UNIVERSITY OF OKLAHOMA

GRADUATE COLLEGE

CHARACTERIZATION AND PREDICTION OF FLASH FLOOD SEVERITY

A DISSERTATION

SUBMITTED TO THE GRADUATE FACULTY

in partial fulfillment of the requirements for the

Degree of

DOCTOR OF PHILOSOPHY

By

MANABENDRA SAHARIA
Norman, Oklahoma
2017

CHARACTERIZATION AND PREDICTION OF FLASH FLOOD SEVERITY

A DISSERTATION APPROVED FOR THE
SCHOOL OF CIVIL ENGINEERING AND ENVIRONMENTAL SCIENCE

BY

_____
Dr. Yang Hong, Chair

_____
Dr. Jonathan J. Gourley

_____
Dr. Randall Kolar

_____
Dr. Jeffrey Basara

_____
Dr. Keith A. Strevett

This dissertation is dedicated to my family.

To my parents, Ramesh Chandra and Nilakhi Sahariah, for the sacrifices they made to give me the best possible education. I will forever be in their debt.

And to my brother, Dhiraj, for his love and affection.

Acknowledgements

I have come to understand over the years that life is a highly non-linear process where any outcome is influenced by a large number of causative processes. It is beyond my ability to comprehensively list all the people who have contributed to my learning throughout the years. So, if you chance upon this acknowledgement, please know that I value you and all the opportunities, mentoring, and friendships over the years.

It is difficult to overstate my gratitude towards my PhD advisors - Prof. Yang Hong and Dr. Jonathan J. Gourley. Without their active guidance, enthusiastic encouragement, and steadfast support, this journey would not have been possible. Also, I am thankful to the other members of the committee – Dr. Randall Kolar, Dr. Jeffrey Basara, and Dr. Keith A. Strevett for their support.

A special order of gratitude towards Dr. Pierre-Emmanuel Kirstetter, a researcher par excellence, whose advice and mentoring on technical and finer aspects of research I value dearly. Finally, I would like to thank all my colleagues in the HyDROS research group for the stimulating conversations and the congenial work environment.

I would also like to thank Prof. Rajib Kumar Bhattacharjya (IIT Guwahati), Dr. Sharad K. Jain (National Institute of Hydrology/IIT Roorkee), Dr. Parthasarathi Choudhury (NIT Silchar), Dr. Parthajit Roy (NIT Silchar), and Prof. Dong-Jun Seo (UTA) for encouraging me to tread the world of research during my Undergraduate and Master's degree.

I feel indebted and fortunate to be emerging from my formal education and I look forward to contributing to the world in earnest.

Table of Contents

List of Tables

List of Figures

Abstract

Flash floods, a subset of floods, are a particularly damaging natural hazard worldwide due to their multidisciplinary nature, difficulty in forecasting, and fast response that limits emergency responses. The purpose of this work is to develop a framework of characterizing floods and flash floods based on a multitude of explanatory variables that describe the geology, topography, pedology, climatology, and rainfall spatial variability. Until now, flash flood characterization studies in the United States have been limited in scope due to the lack of a comprehensive database matching flood characteristics such as peak discharges and flood duration with geospatial and geomorphologic information. In this study, A long data record spanning 78 years from the United States Geological Survey (USGS) stream gauge network is combined with National Weather Service (NWS) flooding thresholds to study floods at basin and event scale, with special focus on the rise time and unit peak discharge. A new metric for flash flood severity called 'flashiness' is also proposed that represents the rate of rise of the hydrograph during flooding conditions and thus captures both the magnitude and timing aspects of floods.

Associations between flashiness and geophysical variables are initially constructed at locations where there is known information from both discharge observations and the geospatial datasets. These relationships are first investigated through first-order characterization of trends and their variability. Since we don't have discharge observations everywhere, a multi-dimensional statistical modeling approach is built upon these associations to regionalize flashiness to all ungauged locations across the Continental United States (CONUS). Several localized flash flood hotspots were

identified outside of the originally defined regions including the western slopes of the Appalachians in Tennessee, Kentucky, and West Virginia. Furthermore, a high-resolution Multi-Radar/Multi-Sensor (MRMS) rainfall reanalysis dataset (1 km/5-min resolution) from 2002-2011 was used to quantify the relative impact of sub-basin scale rainfall spatial variability and geomorphology on flashiness. It was found that the percentage contribution of rainfall spatial variability to flashiness is 9% more for flash floods compared to floods.

Results from this research highlight how the trend and variability of flooding variables such as rise time, unit peak discharge, flash flood severity etc. could be explained using a large number of explanatory variables. It also demonstrates how complex non-linear association between the hydrologic response and variables representing causative processes could be modeled with reasonable skill to predict in ungauged locations.

Chapter 1. Introduction

Flash Floods are naturally occurring events that have been defined by the National Weather Service (NWS) as "a rapid and extreme flow of high water into a normally dry area, or a rapid water level rise in a stream or creek above a predetermined flood level, beginning within six hours of the causative event (e.g., intense rainfall, dam failure, ice jam). Flash floods are swift flood responses to intense rainfall or release of water over a small area. Inundation over dry land occurs within minutes to a few hours of the rainfall event, potentially causing devastating impact on lives and infrastructure (Hong et al., 2012).

Ashley and Ashley (2008) found floods to be the second-deadliest U.S. weather-related hazard after heat. They compiled a nationwide database of flood fatalities across the contiguous United States from 1959 to 2005 with detailed event and demographic information and found that the majority of the fatalities were caused by flash floods. Pielke and Downton (2000) found that flood damage costs for the United States has steadily increased throughout the twentieth century. For the water year 2014 (October 1, 2013 – September 30, 2014) alone, direct flood damages totaled $2.86 billion in the United States according to the Flood Loss Report compiled by the National Weather Service (NWS, 2014). In 2014, 55 flood-related fatalities were recorded, 29 were attributed to vehicle-related accidents and 39 to flash flood events (NWS, 2014). An increasing trend of heavy precipitation at both continental (Groisman et al., 2004) and global scale (Groisman et al., 2005), combined with rapid urbanization, is expected to increase the frequency and impact of flash floods. Studies such as Mallakpour and

Villarini (2015) and Hirsch and Archfield (2015) have presented evidence that the frequency of flooding has increased over the decades but not the magnitude.

But despite posing significant threat to economy and human life, there is a lack of research into the spatial distribution of flash flooding across the United States as well as its causative processes. Floods, and especially flash floods, are poorly understood and documented and to perform a spatially and temporally comprehensive characterization, we need appropriate databases of flooding events along with data on variables that potentially influence these floods. Also, we need to go beyond the state-of-the-art by not only investigating first-order dependencies but also variability in the associations between flooding characteristics and variables describing causative processes related to geomorphology, climatology, and causative rainfall of a flooding event. The overarching goal of this research is to identify the processes that most significantly impact flooding from climatological to flood event scale.

1.1 The need for flood and flash flood characterization

Flood and flash flood responses are dictated by a complex interaction of various runoff generating processes and conveyance of water out of the basin. Understanding how space and time scales of floods vary with these causative processes is the key to understanding the nature of floods and improving hydrologic modeling. To investigate the spatial, temporal, and geographic distribution of floods, we must first have a centralized database that collates quantitative information regarding floods. The flooding information combined with other geospatial datasets covering geomorphology, climate, and precipitation allows us to uncover a general picture of flooding across the US. This dissertation characterizes flooding across the US from continental to flood event scale.

However, such databases are not easily available as formal records on previous floods are scattered across disparate sources. Due to this limitation, flood characterization studies have been performed mostly based on case studies or limited databases. Costa (1987a) described the hydraulic characteristics of twelve of the largest floods of small basins ever measured by the U.S. Geological Survey (USGS) in the conterminous United States (CONUS) and related them to basin morphometry of the channels. He concluded that basin physiography and geology, in addition to rain intensity and duration, are major factors in maximizing runoff. In order to devise a procedure to distinguish flash floods from other floods, Bhaskar et al. (2000) developed a Flash Flood Index. The index utilizes characteristics describing the shape of the flood hydrograph and shows weak to moderate correlation with additional hydrograph variables such as unit peak discharge and direct runoff volume. Merz and Blöschl (2003) identified the causative mechanisms of various types of floods using 11,518 maximum annual flood peaks in 490 Austrian catchments. They studied long-rain, short-rain, flash floods, rain-on-snow, and snowmelt floods and found that 43% of floods are long-rain floods and only 3% are snowmelt floods. Gaume et al. (2009) reported the compilation of an inventory containing 550 documented flash flood events in seven hydrometeorological regimes in Europe. Marchi et al. (2010) performed a detailed study of 25 selected extreme flash floods in Europe to identify causative processes and related them to climate and basin morphology. They characterized these events in terms of basin morphology, flood-generating rainfall, peak discharges, runoff coefficient, and response time to identify implications for flash flood risk management. To approximate the basin behavior in response to rainstorms, Perucca and Angilieri (2011) evaluated the flash

flood hazard of del Molle basin in Argentina by analyzing different morphometric properties. The study reported the probability of a serious flash flood hazard in the basin and suggested implementation of mitigation measures. Such studies have provided important insights into understanding floods in ungauged locations. Castellarin (2007) found that the reliability of probabilistic regional envelope curve (PREC) flood quantiles for ungauged sites is comparable with the reliability of regional estimates produced by the application of the index flood approach. Gaume et al. (2010) reduced the uncertainties in estimating regional flood quantiles by employing a Bayesian method on flash flood events occurring in ungauged catchments. Ruiz-Villanueva et al. (2013) characterized 41 flash flood events in small mountain basins of Central Spain and analyzed their frequency, severity, seasonality, synoptic meteorological causes, as well as the human impacts in terms of damage and fatalities. These methods can be used to reconstruct floods in ungauged basins.

This study provides a more comprehensive characterization of floods across the US due to a more spatio-temporally representative sample of observations. Previous studies don't go beyond first order characterization of trends while this study investigates the trend as well as variability in the relationship between flooding characteristics and variables describing causative processes. It also proposes a new definition of flash flood severity called flashiness that represents the potential of a basin to produce a rapid and improves upon the discharge frequency-based approaches adopted in studies such as Smith and Smith (2015). Finally, a multi-dimensional modeling approach was built upon these association to regionalize flashiness across ungauged locations of the United States.

Moreover, there is no consensus on how the spatial organization of rainfall impacts basin response. Rainfall is a highly heterogeneous process over a wide range of scales in space and time (Fabry, 1996; Marani, 2005; Rodriguez- Iturbe and Rinaldo, 1997) and the influence of rainfall spatial variability on hydrologic response of watersheds has been a recurrent theme in hydrology for decades. But the extent to which spatial heterogeneity of rainfall impacts catchment response and its influence in comparison to basin morphology is poorly understood. Greater availability and significant improvement in high-resolution radar rainfall data in recent decades has resulted in an increasing number of studies in this area. Still, the literature has not yielded a consensus on how these rainfall heterogeneities impact hydrologic responses, which has implications for flood forecasting and accurate process representations in distributed hydrologic models. At larger spatial scales, catchment responses are often simpler as much of the hydrologic system heterogeneity is subsumed and averaged (Sivapalan et al., 2003). But prediction becomes increasingly difficult at smaller spatial scales, as runoff is more intricately linked to details of landscape structure, thereby exhibiting greater space-time variability (Merz and Blöschl, 2004). The spatial variability in precipitation also adds to the variability in response by partially activating basins to produce a hydrologic response and to different magnitudes, especially when storm size is much smaller than the catchment. Because of this, flood forecasting models often rely on basin-averaged rainfall information. On the other hand, several studies have found that basin flood responses are sensitive to the spatial structure of rainfall (Dawdy and Bergmann, 1969; de Lima and Singh, 2002; Douinot et al., 2016; Kirstetter et al., 2015, p. 201; Lobligeois et al., 2014; Mei et al., 2014; Rafieeinasab et al., 2015; Viglione et al., 2010; Wilson et

al., 1979; Wood et al., 1988). Hydrologists have sought to understand the link between rainfall space-time variability and hydrologic responses for several decades, but it remains an open-ended question in hydrology.

Thus, from the perspective of improving flood forecasting and as a diagnostic tool, it is important to systematically quantify the impact of different explanatory factors on catchment responses for a variety of space and time scales and basin physiography.

1.2 Hypothesis and objectives

The dissertation establishes a framework for characterizing flooding from climatological to event scale based on a multitude of causative factors related to geology, topography, pedology, climatology, and rainfall spatial variability to understand hydrological behavior. To that end, this study proposes two hypotheses –

1. If the hydrologic responses of the basin are influenced by a large number of factors (namely geomorphology, climatic regime, spatial organization of rainfall, soil type, land use/land cover etc.), then these relationships could be used to explain the trend and variability of flooding variables such as rise time, unit peak discharge, flash flood severity etc.
2. If this complex association between the hydrologic response variables and causative processes could be modeled with reasonable skill, it could be used to predict hydrologic variables beyond locations where observation dataset is available as well as disaggregate the influence of individual variables.

The study is a part of the larger project called Flooded Locations And Simulated Hydrographs (FLASH) which encompasses a suite of products to advance the state of the science in flash flood prediction (Gourley et al., 2017). This dissertation, till now, has

resulted in two publications concerning the characterization of floods (Saharia et al., 2017) and the mapping of flash flood severity in the United States (Saharia et al., 2016). Specific objectives of this work are listed below:

1. Perform a spatially and temporally comprehensive flood characterization over the CONUS.
2. Propose a new definition for flash flood severity and quantify the relative influence of a large number of causative factors. Predict flash flood severity across the CONUS using a multidimensional modeling framework.
3. Quantify the impact of rainfall spatial variability on flash flood severity using high-resolution rainfall data.

1.3 Structure of the dissertation

The research work presented in this dissertation consists of three studies that describe the progressive development of a framework to characterize floods and flash floods. Chapter 2 describes the various datasets used in this study, such as the flash flood observation database, the MRMS radar precipitation, and the spatial datasets describing physiography and climatology.

Chapter 3 describes how flooding characteristics are examined to identify variation of space and time scales of floods with climatic regimes and geomorphology. Flood events were characterized by linking flood response variables in gauged basins to spatially distributed variables describing climatology, geomorphology, and topography. The availability of a representative and long archive of flooding events spanning 78 years over a variety of hydroclimatic regions results in a spatially and temporally comprehensive flood characterization over the continental U.S.

Chapter 4 introduces a new variable called “Flashiness” as a measure of flood severity by utilizing the long archive of flooding events. It is modeled as a function of a large number of geomorphological and climatological variables, which is then used to extend and regionalize the flashiness variable from gauged basins to a high-resolution grid covering the conterminous United States. Six flash flood “hotspots” are identified and additional analysis is presented on the seasonality of flash flooding. The findings from this study are then compared to other related datasets in the United States including National Weather Service storm reports and a historical flood fatalities database.

Chapter 5 explores the impact of rainfall spatial variability on flash flood severity by using a high-resolution rainfall and flooding dataset spanning 2002-2011. The study employs an observation-based big data approach to develop a robust understanding of how rainfall spatial variability impacts flash flood severity and quantify its contribution relative to basin physiography.

Finally, Chapter 6 summarizes the findings and conclusions made from the studies. Suggestions are also provided on how the work can be extended to improve the characterization of flooding.

Chapter 2. Datasets

2.1 Unified Flash Flood Database

In the United States, flood characterization has been done mostly through limited case studies or for a part of the country since the available information is usually sparse and non-homogeneous. Most flood databases do not catalogue sufficient information such as geospatial and geomorphologic data to be adequate for flood characterization studies. A comprehensive flood database should have certain information such as flood response variables (e.g. flooding rise time, recession time, etc.), peak discharge information, gridded rainfall rate data and as many geomorphologic parameters of the basins as possible to evaluate specific parameters that improve analysis of the driving geomorphologic and climatological factors, and hydrologic simulations. Some of the existing hazard databases that catalogue flooding events include the freely-accessible Emergency Disasters Database (EM-DAT) by the Center for Research on the Epidemiology of Disasters (CRED), that covers natural and man-made disasters from 1900-present (http://www.emdat.be/). The United Nations Office for the Coordination of Humanitarian Affairs (OCHA) also maintains ReliefWeb (http://www.reliefweb.int/) which publishes disaster reports in real-time. The International Flood Network (IFNET) publishes a flood event database based on voluntary submission of events that caused 50 or more casualties between 2005-2007 (http://www.internationalfloodnetwork.org/). The Dartmouth Flood Observatory (DFO) maintains a Global Archive of Large Flood Events (http://floodobservatory.colorado.edu/) which is one of the most comprehensive flood databases derived from a variety of sources such as remote sensing images and

government reports (Brakenridge and Karnes, 1996). However, even though the database has good global coverage, it is not exhaustive enough and its events are only geo-referenced up to 2006, which limits its usability in evaluating and improving flood models. Adhikari et al. (2010) also reported a digitized global flood inventory (1998–2008) with georeferenced flooding events.

The Unified Flash Flood Database released by the HyDROS group at the University of Oklahoma is a curated database of flooding information from a variety of sources such as gauge measurements of streamflow by US Geological Survey (USGS), flash flooding reports in the National Weather Service Storm Events Database, and public survey responses on flash flood impacts collected during the Severe Hazards Analysis and Verification Experiment (Gourley et al., 2010; Ortega et al., 2009). The high-resolution information provided by SHAVE, spatial coverage of NWS reports, and automated data collection mechanism of USGS streamflow records makes it one of the most representative flash flood databases in the United States (Gourley et al., 2013). It is publicly available for no cost at: https://blog.nssl.noaa.gov/flash/database/

Michaud et al. (2001) have depicted the distribution of large floods in the U.S. using data from 130 USGS stations, but only for basins less than 200 km^2. O'Connor and Costa (2004) was the first study to systematically analyze large portions of the USGS streamflow dataset comprising largest 10% of annual peak flows from 14,815 stations. While it states that specific basins of high unit peak discharge correspond to relatively high topographic relief, it only provides a qualitative assessment of this relationship due to unavailability of geomorphological data. Other studies have uncovered flooding characteristics in a portion of the country using the same USGS data, such as Villarini

and Smith (2010) in the eastern U.S. and Mallakpour and Villarini (2015) in the central U.S. Smith and Smith (2015) uses a similar dataset to identify the "flashiest" watersheds in the contiguous United States based on the frequency of discharge peaks exceeding 1 $m^3s^{-1}km^{-2}$. They noted urban areas were frequently affected by flash flooding in the south-central U.S. (i.e., Tulsa, Oklahoma and St. Louis, Missouri) up through the mid-Atlantic (i.e., Baltimore, Maryland) as well as the Pacific Northwest.

This work uses automated streamflow measurements from the USGS. USGS collects instantaneous streamflow data at intervals ranging from 5 to 60 minutes for 10,106 gauges in the database. The NWS coordinates with local stakeholders and the USGS to define stages corresponding to action stage, minor, moderate and major flooding for 3,490 stream gauge locations. This subset of gauges from the USGS network has defined flooding thresholds which is useful information for many applications including modeling. These thresholds are used to extract flooding events from the streamflow record. Action stage is defined as the stage at which NWS forecasters take "mitigation action for possible significant hydrologic activity" and it often corresponds to bankful conditions. In fact, 41% of USGS stations have identical action stage and bankful stages, differing on average by 1.3%.

USGS also supplies regulation codes for these gauges, which is used to further screen out the gauges that have some amount of anthropogenic influence from regulation or diversion. After removing gauges with anthropogenic influences and no defined action stage, we are finally left with a data sample of 70,273 flooding events from 1649 stations. Flood events are defined when streamflow exceeds the defined action stage for that gauge. There must be a 24-hour difference between when streamflow drops below action stage

to the next rise for it to be counted as a separate event. The primary database comes with the following information for each gauge: the USGS Gauge ID, latitude (decimal degrees), longitude (decimal degrees), start time (UTC) at which the flow first exceeded the action stage threshold, end time (UTC) when the flow dropped below the threshold, peakflow magnitude (m^3/s), peak time (UTC) at which peakflow occurred (UTC), and the difference between the time at which the discharge first exceeded action stage and reached its maximum value, defined as the flood rise time (in hours).

2.2 Physiographic and climatological data

The Unified Flash Flood Database detailed above was further enhanced with geomorphologic and climatological attributes derived for each basin in the dataset. Spatially distributed parameters were introduced to elucidate and quantify how the underlying, static basin characteristics influence flood response. Several geomorphological attributes were extracted from the Digital Elevation Model (DEM) data of the National Elevation Dataset (NED; http://ned.usgs.gov/) as potential explanatory variables of flash flood severity. Flow accumulation and flow direction information was extracted by delineating basins with USGS stations. The 30-m DEM was resampled to a 1-km grid using the National Hydrography Dataset (NHD; http://nhd.usgs.gov/) to ensure that DEM-based flow accumulation computations agree with the actual river network across the CONUS. The geomorphologic parameters were derived from the grid-based delineated catchments using custom libraries developed using MATLAB. Soil datasets from the STATSGO database (Miller and White, 1998) were utilized to derive variables such as mean depth-to-bedrock and K-factor (erodability). Land cover and land use data from the National Land Cover Dataset (Fry

et al., 2011) were used to estimate the runoff curve number. Lastly, in addition to the geomorphological variables, the hydroclimatic variables of mean annual precipitation and temperature were extracted from the 30-year datasets (for period 1981-2010) prepared by the PRISM Climate Group of Oregon State University (http://www.prism.oregonstate.edu/normals/). Custom libraries developed in MATLAB were utilized to derive different parameters based on the resulting grid-based delineated catchments which have been described in the later chapters.

2.3 Multi-Radar/Multi-Sensor (MRMS) Precipitation

Traditionally, rainfall data has been collected using manual and automatic rain gauges. The process has now evolved with radars providing rainfall data with near real-time updates. An increasingly extensive coverage of radars has led to the development of mosaic radar rainfall products over the CONUS with high spatio-temporal resolution. The MRMS project, initiated by the NOAA NSSL, has revolutionized the way precipitation is measured by producing a seamless high-resolution dataset that updates in the order of two minutes without human intervention. A complete description of the MRMS system can be found in Zhang et al. (2015) along with the Quantitative Precipitation Estimation (QPE) generation process that comes from the preceding National Mosaic and Multi-Sensor QPE (NMQ) system (Zhang et al., 2011). MRMS system currently centralizes collection and collation of data from 180 operational radars and ~7000 hourly gauges across the CONUS and southern Canada. The radar data is integrated with atmospheric, environmental, satellite, lightning and rain gauge observations to generate a suite of products suitable for weather and hydrologic modeling (Zhang et al., 2015). The use of a multi-sensor network increases the accuracy of rainfall

estimation compared to a single-radar framework, addressing the issue of significant rainfall estimation errors offsetting the improvements afforded by incorporation of rainfall spatial variability in hydrologic modeling (Ogden et al., 2000; Quintero et al., 2012; Schröter et al., 2011; Villarini et al., 2010).

Figure 2.1 shows the MRMS CONUS domain bounded by latitudes 20º-50ºN and longitudes 130º-60ºW along with the radar beam height (in KM) used in the hybrid scan reflectivity computation. The radar coverage is not uniform across the country and western CONUS has large areas with high radar beam height, which decreases the accuracy of surface precipitation estimation (Kirstetter et al., 2015). Figure 2.2 shows the cumulative distribution function of the radar beam height across the country. Approximately 40% of the geography is in an area with radar beam height of less than 1 km. This information is used for quality control of the dataset as described in Chapter 5. For performing more comprehensive studies and analyses, a reanalysis MRMS product has been recently produced for a period from 2001 to 2011. The reanalysis domain is analogous to the MRMS domain with products on a regular 0.01º grid with 7000 columns and 3500 rows for a total of 24,500,000 grid cells. The precipitation rainfall rates produced for this period are used to characterize the rainfall spatial variability and its impact on the flooding events reported in the Unified Flash Flood Database.

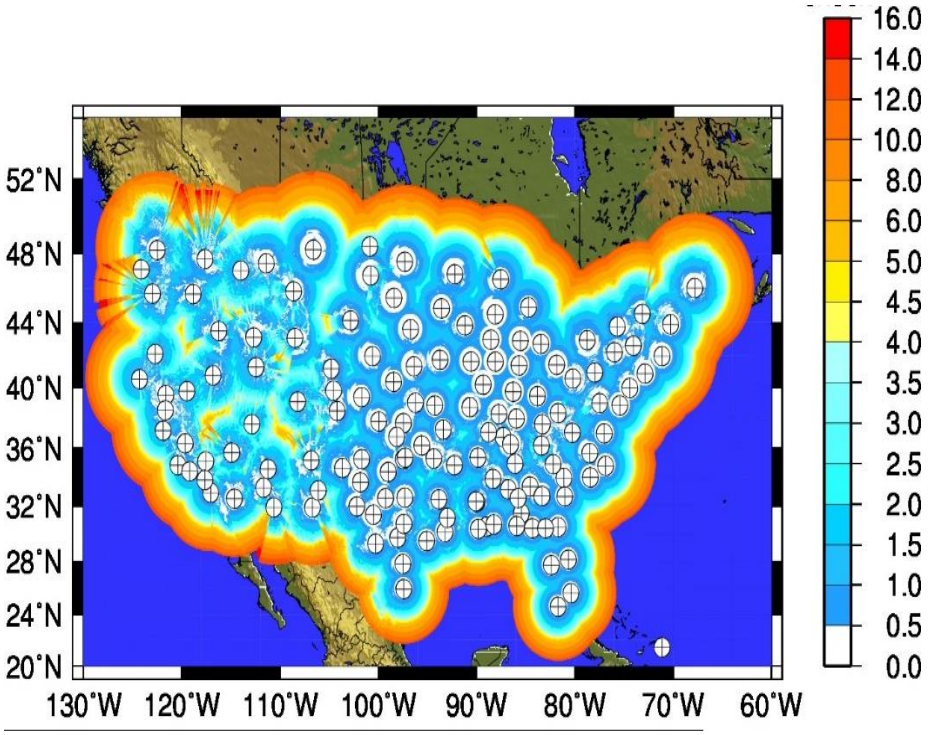

Figure 2.1: MRMS domain and locations of the US WSR-88D radar sites within the CONUS domain, along with the radar beam height.

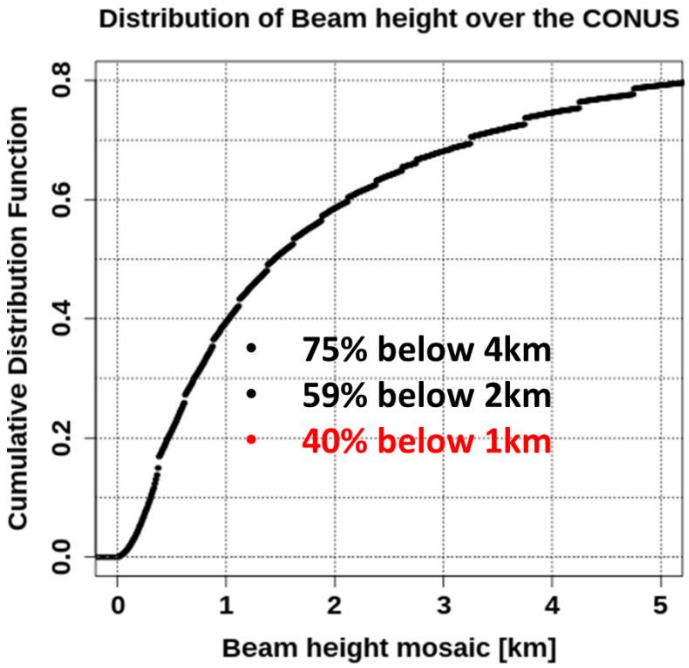

Figure 2.2: Distribution of MRMS radar beam height over the CONUS

Chapter 3. Characterization of Floods in the United States

3.1 Introduction

Flood hazard studies at the continental and global scales increasingly receive more attention as the destructive effects of flooding events are given more importance in public policy. However, floods have still not received systematic and comprehensive characterization studies commensurate with their social and economic impacts.

Benefiting from the representativeness and length of the Unified Flash Flood Database, this study provides a spatially and temporally comprehensive flood characterization over the CONUS. The long USGS component of the database containing 70,273 flooding events from 1649 stations is suitable for characterizing floods because it contains most of the necessary attributes such as flooding rise time, peak discharge, basin area, etc. This study for the first time, employs a large-events database based on NWS definitions of floods instead of a frequently-adopted case study or frequentist approach which allows us to base our analyses and conclusions on real definitions of floods. It examines flood regimes across the CONUS to determine how space and time scales of floods vary with climatic regimes, seasons, and geomorphology. This characterization of flood events paves the way towards improving hydrologic forecasting and risk management.

The purposes of this analysis are to (i) present an overview of the database that covers flooding events over more than 70 years from 1936-2013, (ii) characterize flooding events according to geomorphological basin attributes and climate classes, (iii) establish new relationships and envelope curves taking advantage of the lengthy historical

record of floods, (iv) explore the results from the perspective of improving flood forecasting and risk management. The study is organized as follows. Section 3.2 provides an overview of the spatial and temporal distribution of floods over the CONUS. Sections 3.3 characterizes floods based on physiographic factors. Sections 3.4 and 3.5 characterizes unit peak discharge and flooding rise time, respectively, based on geomorphologic parameters such as basin area, relief ratio, and shape factor. Finally, Section 3.6 provides a summary of findings and concluding remarks.

3.2 Spatial and temporal distribution of floods

In order to investigate the potential dependence of floods on climatic regime, the analysis used the Köppen-Geiger Climate Classification over the U.S given in Kottek et al. (2006). Figure 3.1 shows the distribution of all USGS stations in the database over the CONUS segregated as per the Köppen-Geiger climate classes. Six classes were utilized in this study: Warm temperate fully humid extremely continental (Cfa), Warm temperate summer dry warm summer (Csb), snow fully humid hot summer (Dfa), snow fully humid warm summer (Dfb, West and East) and Arid steppe cold arid (BSk). The number of flooding events and gauges in each climate class is given in Table 3.1, along with the number of flooding events normalized by the number of gauges in each regime to enable comparison between different climate classes. Cfa has the highest number of 39,872 events while Dfb (W) has the lowest with 905 events. Basins in the eastern half of U.S. that comprises of Dfb (E), Dfa, and Cfa have higher number of flooding events per gauge than the western half of U.S. comprising Csb, BSk, and Dfb (W).

Table 3.1: Number of flooding events and gauges in each climate class along with normalized values of number of flooding events. Floods are defined by discharge exceeding action stage, as defined by National Weather Service employees and local stakeholders.

Climate Classes	Flooding events	Gauges	Flooding events/Gauges
Csb	1688	78	21.64
BSk	1129	110	10.26
Dfb (W)	905	84	10.77
Dfb (E)	9901	230	43.05
Dfa	16778	313	53.60
Cfa	39872	827	48.21

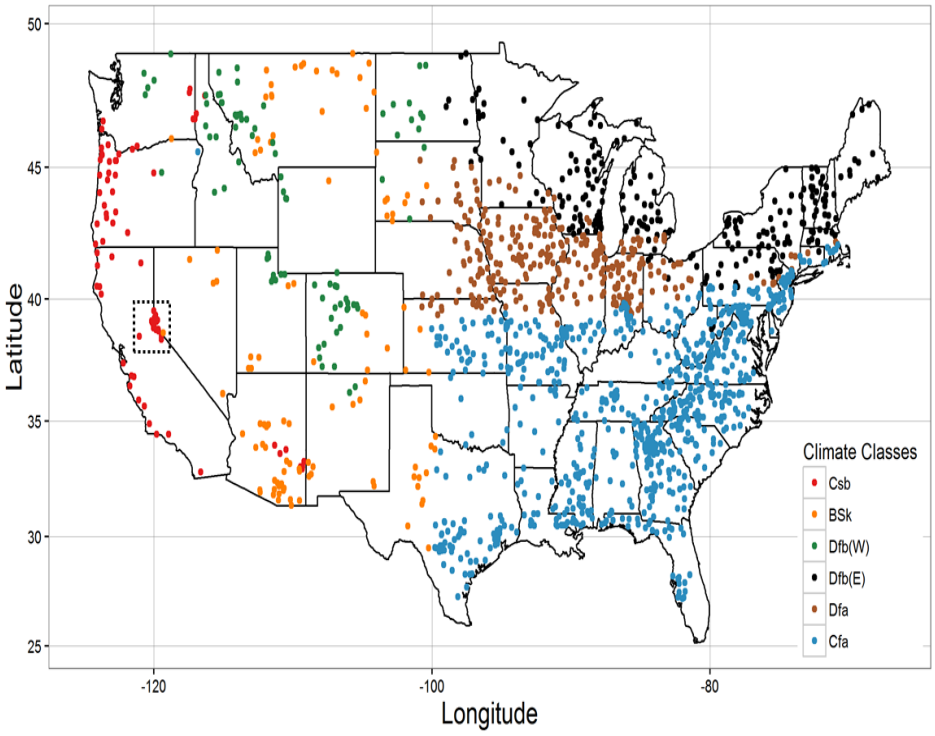

Figure 3.1: Distribution of USGS streamflow stations used in this study color-coded by Köppen-Geiger Climate Classes. The black box within the Csb region is a sub-class called Csb 1 and the rest of Csb outside the box is termed Csb 2 in this study.

Precipitation, being the primary driver of floods, is important to explain the variability of flooding events. The summary statistics for average annual precipitation computed for the six climate classes is provided using the box-and-whisker plot of Figure 3.2. The band inside the box is the second quartile (median), while the bottom and top of the boxes correspond to the first (25^{th} percentile) and third quartiles (75^{th} percentile), respectively. The mean is given by the open circle inside the box. The whiskers extend to the extremes of the observations and outliers outside 1.5 times the inter-quartile range are plotted as filled circles. The highest annual precipitation of 1537 mm/y falls in the Csb region, which is expected as moisture-laden westerlies from the ocean encounter the high mountain ranges of California, Oregon, and Washington, including the Olympic Mountains, the Cascades, and the Sierra Nevada range. After Csb, areas in the East such as the southeastern US (Cfa), eastern and midwestern US from the Atlantic to the 100th meridian (Dfa) and the Great Lakes region with New England (Dfb (E)) experience high precipitation. The semi-arid region of BSk that acts as a transition zone between humid and desert climate has the lowest annual precipitation among the six classes, while the Dfb (W) region that contains the Rocky Mountain range receives slightly higher precipitation.

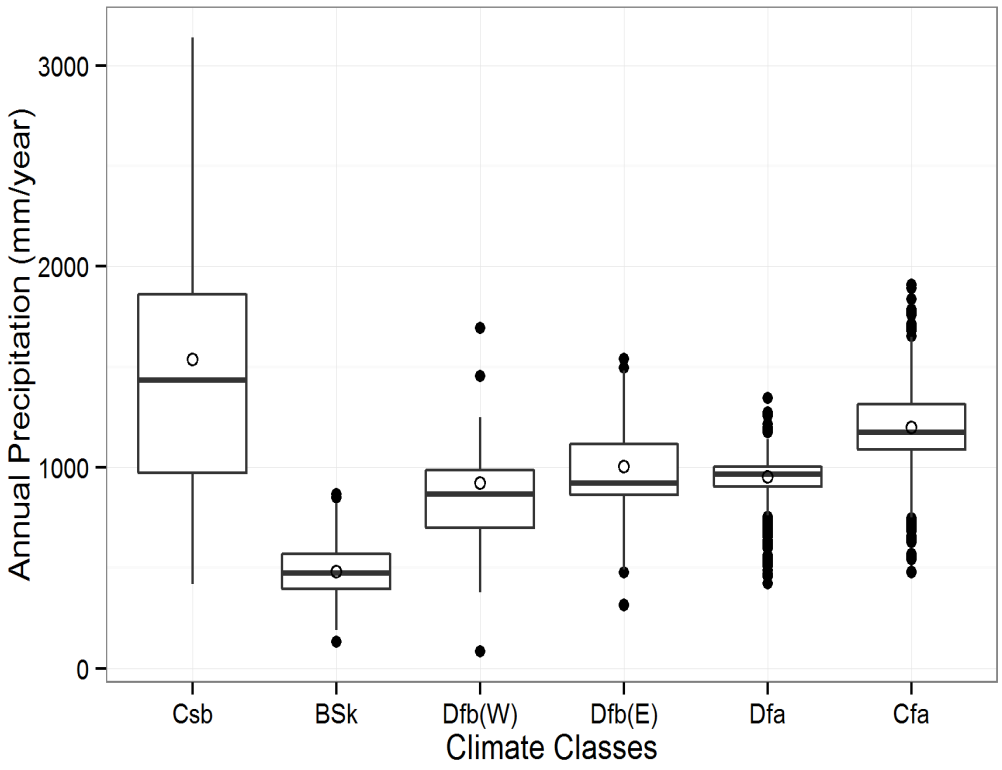

Figure 3.2: Box-and-whisker plot of annual precipitation in different climate classes.

Even though the dataset spans 78 years, most the data (92.9% of events) is concentrated in the last two decades. The number of gauges also doesn't remain constant during this period. So, to detect any temporal trend in the most extreme floods, the number of major stage floods in each year were normalized by the number of action stage floods for the past three decades. This was performed on the dataset for the CONUS as well as for the different climate classes. No clear trend was observed nationally; however, Dfb (E) suggests an increasing trend as shown in Figure 3.3. A similar increasing trend in annual maximum daily flow was observed in the northeastern U.S. by Lins and Slack (1999) that was attributed to precipitation patterns linked with the persistent high index phase of the North Atlantic Oscillation at that time. However, a detailed analysis of this

trend would need additional studies involving climate datasets and is beyond the scope of this study.

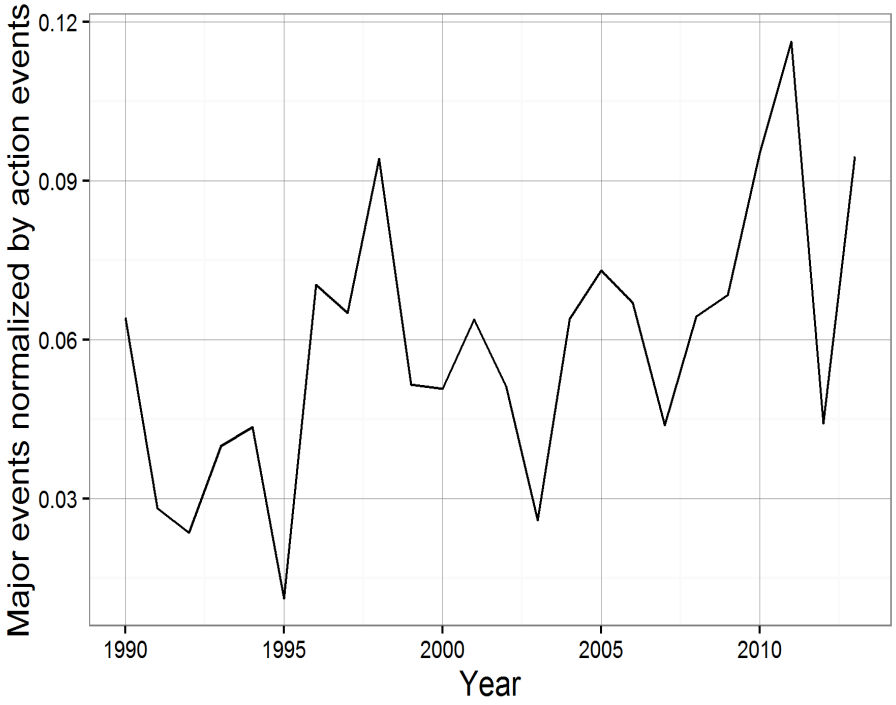

Figure 3.3: Temporal evolution of the number of the events that exceeded major flood stage divided by the number of action stage events each year for Dfb (E).

The regional variations of flood frequency are evaluated on a monthly basis for a better understanding of flood dynamics and the driving factors. Figure 3.4 shows the monthly distribution of flooding events normalized by the total number of events in the various climate classes. The northern migration of the jet stream during the winter brings most of the precipitation to the West Coast, which experiences the highest number of flooding events among all classes during the November-March period. Michaud et al. (2001) found that as one moves inland, the primary flood season shifts to the warm season: late spring/early summer in the northern intermountain West and late summer in the more southerly monsoon-dominated regions. The monthly frequency confirms this,

as the other climate classes experience more flooding events than the West Coast during the warm season. The intermountain West in the Dfb (W) region experiences a high number of floods during the onset of the warm season (April-July) while the semi-arid region of BSk, which receives monsoon precipitation, experiences the highest number of floods in the late summer months (June-September). Basins in the Great Lakes region of Dfb (E) tend to be flooded more during the spring season while the Southeast in Cfa shows the lowest monthly variation of flooding, with a higher tendency of being flooded in early spring.

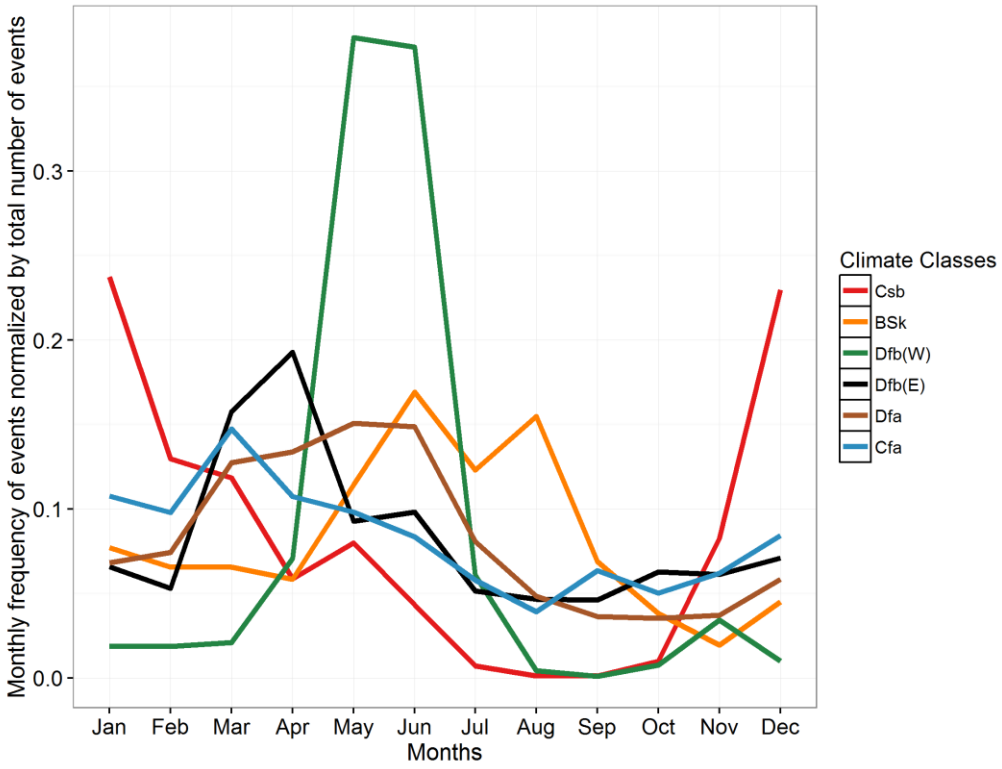

Figure 3.4: Monthly distribution of flooding events normalized by the total number of events in different climate classes.

The number of flooding events in a climate class is correlated with the average annual precipitation given in Figure 3.2. Except for Csb, which is driven by synoptic-scale precipitation events during the cool season, the next two classes experiencing the

highest annual average precipitation, Cfa and Dfa, get the largest number of floods during spring and early summer. As we move westward to basins in Dfb (W) and BSk, deep moist convection plays a larger role with the occurrence of highest number of floods occurring in late-spring and summer.

3.3 Characterization of floods based on physiographic factors

The terrain of a catchment influences catchment response through the combined effects of orography on precipitation rates and topographic relief on streamflow evolution. Geomorphologic analysis is thus of vital importance in describing the hydrologic behavior of basins as it influences factors such as response times and peak discharge values. Relationships between flooding variables and geomorphological parameters are very useful in modeling as geomorphology changes very slowly and most of these parameters can be easily calculated from DEM data. Studies such as Collier and Fox (2003) and Collier (2007) identified several morphological characteristics such as catchment slope and ratio of catchment area to mean drainage path length that have a large correlation with basin susceptibility to flooding. Apart from exploring the general interdependence between flooding variables and basin area, this study also explores several other variables such as relief ratio and shape factor to determine how various basins respond in different regions.

The relief ratio is the ratio between the total relief of a basin (elevation difference of lowest and highest points of a basin) and the longest dimension of the basin parallel to the principal drainage line (Schumm, 1956). This dimensionless height-length ratio allows for comparison of relative relief of basins with varying topography. We can generally anticipate that a higher relief ratio would be associated with a basin more prone

to flooding with faster concentration of streamflow. Higher terrain gradients with generally shallow soils imply that a greater proportion of the water becomes infiltration-excess runoff, while runoff is more likely to be saturation-excess in gently sloping basins. The relation between relief ratio and basin area for different climate classes is given in Figure 3.5. The general relationship of decreasing basin relief with increasing basin area is in conformity with reported literature (Dade, 2001; Marchi et al., 2010).

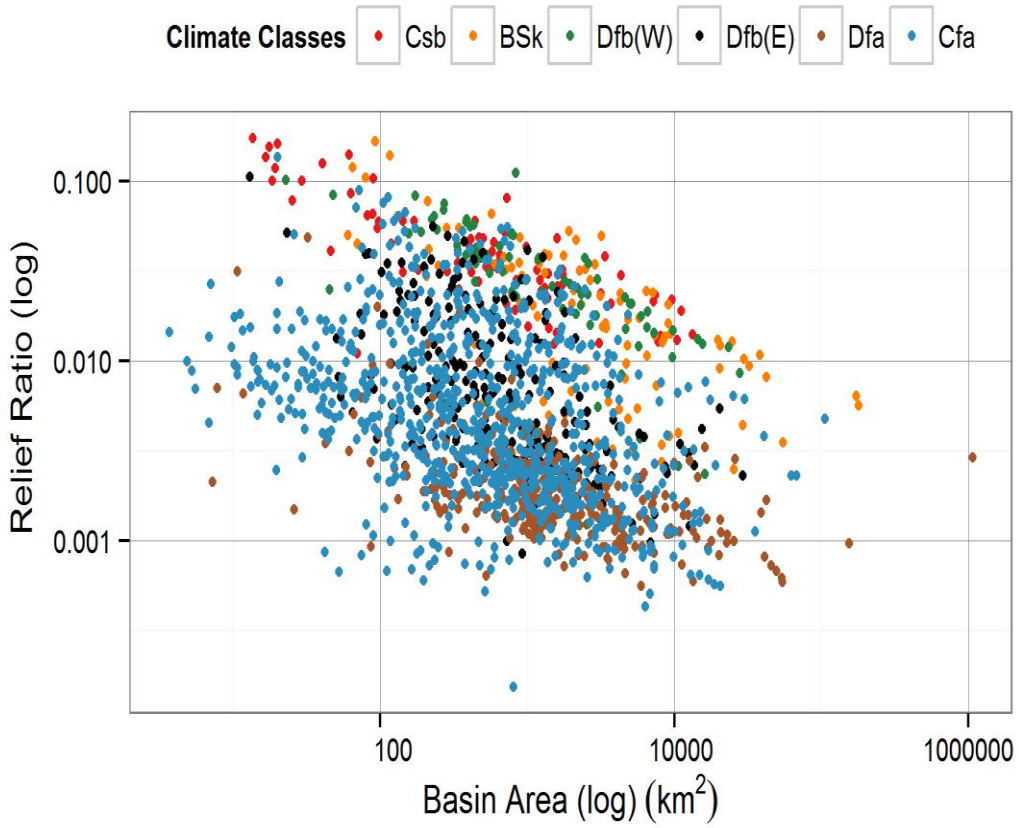

Figure 3.5: Relief ratio plotted as a function of basin area where the colors correspond to different climate classes (refer to legend). The sample size of each climate class is reported in Table 3.1.

The summary for values of relief ratio over the six climate classes is given by the box-and-whisker plot of Figure 3.6. Values of relief ratio over the CONUS range from 0.0002 to 0.17, with an average value of 0.008 which is comparable to values reported in other studies (Costa, 1987a; Marchi et al., 2010). From the box-and-whiskers plots, it can be seen that basins in the western half of the CONUS, i.e. West Coast (Csb), Rocky Mountains (Dfb (W)) and the intermountain West (BSk) have higher average relief ratio values than the basins in the eastern half (Dfa, Dfb (E) and Cfa). The highest mean values of relief ratio are found in the Rocky Mountain range of Dfb (W) and the West Coast (Csb), both of which also experience some of the highest number of flooding events in the CONUS. The lowest value is in Dfa, which covers most the Midwest (High Plains).

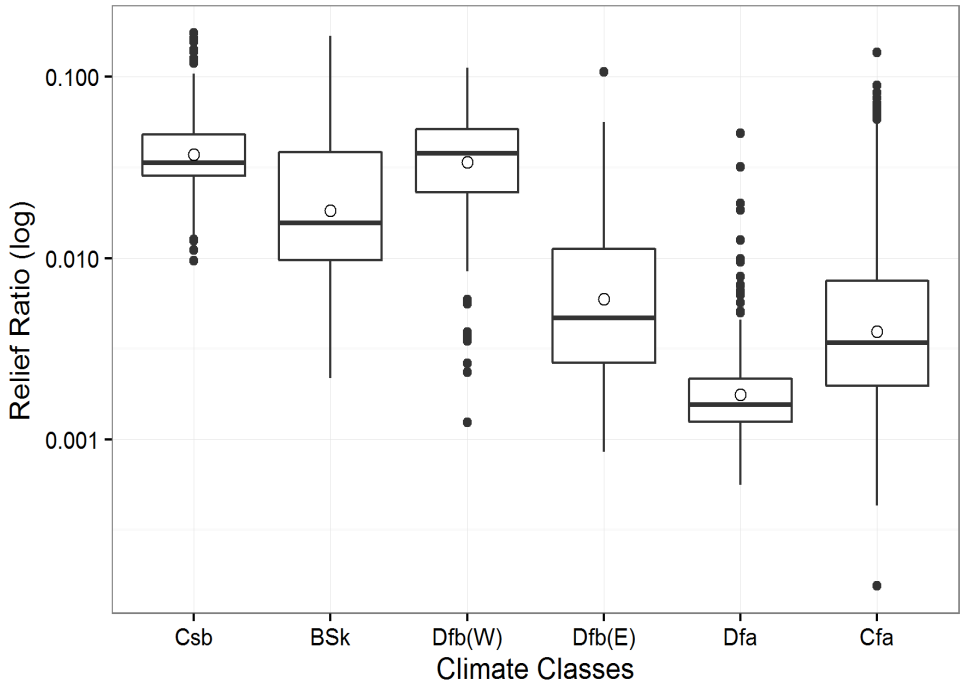

Figure 3.6: Box-and-whisker plot of relief ratio in different climate classes. The horizontal line within the box is the second quartile (median), the open circle is the mean, and the bottom and top of the boxes correspond to the first (25th percentile) and third (75th percentile) quartile respectively. The whiskers extend to the extreme values and filled circles are the outliers outside 1.5 times the inter-quartile range.

3.4 Characterization of floods based on unit peak discharge

The relationship between peak discharge and basin area is well-understood and has been explored in several studies (Furey and Gupta, 2005; Gupta et al., 1996; Marchi et al., 2010; Smith, 1992). A strong correlation between drainage area and discharge is intuitive as it is expected that channels in larger catchments will collect and carry proportionately larger discharges. This relationship will be linear if the unit peak discharge (i.e. the ratio between peak discharge and upstream basin area) is spatially constant. However, in reality, spatial heterogeneity is introduced in the amount of peak discharge per unit area by various factors such as slope, vegetation, rainfall intensity, and spatial rainfall coverage over the basin, etc. The peak discharge values in this study vary greatly in magnitude as the basin sizes vary over several orders of magnitude from 3.68 km^2 to 1,061,895 km^2. Figure 3.7 and Figure 3.8 shows the summary statistics of unit peak discharges and basin area respectively for the six climate classes. Both the highest median unit peak discharge and smallest basin area occurs in West Coast (Csb).

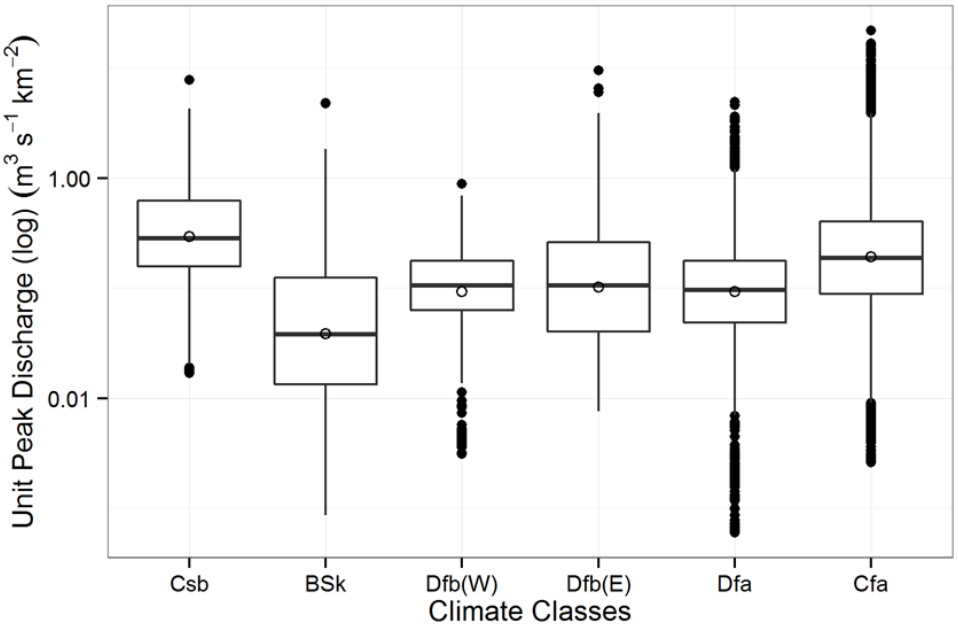

Figure 3.7: Box-and-whisker plot of unit peak discharge in different climate classes

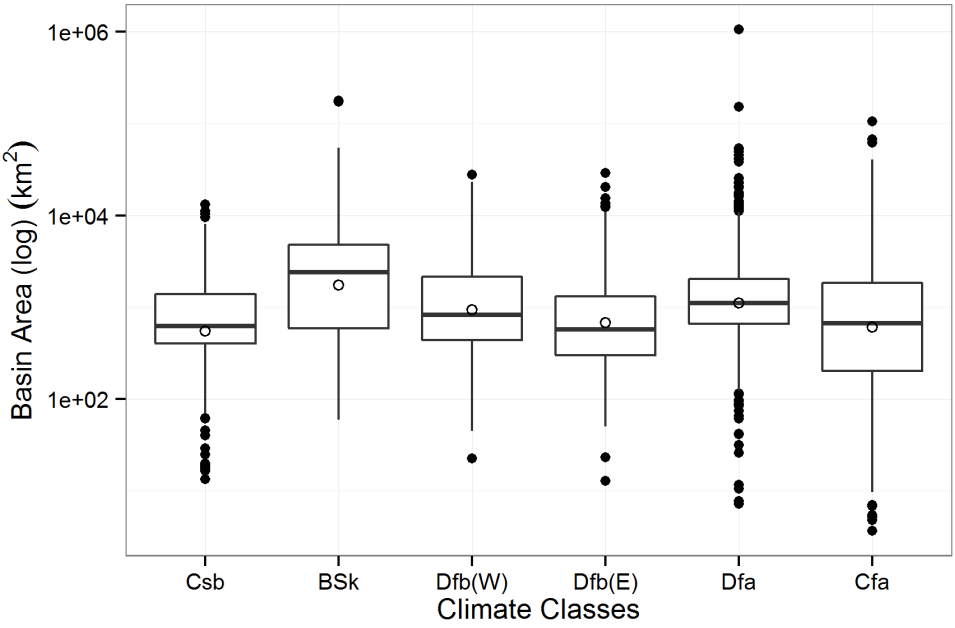

Figure 3.8: Box-and-whisker plot of basin area in different climate classes.

Envelope curves provide an effective summary of historical floods in a study area and have been widely used in previous studies on extreme floods (Jarvis, 1926; Crippen and Bue, 1977; Herschy, 2002; Castellarin, 2007). The dependence between basin area and unit peak discharge for each climate class is explored using log-log diagrams, envelope curves and quantile plots. A simple power-law formula (Eq. 3.1) used in previous studies is selected here.

$$Q_u = \alpha A^{\beta} \quad \textbf{(3.1)}$$

where Q_u is the unit peak discharge ($m^3\ s^{-1}\ km^{-2}$), A is the contributing basin area (km^2), coefficient α is known as reduced discharge and β is a scaling coefficient (Gaume et al., 2009). The values of α and β were determined by fitting a regression line between log (Q_u) and log (A) values for each climate class. The regression was computed on the entire sample and shifted to identify the upper envelope. While α is independent of A, the constant β represents the degree to which unit peak discharge varies with basin area. Atmospheric humidity and surface characteristics affect the unit peak discharge values of basins. The lower the value of β, the faster the proportionate decrease of unit peak discharge with the contributing basin area.

The envelope curves are the straight lines on the log-log diagram developed for different levels of floods and each climate class that can be seen in Figure 3.9 and Figure 3.10 respectively. The National Weather Service has defined flood stage levels in selected gauging stations across the country such as action, minor, moderate and major stage. Flood levels exceeding action stage are closely related to bank-full

conditions and require the authorities to start taking mitigation procedures for possible flooding; minor stage causes minimal property damage; moderate stage causes some inundation in roadside structures and roads near streams; and major stage causes extensive inundation of structures and roads. The solid lines are the envelope curves for the four levels of floods in CONUS and the dotted line is the envelope curve for major floods in Europe ($Q_u = 97.0\ A^{-0.4}$) for comparison, as proposed in Gaume et al. (2009).

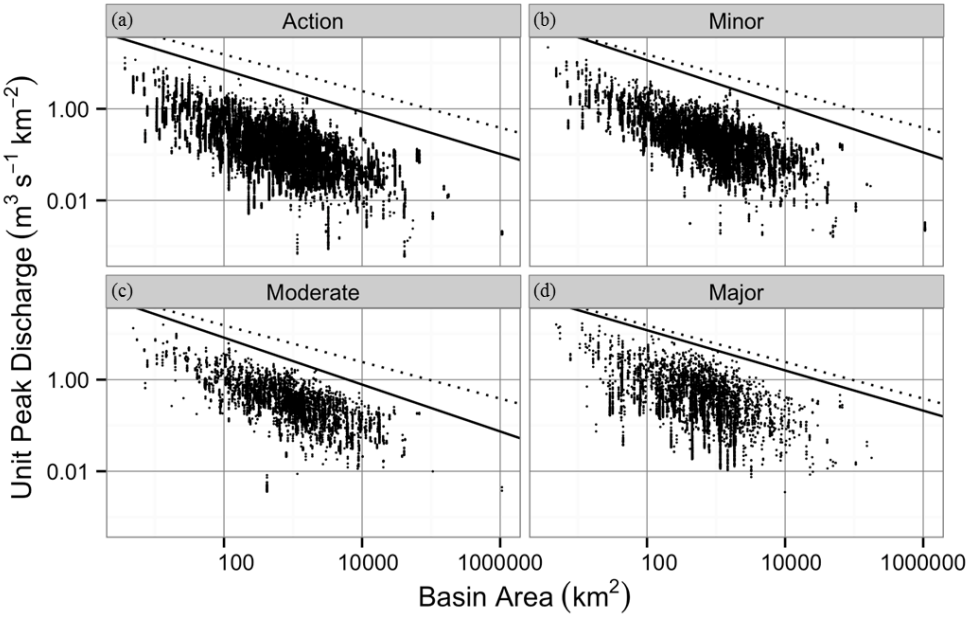

Figure 3.9: Unit peak discharges versus basin area along with their CONUS-wide envelope curves for (a) action, (b) minor, (c) moderate, and (d) major stage floods. The solid line is for CONUS-wide envelope curves while the dotted line is the envelope curve for 25 extreme floods across Europe as reported in Marchi et al. (2010).

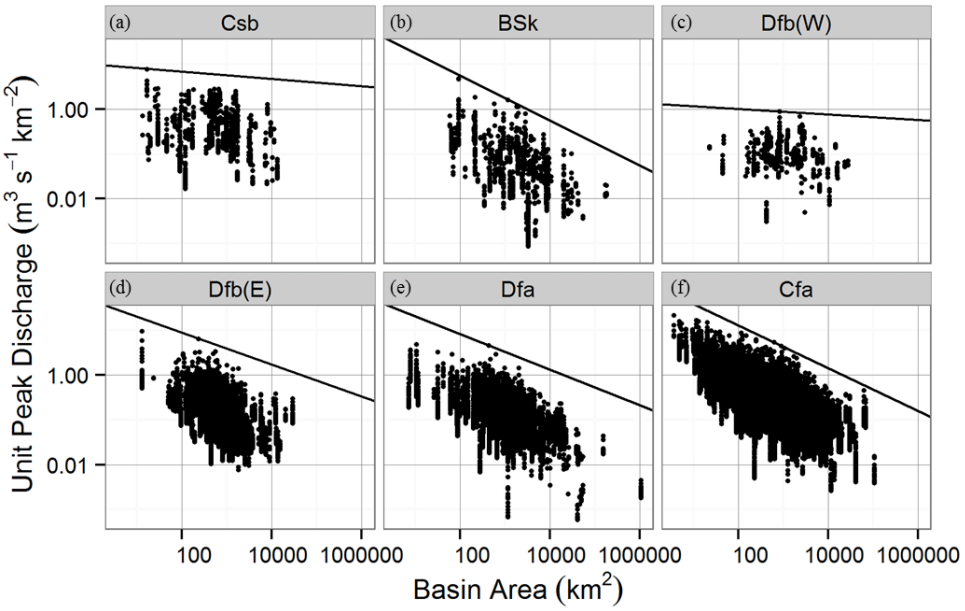

Figure 3.10: Unit peak discharges versus basin areas along with their envelope curves for the (a) warm temperate summer dry warm summer (Csb) (b) arid steppe cold arid (BSk), (c) snow fully humid warm summer west (Dfb(W)), (d) snow fully humid warm summer east (Dfb(E)), (e) snow fully humid hot summer, and (f) warm temperate fully humid extremely continental (Cfa) climate classes.

Table 3.2 gives the α and β values of the CONUS-wide envelope curves for the four flood stages and the exponent (β) in the power-law relationship varies according to stage. The most extreme floods in the CONUS corresponding to the major stage have a β value of -0.44, which is very near to the value of -0.40 proposed for European extreme floods by Gaume et al. (2009) and Marchi et al. (2010). This can also be seen in Figure 3.9, where the solid line corresponding to the major stage is nearest to the European envelope curve. The reported β value for major stage floods in CONUS is greater than the value of -0.643 proposed for global extreme floods (Herschy and Fairbridge, 1998) and -0.57 for mostly riverine floods in Europe (Herschy, 2002). Nonetheless, the asymptotic increase of the envelope curves derived in this study with increasing flood severity toward the

European curve supports the argument that there is a global envelope or upper limit to unit peak discharges.

Table 3.2: Coefficients of CONUS-wide envelope curves describing relationship between unit peak discharge and basin area for the different flood stages.

Unit peak discharge versus Basin area		
Flood stage	**α**	**β**
Action	59.322	-0.460
Minor	116.749	-0.503
Moderate	87.813	-0.512
Major	91.267	-0.440

Table 3.3 gives α and β values of the envelope curves according to climate classes. While some of the values are comparable, the range of basin areas as well as sample sizes is greater in this study than in the European studies (Gaume et al., 2009; Herschy, 2002; Marchi et al., 2010). Within the CONUS, the approximate value of β is highest for Csb class (-0.081) and lowest for BSk (-0.501). With the lowest annual average precipitation (479 mm/yr) as well as lowest annual maximum rainfall (866 mm/yr) as given in Figure 3.2, the arid basins in the BSk class experience the most drastic reduction in unit peak discharge values with basin area compared to other classes. Basins in the West Coast of the U.S. falling in climate class Csb have the highest annual average rainfall (1537 mm/yr) among the six classes which results in higher values of unit peak discharge, and these basins show the slowest decrease in unit peak discharge values with basin size. Upon further analysis, a discontinuity in range of basin areas of in West Coast was

observed. On dividing the events based on a 250-km^2 threshold, the two areas were found to be geographically distinct where the larger basins were in Coastal California (Csb 1) and the smaller basins were mostly in the Sierra Nevada mountain range along with some isolated basins in Northern and Southern California (Csb 2). The basins in Csb 1 with an average size of 1700 km^2 are much larger than those in Csb 2 with an average basin size of 77 km^2. Computing the envelope curves for these two sub-regions, we get β values of -0.56 for Csb 1 and -0.31 for Csb 2. Interestingly, the unit peak discharges in basins with contributing areas less than 100 km^2 of BSk and Csb are similar. This means that flash flooding resulting from intense, convective cells in these arid basins results in similar peakflows as those experienced in the Pacific Northwest that receive much more rainfall on average. However, the unit peak discharges in BSk at larger scales (> 100 km^2) are much lower due to the influence of drier surface conditions, evaporation, and the smaller space-time scales of the causative precipitation systems. Basins in the eastern half of the CONUS exhibit similar values of β, but there is a general increase in α going from north to south. This means that the effective scales of the causative rainfall have similar characteristics in the east with increasing rainfall intensities as one moves south.

Table 3.3: Coefficients of envelope curves between unit peak discharge and flooding rise time versus basin area for the different climate classes.

	Unit Peak Discharge v/s Basin Area		Flooding Rise Time v/s Basin Area	
Climate Classes	α	β	α	β
CONUS	108.000	-0.470	0.001	0.434
Csb	9.864	-0.081	0.027	0.174
Csb 1	203.000	-0.560	0.201	0.042
Csb 2	18.000	-0.310	0.045	0.118
BSk	55.123	-0.501	0.038	0.085
Dfb (W)	1.351	-0.063	0.118	0.086
Dfb (E)	45.217	-0.356	0.008	0.413
Dfa	51.736	-0.399	0.007	0.307
Cfa	116.846	-0.478	0.002	0.493

In comparison to floods in Europe reported in Gaume et al. (2009) and Marchi et al. (2010), we find similarities in the following characteristics. First, the highest unit peak discharges tend to occur in basins near the ocean that also have mountainous terrain. These conditions are met both in the Cevennes-Vivarais region of the Mediterranean and also along the West Coast of the US. The seasonality of the events are different, however, with the Mediterranean ones generally occurring in autumn and the West Coast events occurring in the cool season. Similar to Europe, the unit peak discharges generally

decrease moving inland. The dependence of unit peak discharge on basin area is attributed to the spatial scales of the rainfall forcing that can be exacerbated by evaporation and dry surface conditions. The U.S. has some regions that are quite distinct from Europe. In particular, the BSk region of the desert Southwest is influenced by warm season, monsoon rainfall that exhibits very high unit peak discharges that depend strongly on basin area. Finally, the largest unit peak discharges in the U.S. occur in the Cfa region of the Southeast. Some basins are situated in the Appalachian mountains but this large class includes a wide variety of surface characteristics including plains. The causative rainfall in this most extreme class is also variable ranging from land-falling tropical storms from the Gulf of Mexico and Atlantic Ocean to localized, convective thunderstorms. The seasonality of Cfa events is quite different from those in Europe with a peak in the early spring months and a minimum during the late part of the warm season.

Beyond this first order characterization of trends with envelope curves, the relationship between unit peak discharge and area can be further quantified in terms of variability, which would be a prerequisite for any prediction in ungauged basins. More meaningful information can be extracted from quantile plots, as shown on Figure 3.11 with the 10^{th}, 25^{th}, 50^{th}, 75^{th} and 90^{th} quantile of unit peak discharge values conditioned on drainage area over all climate classes in the CONUS. The first order relationship is provided by the conditional median, the interquartile area provides an estimate of the uncertainty of the relationship, and the 10^{th} and 90^{th} deciles describe the extreme values. Ultimately, the derivation of a conditional probability density function (PDF) of unit peak discharge for any particular value of basin area can be the basis for the modeling of flood behavior at ungauged basins. These relationships can be especially helpful for modeling

in ungauged basins for which trustworthy flow measurements are not available, but drainage areas can be readily calculated from DEMs. Using these relationships, it will also be possible to ascribe an uncertainty band to anticipated unit peak discharge values of an ungauged basin based on upstream basin area and climate class. This information could potentially be useful to predict the behavior of the extremes, even in future climate scenarios, thus informing risk management practices. It will be further developed in a future study.

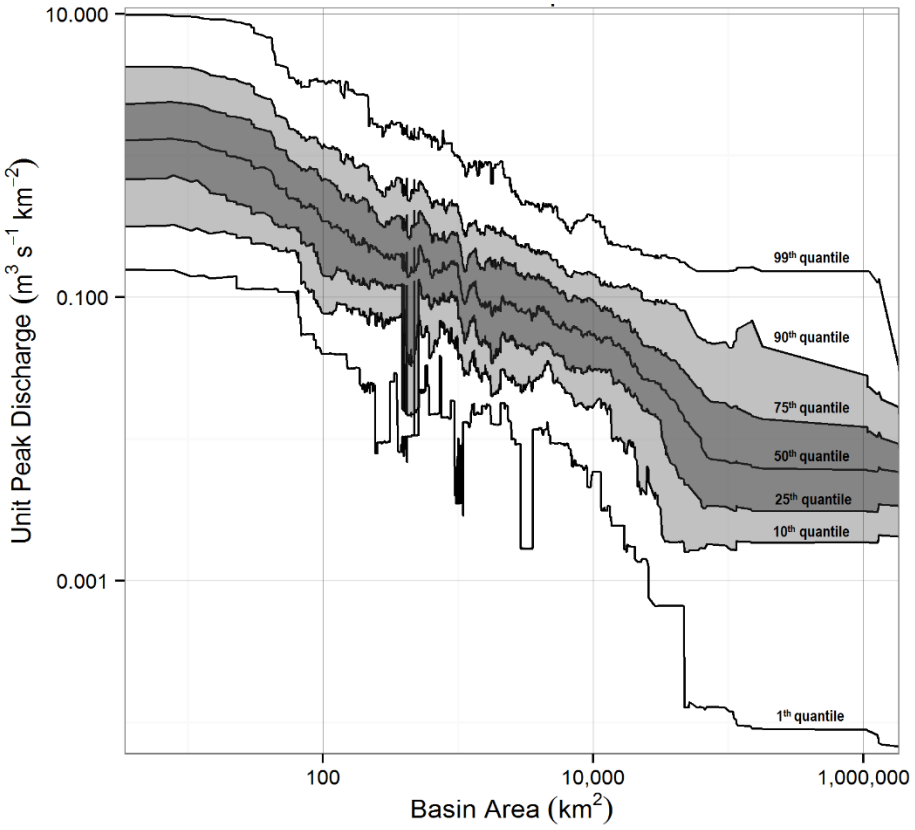

Figure 3.11: Quantiles (10-90th percentile) of unit peak discharges versus basin area for all 70,273 flooding events spanning 78 years over the CONUS.

3.5 Characterization of floods based on flooding rise time

The National Weather Service defines flash floods as those caused by heavy or excessive rainfall in a short period, generally less than 6 hours. The short lead time is an important aspect of flood risk management and associating flood response times with morphological and topographic parameters such as basin area is a critical element of our analysis. It is essential for flood forecasting and risk management. Similar studies such as Creutin et al. (2013) and Marchi et al. (2010) used the concept of lag-to-peak or lag time, which is the duration between the time of the centroid of the generating rainfall sequence and the time of the discharge peak. However, historical gridded rainfall information is not available for all events, given our lengthy dataset of river discharge. The present study utilizes a stream discharge response variable called flooding rise time, which is the difference between the time when flow exceeded the action stage flooding threshold (closely related to bank-full conditions) and the time at which the peakflow occurred. It can be regarded as a proxy for the lag time which is analyzed below as a function of basin area. There is a wide range of values of flooding rise time with an average value of 20.6 hours and a median of 10 hours. Figure 3.12 reports the relationship between flooding rise time and basin area for the six climate classes. The lower bounded curve enclosing all flooding rise times for each value of watershed area was derived, similar to what was derived for lag time in Marchi et al. (2010).

A power-law relationship (Eq. 3.2) was used to represent the lowest bound of flooding rise time T_r (h) versus basin area (km^2).

$$T_R = \alpha A^{\beta} \quad \textbf{(3.2)}$$

where β is a scaling coefficient. The values of α and β were determined by fitting a regression line between log (T_r) and log (A) values for each climate class.

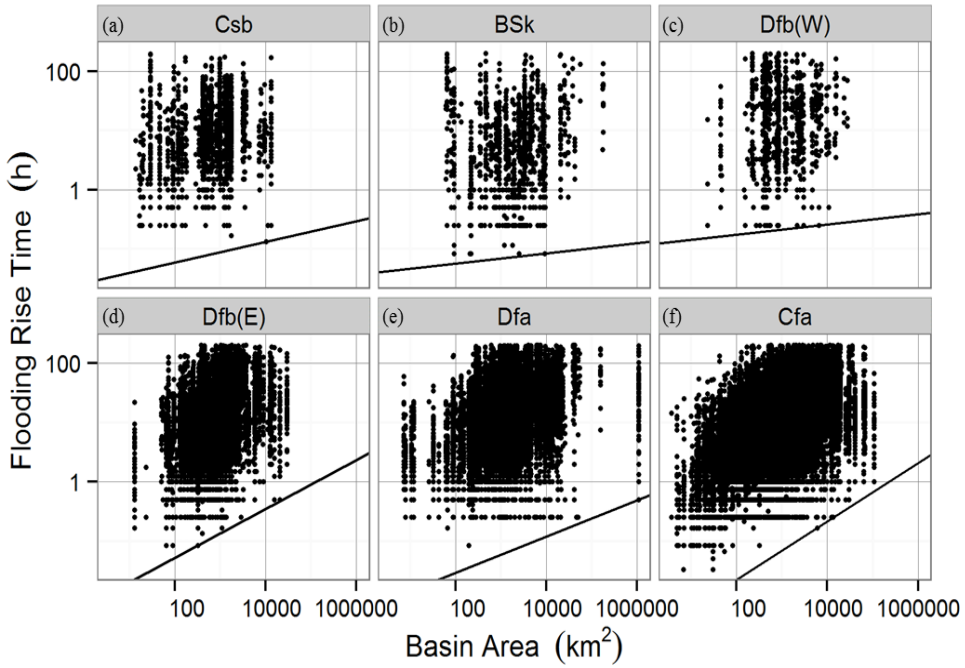

Figure 3.12: Flooding rise times versus basin area along with their envelope curves for the (a) warm temperate summer dry warm summer (Csb) (b) arid steppe cold arid (BSk), (c) snow fully humid warm summer west (Dfb(W)), (d) snow fully humid warm summer east (Dfb(E)), (e) snow fully humid hot summer, and (f) warm temperate fully humid extremely continental (Cfa) climate classes.

Table 3.3 gives the α and β values for the various climate classes as well as CONUS. Higher values of the β exponent indicate a faster increase of flooding rise time with basin area. The β value is the highest for Cfa (0.493) and lowest for Csb 1 (0.042). Figure 3.12 shows that the time at which floods reach their peak values after exceeding flood stage occurs more quickly at small basin scales, as one would expect. Examination of the scatter plots, envelope curves, and β values reveal a distinction between basins in the western

(Csb, Csb 1, Csb 2, BSk, and Dfb(W)) and eastern half of the U.S. (Dfb(E), Dfa, and Cfa). Basins in the eastern half of U.S. with β values of 0.042-0.174 exhibit faster increases in flooding rise times with basin area than in western half with β values of 0.307-0.493. The arid intermountain West BSk stations tend to have quicker flooding rise times for a given basin area. This is most likely a result of the causative precipitation from intense convective cells that yield quick-responding flash floods during the monsoon. Further, many of the BSk stations are situated in steep terrain which contributes to these fast responses. In contrast, the Dfb (W) stations are not significantly displaced geographically from the BSk stations, but they are at much higher altitude. The high data density at slow flooding rise times is interpreted to be a result of snowmelt influences on flood peaks. Snowmelt generally occurs more gradually as compared to stream response to intense convective cells and likely explains this discrepancy. This inference is supported by Figure 3.4, which shows that the Dfb (W) floods tend to occur earlier in the late spring months as compared to Bsk. The West Coast (Csb) consists of two distinct sub-regions based on basin area and events in Csb1, which is mostly the mountainous Sierra Nevada range, have very small exponent value of 0.042, which is a reflection of the small size of basins in this sub-region. While Csb2 has a slightly higher value of 0.174 as the basins are bigger than those in Csb1.

3.6 Conclusions

A systematic analysis of spatial and temporal characteristics of floods in the United States was performed based on USGS observations combined with NWS flood stage thresholds. Flood thresholds were studied to explore the influence of

geomorphology and climatology. Flooding variables investigated are the unit peak discharge and the flooding rise time. The results are summarized as follows:

- Regions such as the West Coast (Csb) and southeastern United States (Cfa), which experience the most extraordinary precipitation, have the highest unit peak discharges. The dependence of unit peak discharge on basin area is determined by the spatial scales of the causative rainfall as well as the atmospheric humidity and aridity of the basin's soils.
- Analysis of the monthly frequency of flood events shows great variations among the different climate classes. While the West Coast experiences the highest number of floods during the cool season, the peak flood season shifts towards the warmer months as one moves further inland to basins within the Intermountain West.
- Unit peak discharge and flooding rise time depend on catchment area for all the climate classes. In mountainous areas, especially in the Rocky Mountains, relief has a greater impact on both unit peak discharge and rise time than basin area.
- The envelope curves developed for unit peak discharges and basin area are consistent with the studies of floods in Europe and worldwide. In general, the magnitude of the unit peak discharges depends on the causative rainfall, which tends to be more intense in the Southeast U.S. and the West Coast. The unit peak discharges of floods in the monsoon-dominated desert Southwest are modulated by dry atmospheric and land surface conditions, which becomes more apparent with increasing basin scale. Finally, the seasonality of the U.S. floods is quite variable compared to Europe. This variability is attributed to the diversity of

flood-causing storms ranging from rainfall organized at synoptic scales but with orographic enhancements in the West Coast during the cool season to monsoon thunderstorms during the warm season in the desert Southwest to land-falling tropical storms and localized, intense thunderstorms in the Southeast.

- Flooding rise times are quickest in the desert Southwest (BSk) due to the coincidence of intense thunderstorms and steep terrain. Basins in the nearby Dfb (W) Intermountain West region are much slower to respond, presumably due to the influence of snowmelt.

This study proposes a general picture of the flood characteristics over the U.S. As a continuation, we will employ more sophisticated modeling techniques to analyze the impact of variables such as shape factor, curve number, event-scale precipitation variability indices, etc. on the flooding variables. The eventual goal is to use this dataset to make better prediction of floods in the vast number of ungauged basins.

Chapter 4. Mapping Flash Flood Severity in the United States

Floods have gained increasing global significance in the recent past due to their devastating nature and potential for causing significant economic and human losses. Several approaches have been attempted to identify and characterize flash floods, such as geomorphology-based (Costa, 1987a; Gaume et al., 2009; Marchi et al., 2010), frequency-based (Reed et al., 2007; Vogel et al., 2001), and flash flood guidance (Georgakakos 2006) among others. This work utilizes 70,273 flooding events from 1649 stations spanning 78 years to map flash flood severity over the CONUS using a novel approach that combines flooding data with geo-climatic information. A natural flood generally begins with snowmelt or intense rainfall. The characteristics of the underlying basin then dictate the speed at which water is conveyed through the basin and the magnitude of the maximum discharge. We concentrate on those floods with faster rise times and higher peak flows due to their devastating nature and lack of time to take mitigating actions.

The purposes of this study are to (i) propose a new variable called flashiness to describe the severity of flash flooding across the U.S., (ii) identify hotspots and evaluate their seasonal behavior, (iii) extend the flashiness analysis beyond gauged basins to a continuous grid over the CONUS based on spatially distributed variables describing basin topography, hydroclimatology, underlying geology, and geomorphology, and (iv) identify flash flood prone areas that are not highlighted in the observation database. It is suggested that this analysis can be used for regional and community planning and mitigation purposes. The paper is organized as follows. Section 4.1 proposes the flashiness variable, which is then evaluated spatially and seasonally in section 4.2. The

relationships of variables that describe flashiness are explored in section 4.3. Section 4.4 then regionalizes the flashiness variables to all grid points in the U.S., permitting an analysis of the potential for severe flash flooding in ungauged basins. This section evaluates the flashiness maps through comparisons to related databases. The summary and conclusions are provided in section 4.5.

4.1 A new metric for flash flood severity

A new variable called "Flashiness" is introduced in this paper as a measure of flood severity. It is defined as the difference between the peak discharge and action stage discharge normalized by the flooding rise time and basin area as given in Eq. (4.1) and visualized in Figure 4.1. The flashiness metric gives the rate of rise of the hydrograph during flooding conditions and thus captures both the magnitude and timing aspects with higher values corresponding to more severe floods. Let Φ be the flashiness, S the number of gauging stations, and N_i the number of events for a given gauge i, i=1,...,S. Thus, the flashiness for a given event j, j=1,...,N_i, at a given location i is,

$$\phi_{ij} = \frac{Q_{ij}^{(p)} - Q_{ij}^{(a)}}{A_i . T_{ij}} \tag{4.1}$$

where $Q^{(p)}$ denotes the peak discharge (m^3/s), $Q^{(a)}$ the action stage discharge (m^3/s), A is the basin area (m^2), and T the flooding rise time (s). An empirical cumulative distribution function (ecdf) function was then used to scale the values between 0 and 1 (Eq. 4.2). The standardized version of Φ is

$$\tilde{\phi}_{ij} = \frac{1}{\sum_{i=1}^{S} N_i} \sum_{i=1}^{S} \sum_{j=1}^{N_i} \mathbb{1}_{\{\varphi_{ij} \leq t\}} \tag{4.2}$$

where $\mathbb{1}_{\{E\}}$ is the indicator function yielding 1 if the condition E is true and 0 otherwise. The flashiness information is available at two levels: event and basin. Event-level flashiness given in Eq. (4.2) is computed for all 70,596 flooding events. The characteristic scaled flashiness variable for a given basin *i* is summarized by the median value computed from all flooding events N_i observed at that station.

$$\{\tilde{\phi}_i : \mathbb{P}[\tilde{\phi}_{ij} \leq \tilde{\phi}_i]\} = \frac{1}{2}, for\ j \in \{1, \dots, N_i\} \tag{4.3}$$

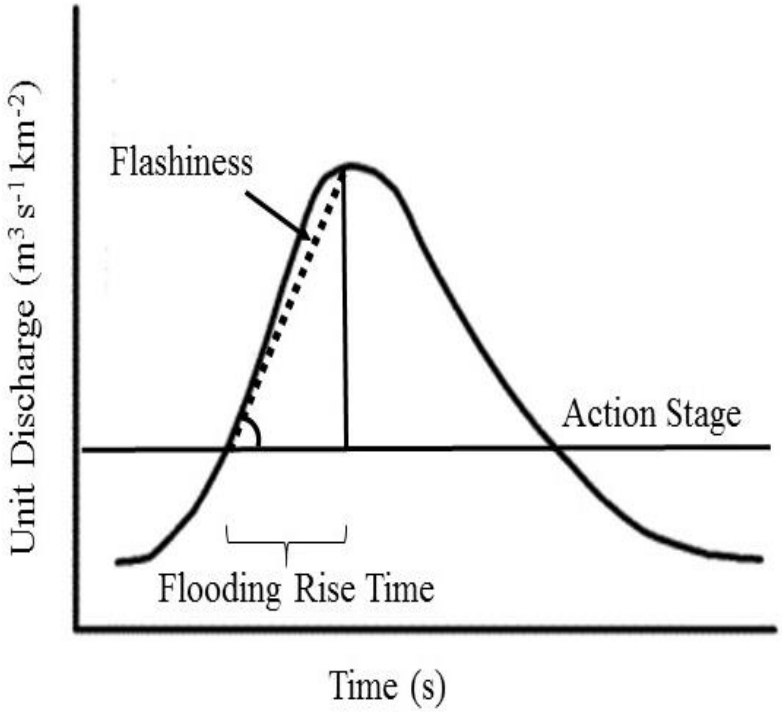

Figure 4.1: Graphical representation of the definition of event-level flashiness

Often, frequency-based approaches such as the discharge peak-over-threshold occurrences in Smith and Smith (2015) are used to quantify basin response as being

flashy or not. The frequency of peaks-over-threshold highlights small basins, typically in urban areas, that are situated in hydroclimatic regimes with persistent and heavy annual rainfall such as the south-central US, mid-Atlantic, and Pacific Northwest. However, this frequency-based definition of flashiness fails to identify those regions that may not flood on a frequent basis, but when they do flood, it can be catastrophic. Some dramatic examples include Big Thompson Canyon in July 1976, which killed 145 people, the great Colorado flood of September 2013 (Gochis et al., 2014), both of which are situated along the Front Range of the Rocky Mountains, and the Arizona-Utah border canyon flash flood that killed up to 20 people in September 2015. It is postulated that the paucity of these flash floods is even more devastating than they would be if they were persistent because the occupants are less prepared and often unaware of the danger. The flashiness variable used in this study differs from the frequency-based approaches in that it identifies those basins that have a high conditional probability of having a large-magnitude discharge in a short period of time. Flashiness is conditioned on the occurrence of heavy rainfall; thus, it represents the potential for a flashy response to input rainfall. The scaled flashiness variable for a given basin is the median value computed from all flooding events observed at that station.

Figure 4.2 shows the observed flashiness across the CONUS. At this point, the true spatial distribution of flashiness is limited by the density of the USGS stations with defined flooding thresholds. However, several regions emerge as being prone to flash flooding: 1) West Coast, 2) Arizona, 3) Front Range, 4) Flash Flood Alley, 5) Missouri Valley, and 6) Appalachians. High flashiness in the West Coast region is restricted to the coastal basins and the upslope region of the Sierras near Lake Tahoe. Arizona hosts a

large number of flashy basins that range from the low deserts in southeast Arizona all the way up to the Mogollon Rim and the higher terrain plateau in the northern part of the state. Several flashy basins are apparent just to the east of the Rocky Mountains in the Front Range region. In Texas, several flashy basins are clustered around San Antonio, Austin, and Waco along the Balcones escarpment in what is locally known as Flash Flood Alley (Safety, 2005). There is a secondary cluster closer to the Gulf Coast near Houston. Moving further to the northeast, flashiness increases and appears to maximize in the center of Missouri. The Appalachian Mountains in the eastern U.S. exhibit high values of flashiness from Georgia all the way to Maine.

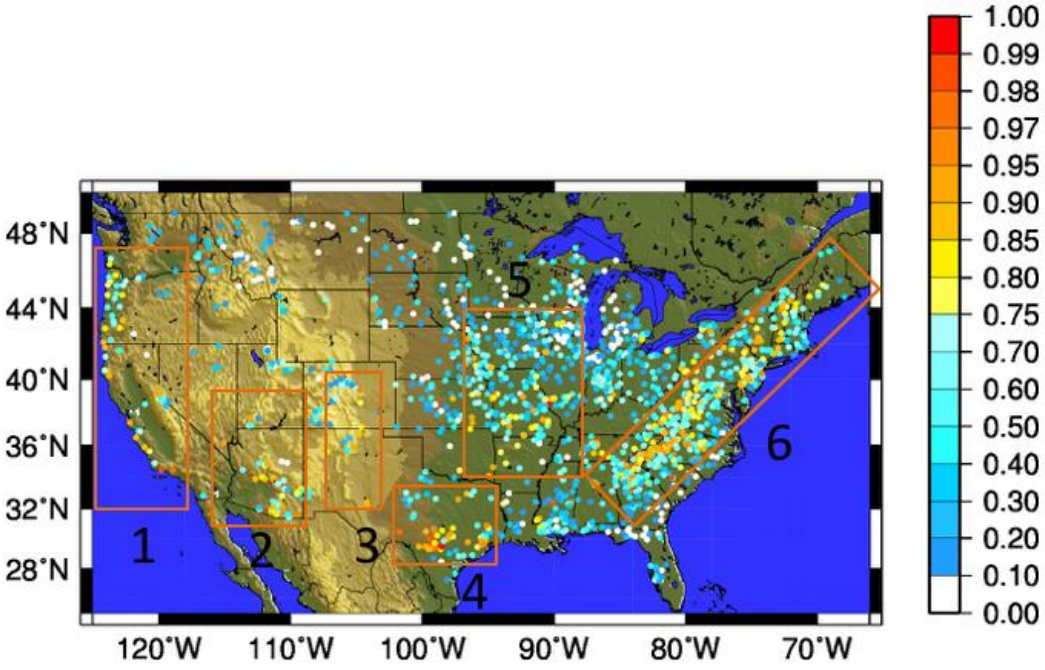

Figure 4.2: Distribution of observed flashiness (0-1) over CONUS. The bounding boxes highlight known flash flood hotspots: (1) West Coast, (2) Arizona, (3) Front Range, (4) Flash Flood Alley, (5) Missouri Valley, and (6) Appalachians.

Flashiness, a continuous variable, may prove to be useful in the definition of a flash flood. To date, many definitions exist and often refer to the stream response to causative

rainfall on the order of a few minutes to hours, typically less than six (US Department of Commerce, n.d.). In the U.S. NWS, the timescale of six hours is used to divide operational responsibility between local weather forecast offices that issue flash flood warnings and regional river forecast centers that issue river flood warnings. Definitions also refer to the basin catchment scale, which is linked to the basin's response time. The European flash flood database described in Gaume et al. (2009) uses a catchment area threshold of 500 km^2. Marchi et al. (2010) used the European flash flood database to examine the characteristics of extreme events. They refer to a maximum basin scale associated to flash flooding of 1000 km^2. A limitation of a basin scale threshold to define flash flooding is the *effective* basin area can be quite small for a localized convective storm near the basin outlet, which can produce a rapid response for a relatively large catchment.

In this study, we apply a subjective 75% quantile threshold on the flashiness variable (corresponding non-standardized flashiness index is 0.0279 $m^{-3}s^{-2}$) to separate basins that have "flashy" and "non-flashy" responses. This cutoff was later verified using actual storm data from the National Weather Service. It is interesting to note that there are no flashy gauged basins as per our definition in the state of Florida as well as a contiguous area stretching from the north central plains westward into the intermountain region of the Rockies. Some caution must be exercised at this point because flashiness can only be assessed in USGS-gauged basins that have flood stage definitions. The state of Wyoming, for example, only has four of these candidates.

4.2 Monthly variability of flash floods by region

A variety of meteorological processes such as convective thunderstorms, tropical cyclones, and orographically enhanced precipitation in complex terrain causes precipitation of varying characteristics and intensity at different times of the year to cause flash flooding (Saharia et al., 2016). A better understanding of the monthly variation of flash flooding is necessary for assessing vulnerabilities and developing flood mitigation strategies. The locations of the regional hotspots identified using basin-level flashiness as shown in Figure 4.2 can be attributed to specific conditions of topography and climate. Figure 4.3 shows the monthly frequency of flash floods using our 75^{th} quantile of flashiness definition for each of the regions.

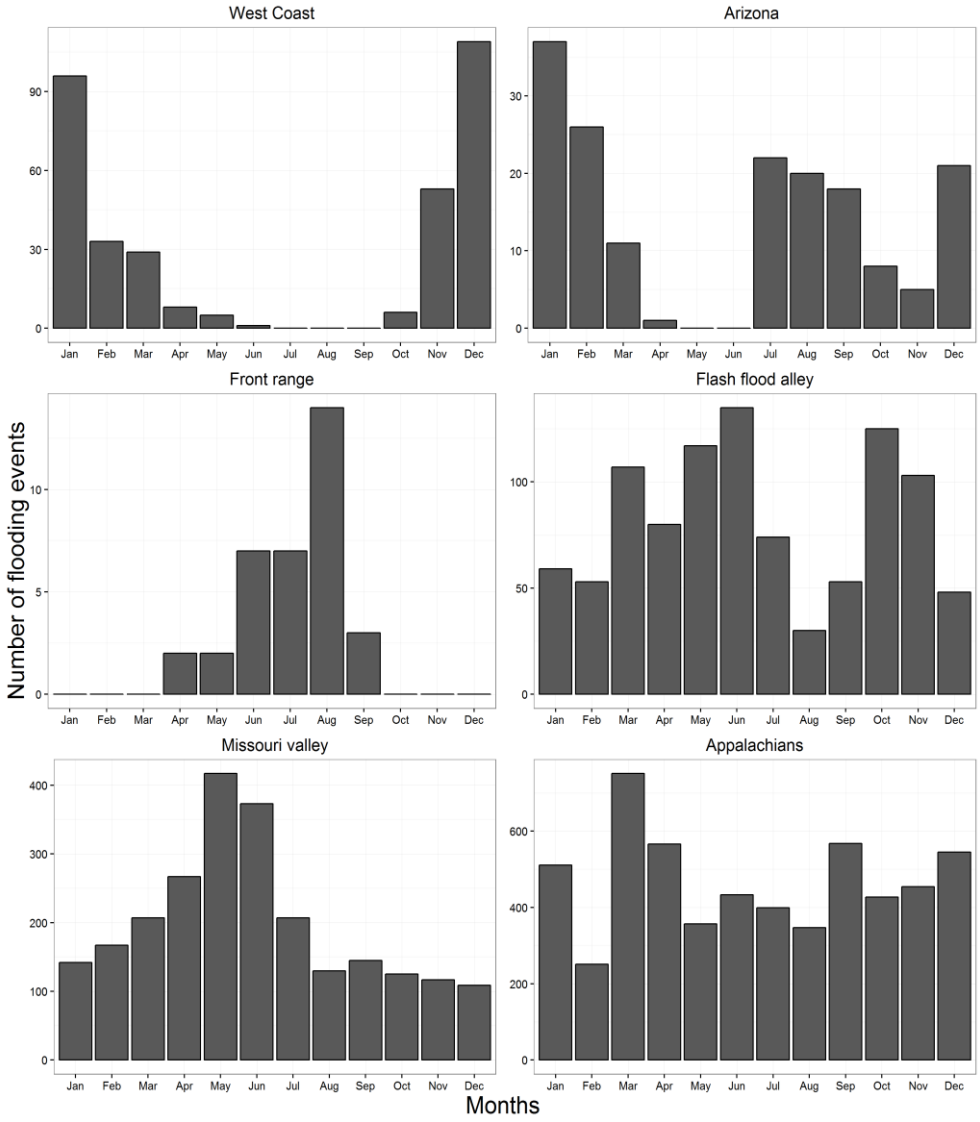

Figure 4.3: Region-wise monthly frequency of events for floods exceeding 75th quantile flashiness, i.e. Flash floods

Flash floods on the West Coast (Figure 4.3a) are clearly a cool season phenomenon that's related to the position of the jet stream, which directs extratropical cyclones with moisture from the Pacific Ocean into the mountains. Orographic enhancement by the topography increases precipitation amounts from the storms that can last several days. These flash flooding events begin to increase in November, reach their maximum frequency in December, and are essentially finished for the season by April. Very few

flash floods occur in this region during the warm season months of May through August. Despite its geographical proximity to the West Coast, the frequency of flash floods in Arizona has a bimodal character (Figure 4.3b). This reflects the same cool season phenomenon experienced on the West Coast, but a smaller, secondary peak occurs from July through September. This region is impacted by the North American monsoon that transports moisture from the Gulf of California northward into the semi-arid and hot deserts. The monsoon-forced flash floods do not occur as frequently as the larger scale storms in the cool season, but they can be particularly catastrophic with intense, localized rainfall. As we move further inland to the Front Range region, the frequency of flash floods increases at the beginning of the warm season and peaks during August (Figure 4.3c). These storms are also related to the larger scale circulation patterns with the North American monsoon. They differ from the Arizona storms in that their moisture fetch tends to be from the Gulf of Mexico up to the upslope region of the Front Range. The shift of the flood season from winter to summer as one moves inland was discussed by Michaud et al. (2001) and is further confirmed here.

The urban corridor spanning from Dallas to San Antonio in south-central Texas, also known as Flash Flood Alley, experiences some of the most dangerous floods in the country. This is caused by a combination of climatic and geomorphologic factors. Tropical air from Gulf of Mexico, tropical cyclones, extratropical cyclones, and orographic uplift over the Balcones Escarpment result in very high precipitation efficiencies in this area, which produces flash floods (Sharif et al., 2010). This area shows a unique variation in flash flooding with only a single month (August) where the frequencies are very close to zero (Figure 4.3d). The approximate bimodal distribution of

flash flood peaks in spring and autumn can be attributed to the synoptic scale patterns that drive the climatological rainfall peaks in these two seasons. Tropical cyclones also contribute in the latter, autumn peak.

Similar to Flash Flood Alley, the Missouri Valley region has a strong peak in flash flooding in the late spring months of May and June (Figure 4.3e). This region is also known to have a secondary rainfall peak in the autumn months like Flash Flood Alley. However, this secondary rainfall maximum is not reflected in the monthly frequency of flash flooding. There are additional factors probably related to the characteristics of the rainfall (i.e., intensity) that apparently is not sufficient to cause many flash floods during the autumn months. The frequency of flash flooding in the Appalachians differs from the other regions with a peak occurring in early spring (Figure 4.3f). Moisture laden air from both the Gulf of Mexico and Atlantic Ocean is forced up the slopes of the Appalachian Mountains and causes rapid formation of runoff. Villarini and Smith (2010) explores the role of tropical cyclones in controlling the upper tail of flood distributions in eastern United States. Villarini et al. (2014) indicated that North Atlantic tropical cyclones are responsible for large flooding over the eastern United States from Florida to Vermont and Maine along with a secondary swath of enhanced flooding in the central United States. Tropical cyclones are more common in autumn and we see a relative maximum in flash flooding in September. Sturdevant-Rees et al. (2001) also noted the large concentrations of unit peak discharges along the Atlantic seaboard and southeastern United States. The lack of flash floods in Florida and the coastal plains of the eastern seaboard states (see Figure 4.2) further highlights the importance of combination of moisture-rich air being forced upward by the terrain in causing flash floods. Konrad (2001) found that these

comparatively flat and permeable areas do not produce large unit discharges despite its proximity to moisture sources and being subject to frequent hurricanes.

4.3 Association of flashiness with basin geomorphology and climatology

Figure 4.4(a-d) shows the spatial distributions of potentially important geomorphologic and climatological characteristics that could influence a basin's response.

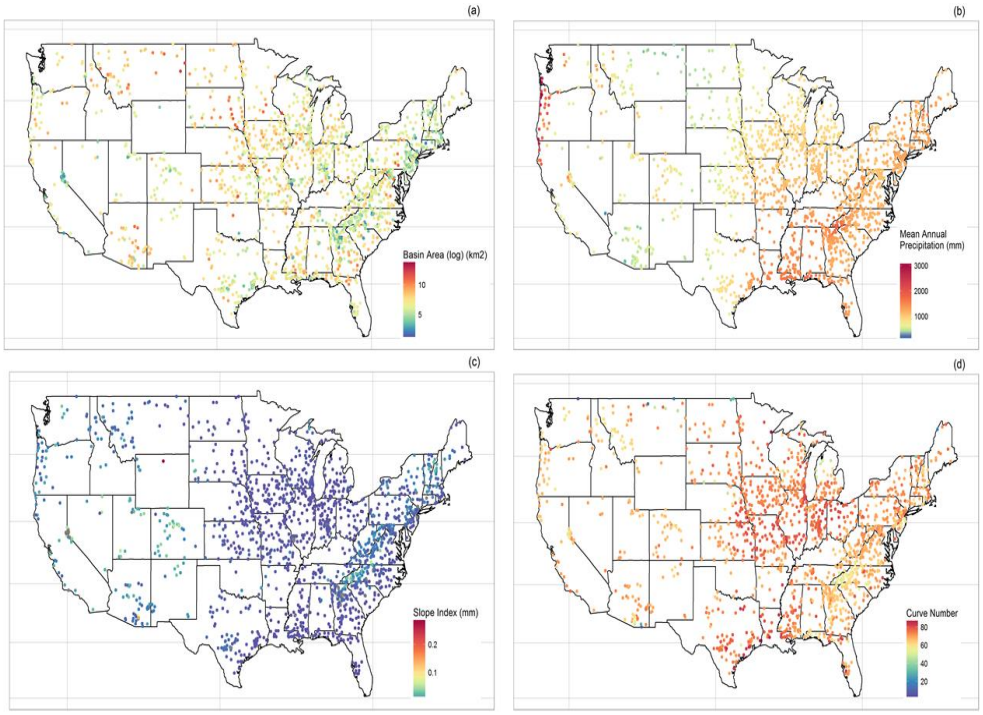

Figure 4.4: Distribution of (a) basin Area, (b) mean annual precipitation, (c) slope index, and (d) curve number over CONUS

In Figure 4.4(a), we see that there are concentrations of relatively small gauged catchments near Lake Tahoe on the California/Nevada border, in some Midwest cities such as St. Louis and Indianapolis, and along the Appalachians extending into the more

populated regions of the Northeast. In comparing Figure 4.4(a) to Figure 4.2, we see many of these basins are deemed as flashy, which is largely driven by the fact that they are small catchments. The climatological rainfall seems to influence flashiness in the Southeast near the Appalachians as well as in the Pacific Northwest, but there are some notable exceptions (Figure 4.4b). Arizona, for example, hosts a number of flashy basins, but it is much more arid than other flashy region. The Slope Index is the DEM-derived slope along the main channel length of a basin and is shown in Figure 4.4c (Costa 1987a). Higher slope indexes are associated to flashy responses in the Appalachians, the Sierra Nevadas of California, and some basins in Arizona. But, again, there are numerous flashy basins that are relatively flat. Finally, the curve number is an empirical parameter that characterizes the runoff response to excess rainfall. It includes many factors such as hydrologic soil group and land cover in order to approximate infiltration, vegetative interception, and soil moisture retention processes on runoff generation. Figure 4d indicates higher runoff potential and thus some correlation with flashiness in Missouri and Flash Flood Alley. In reality, the behavior of a basin's response to rainfall is a result of a complex interaction between a large number of geomorphologic and climatological factors.

The influence of each of the factors described above (i.e., basin area, mean annual precipitation, slope index and curve number) on flashiness is further analyzed using quantile plots in Figure 4.5(a-d). Information regarding the variability of the dependency can be extracted from the quantiles (1^{st}, 10^{th}, 25^{th}, 50^{th}, 75^{th}, 90^{th} and 99^{th}) of basin flashiness conditioned on the evaluated variables. The conditional median provides the first order information of the dependency, while the interquartile area estimates the

uncertainty in the relationship and the 10th and 90th quantiles describe the variation of extreme values of flashiness.

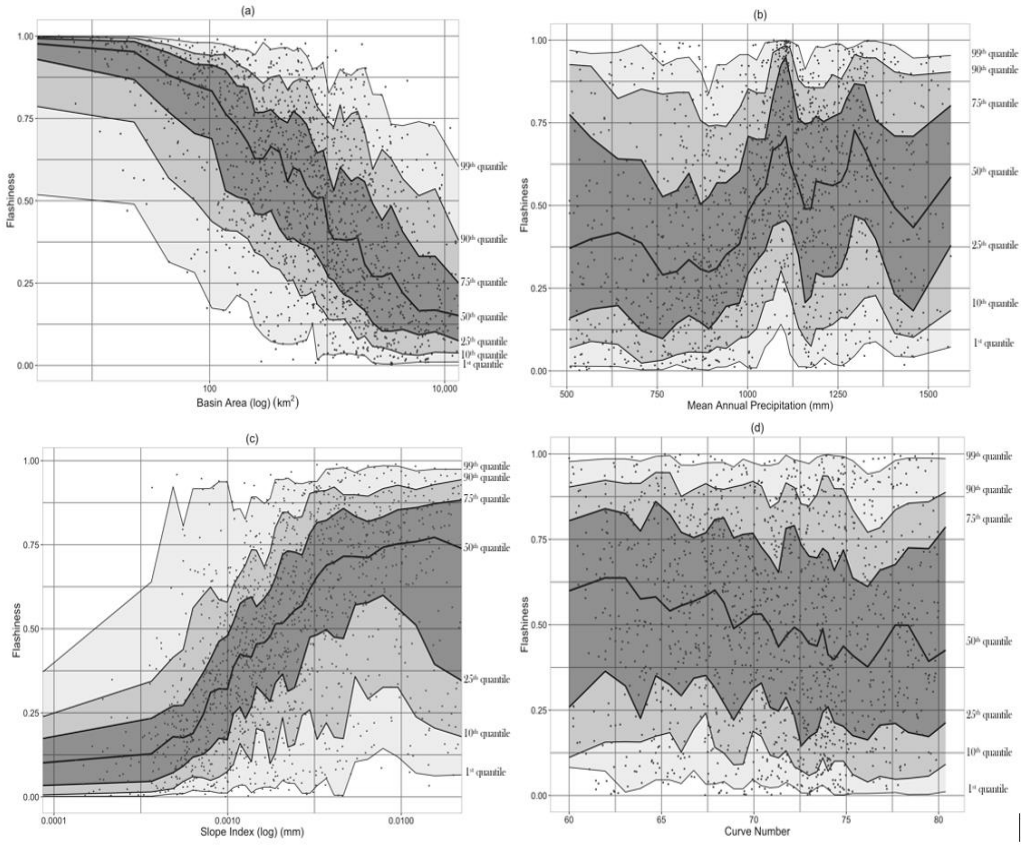

Figure 4.5: 1st-99th quantiles of flashiness versus (a) basin area, (b) mean annual precipitation (c) slope index, and (d) curve number. Dots represent the actual data.

Figure 4.5(a) confirms the anticipated result that flashiness is more common in small catchments. The basin area associated to a median flashiness value of 0.75 (i.e., our subjective threshold for flash flooding) is 145 km^2. Mean annual precipitation is likely to be correlated to the frequency of flooding. It is noted that the flashiness variable describes the potential for fast and extreme runoff generation conditioned on heavy rainfall. In other words, it is not dependent on the frequency of flash flooding. Figure 6(b) shows the quantiles of flashiness with mean annual precipitation across the study region of the

conterminous U.S. The correlation of flashiness to mean annual precipitation is much weaker than that with basin area, but there is a slight increase in flashiness with increasing climatological rainfall amounts.

Basins with steeper topography generally experience flashier floods with higher unit peak discharges and faster concentration times. The relationship between flashiness and slope index in Figure 4.5(c) shows how flashiness of a basin increases as slope index increases, i.e. basins become steeper. This variable influences flashiness approximately equal to the basin's catchment area. These two plots confirm that small catchments in steep terrain are generally expected to have a flashy response, according to our definition. Basin curve number is a widely-used empirical parameter in hydrology that is based on soil and ground cover of an area and is used to approximate direct runoff from a rainfall event. It has a range of 30 to 100, with higher numbers indicating higher runoff potential. Figure 4.5(d) shows how flashiness of a basin depends on curve number. When grouping all the basins together in a single plot, there is no apparent trend in the median flashiness with increasing curve number.

The quantile plots provide valuable information about the variation of flashiness with individual geomorphologic and climatological variables. But in reality, flood processes are influenced by complex interactions between a large number of variables. Thus, this technique is extended into a multi-dimensional approach where the collective influence of a large number of explanatory variables on basin median flashiness can be understood. This can be used to not only predict flashiness in ungauged locations, but detect which explanatory variables have greatest impact on floods in any particular location as well as ascribe a band of uncertainty to predicted flashiness.

4.4 Regionalization of flashiness

The dependence between the various explanatory variables and flashiness is examined using the generalized additive models for location, scale, and shape (GAMLSS Rigby and Stasinopoulos, 2005) technique. GAMLSS was proposed as an extension of the classical Generalized Additive Models (Hastie and Tibshirani, 1990), Generalized Linear Models (McCullagh et al., 1989) and Generalized Additive Mixed Models (Fahrmeir and Lang, 2001). The underlying assumption of all such models is that the variable we want to explain (flashiness, in this case) is a response variable whose distribution function varies according to the value assumed by the explanatory variables listed in Table 4.1. GAMLSS offers several advantages over the previously-mentioned approaches, such as (1) higher flexibility, as the response variable can follow a general distribution function and isn't restricted to follow a distribution from the exponential family; and (2) allows for modeling of not only the location parameter (related to the mean), but also scale and shape parameters (related to dispersion, skewness and kurtosis). Due to its flexibility, GAMLSS has been used to model various hydro-meteorological variables such as precipitation rates (Kirstetter et al., 2015), parameters of the kinematic wave routing parameters (Vergara et al., 2016), and flash flood severity (Saharia et al., 2016).

Table 4.1: Geomorphologic variables included in this study

Geomorphologic parameter	Details
Basin Area	Total upstream area that contributes runoff.

Shape Factor	A dimensionless number that is given by drainage area divided by square of the main channel length, $K = \frac{Drainage\ Area}{Channel\ length^2}$
River Length	Measured along a line centered from the basin outlet to the intersection of the extended main channel and the basin boundary.
Relief Ratio	Relief is the difference in elevation between the outlet and the highest point in the basin and relief ratio is relief divided by the basin length. It is a measure of the basin-wide river slope. Higher the relief ratio, higher is the runoff and shorter is the flooding rise time.
Slope Index	Slope between two points along the main channel upstream from the mouth of the basin at distances equal to 10 and 85% of the total main-channel length (Costa, 1987b).
Slope to Outlet	Local slope computed at a distance of 1 km over the basin outlet.
Basin Curve Number	Soil Conservation Service Curve Number (SCS-CN) is an empirical parameter that characterizes the runoff properties for a particular soil and ground cover (United States Soil Conservation Service, 1972)
Kfact	Relative index of susceptibility of bare, cultivated soil to particle detachment and transport by rainfall.
Rock Depth	Depth to bedrock at the outlet.

Soil Texture (b parameter)	It is a proxy for soil texture. Derived from the STATSGO database (Miller and White, 1998).

Two main assumptions are made: 1) the response variable flashiness is a random variable following a known parametric distribution with density *f* conditional on the parameters μ (mu) and σ (sigma), and 2) the observed α (alpha) values are mutually independent given the parameter vectors μ and σ. Each distribution parameter is modeled as a function of the explanatory variables using monotonic (linear/nonlinear or smooth) link functions. More details are provided by Rigby and Stasinopoulos (2001, 2005), Akantziliotou et al. (2002) and Stasinopoulos and Rigby (2007), particularly on the model fitting and selection. It involves identifying a suitable distribution of flashiness, the explanatory variables and the link functions. The estimation method is based on the maximum likelihood principle and the model selection is carried out by checking the significance of the fitting improvement in terms of information criteria such as the Akaike Information Criterion (AIC), the Schwarz Bayesian Criterion (SBC) and the generalized AIC (Stasinopoulos and Rigby, 2007). Forward, backward, and step-wise procedures were applied to select the meaningful explanatory variables, supervised by diagnostic plots to check the fitting performance as discussed in Stasinopoulos and Rigby (2007). The GAMLSS modeling has been performed using the gamlss package developed for the R language.

A number of conditional two-parameter density functions (lognormal, normal, reverse gumbel, logistic, gamma, etc.) were tested to fit the data and the goodness of fit on the dataset was checked with the AIC for each of the semi-parametric density fits as well as by checking the Gaussianity and independence of residuals. The beta distribution

was found to be the most appropriate to examine the dependence of flashiness on various geomorphological variables. The original beta distribution is given by:

$$f(y|\alpha,\beta) = \frac{1}{B(\alpha,\beta)} y^{\alpha-1}(1-y)^{\beta-1} \tag{4.3}$$

for y = (0, 1), α > 0 and β > 0. In the GAMLSS implementation, α = μ and β > σ. The function above was used to model the conditional flashiness distributions, where the location μ is linked to the expected flashiness value, and the scale σ is representative of prediction uncertainty. After selecting the distribution family, the structure of the model was refined through an iterative procedure by trying several combinations of explanatory variables. The trends for each parameter are fitted using penalized splines, which are more flexible than polynomials or fractional polynomials for modeling complex nonlinear relationships. The geophysical variables retained after analysis are presented in Table 4.2 along with their corresponding statistical significance values.

Table 4.2: Statistical significance of explanatory variables in GAMLSS model. Not retained or not considered variable are marked with '-'. Significance is expressed as p-value.

Variable	p-value
Basin Area (km^2)	<2.2e-16

Shape factor	<2.2e-16
River length (km)	-
Relief Ratio	7.828e-06
Slope Index	<2.2e-16
Slope to outlet	7.473e-11
Annual Precipitation (mm/yr)	8.785e-10
Mean Temperature (Celsius)	<2.2e-16
Curve Number	<2.2e-16
K Factor (Erodability)	-
Depth-to-Rock (cm)	8.796e-08
Soil Texture (*b* parameter)	2.487e-13

Consistency can be observed in the identification of the most important factors with what the spatial analysis suggested as discussed in section 4.4. Drainage area, slope index, the curve number and the hydro-climatic variables of mean annual precipitation and temperature are highlighted by their significance levels. This can be interpreted as a sign of robustness for the GAMLSS model. For validation, the dataset is separated into two randomly selected samples, and the model is trained over a 75% random sample of the observations while 25% is used for validation. The expected values yielded by the GAMLSS model are compared to the observations, and exhibit a correlation of 0.82 (67% of the variance of the data explained) and a negligible bias (0.4%). A similar result (correlation 0.83) is obtained with the validation dataset. The GAMLSS model is then re-calibrated using geomorphological and climatological variables for the entire USGS observation dataset. Figure 4.6 shows a scatter plot of predicted versus observed flashiness. The two populations exhibit a correlation of 0.83 and bias as small as 0.6%. The model displays significant skill to predict the flashiness values, thus we have confidence in the results as they are regionalized to ungauged basins.

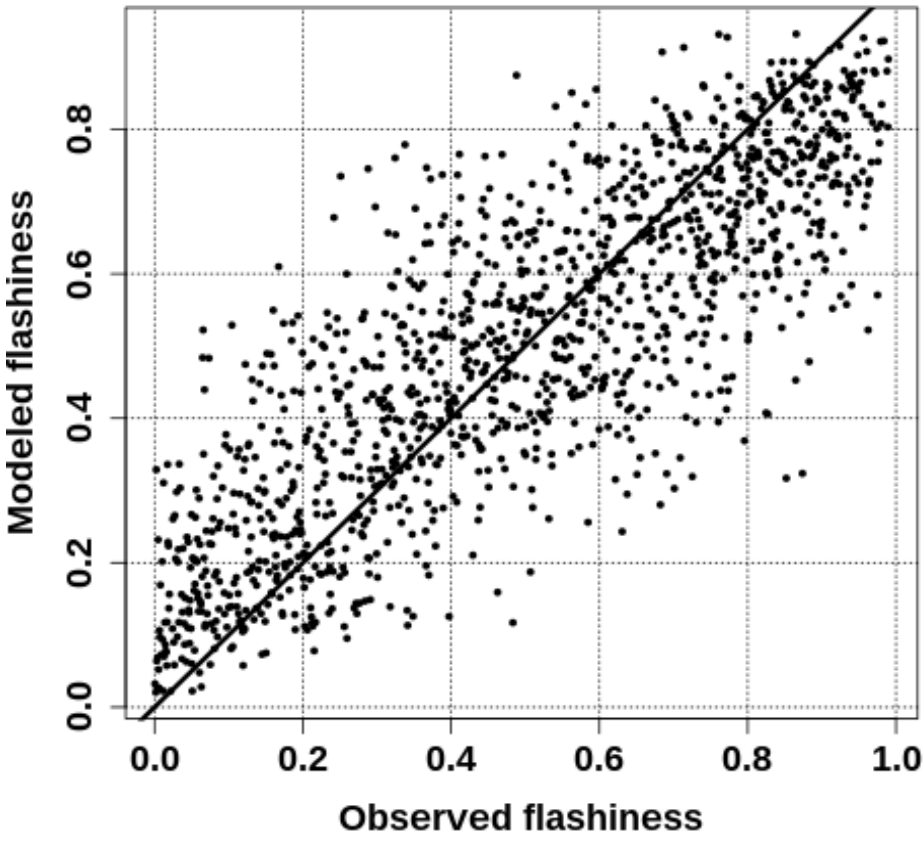

Figure 4.6: Scatter plot of predicted versus observed flashiness. Bias is 0.6% and correlation R=0.83.

The model is used to make predictions of flashiness at every grid point over the CONUS with a spatial resolution of 1 km. Figure 4.7(a) is the expected value of the predicted flashiness values between 0-1 and Figure 4.7(b) shows the standard deviation of predicted flashiness.

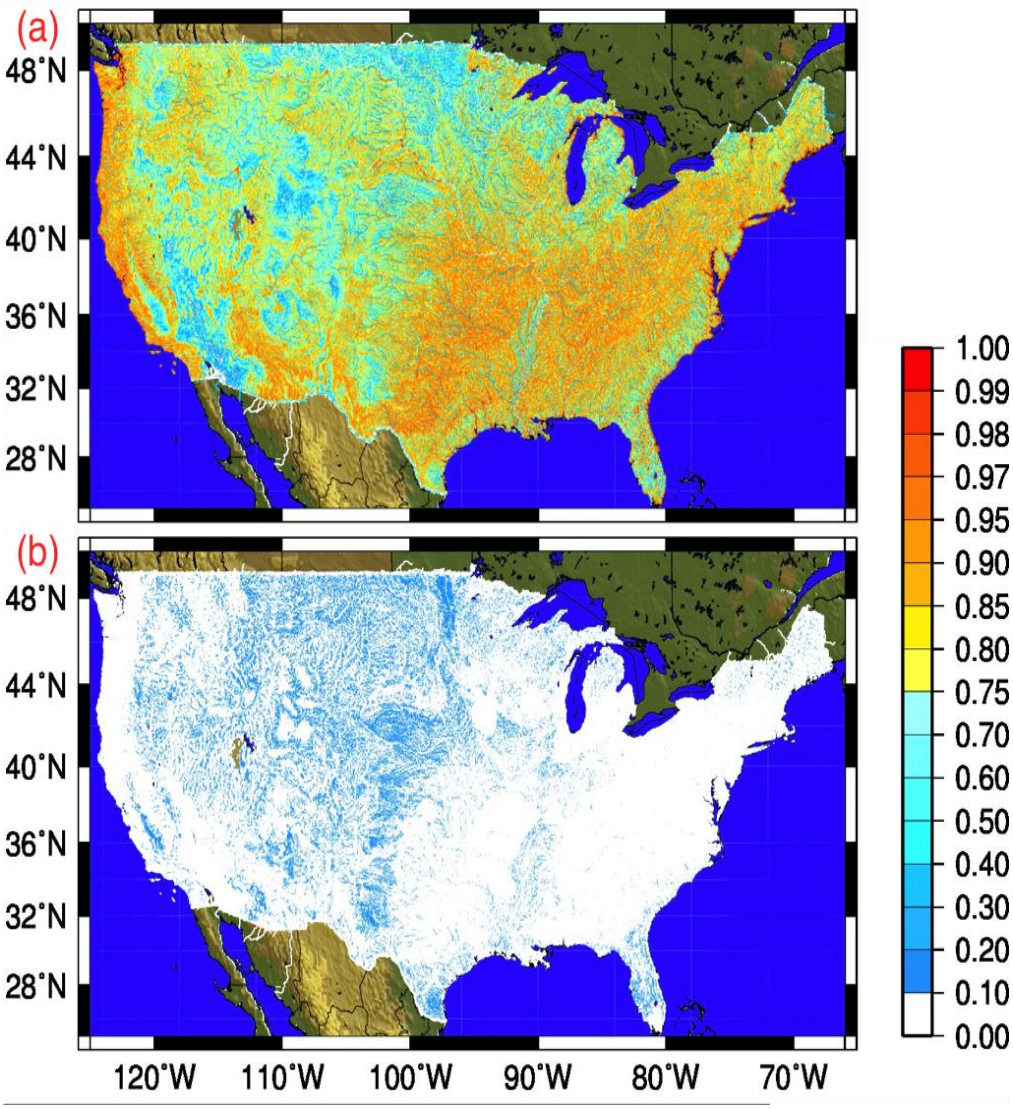

Figure 4.7: Distribution of (a) expectation and (b) standard deviation of predicted flashiness values over CONUS

The real value of this approach is the potential to identify flash flood hotspots in ungauged areas. In the predicted map, we see that the flashy basins on the West Coast are confined to the coastal areas and the upslope region of the inland, Sierra Nevada mountains extending northward. Arizona and the Front Range areas are also better highlighted in the predicted map. In Arizona, the flash flood prone basins are located where there are steep slopes extending from southeast Arizona and along the Mogollon

Rim that separates the lower deserts from the higher plateau region in the north part of the state. The predicted flashiness along the Front Range extends southward from north central Colorado to southeastern parts of the state and then continues southward along the front range of the Rockies in New Mexico. In the observation database, Flash Flood Alley is largely concentrated in central Texas hill country and Houston area. But the predicted map highlights a band of flood prone areas all the way from southwest Texas to Oklahoma, Arkansas, Kansas and Missouri. Villarini et al. (2014) also highlighted the same area on spatial interpolation of maximum and 90^{th} percentile of flood ratios associated with tropical cyclones. The predicted flashiness map highlights several regions that were not identified in the observed flashiness map in Figure 4.2. Several localized hotspots are revealed such as the western slopes of the Appalachians (Tennessee, Kentucky, West Virginia) and a contiguous area in the western Dakotas, eastern Montana, and northeastern Wyoming.

We introduce additional maps related to flash flooding to evaluate the predicted flashiness values in ungauged regions. Ashley and Ashley (2008) compiled a national database of all flood fatalities in the contiguous United States between 1959 and 2005 along with their coordinates, which is shown in Figure 4.8. This fatalities map shows good qualitative agreement with the predicted flashiness map of Figure 4.7(a).

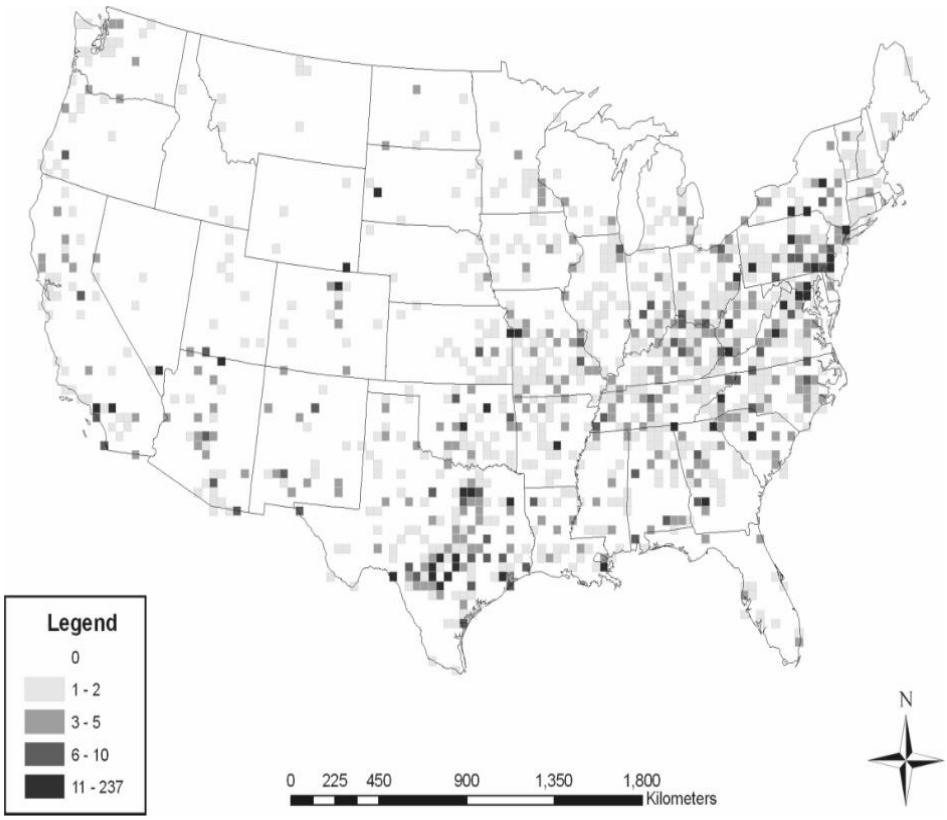

Figure 4.8: Map of flash flood fatalities from 1959 to 2005 (Source: Ashley and Ashley, 2008)

The entire West Coast and Sierra Nevada mountain range has been highlighted in the predicted flashiness map, but it doesn't experience as many flood fatalities as the rest of the country. This may be due to better infrastructure, lower population densities in mountain communities and better community resilience to disasters. The fatalities in the Arizona area are situated geographically similar to the predicted flashiness map. Fatalities in the Front Range tend to occur further north rather than in southeast Colorado and New Mexico, as highlighted in the flashiness map. Low population densities are likely the culprit for the mismatch. Flash Flood Alley and the populated Northeast are the most devastating regions in the country in terms of flood fatalities. Though our observation

database in Figure 4.2 identifies a localized region, the fatalities in Flash Flood Alley are spread over a wider area as shown in Figure 4.7. The extension of Flash Flood Alley by the predicted flashiness map up to the north and east correlates better with the spatial distribution of flood fatalities, attesting to the predictive power of the model in ungauged locations. The Missouri Valley with high flashiness values also experiences large numbers of flood fatalities. The predicted flashiness map also points to the flood prone nature of the entire Appalachians, which is observed in the number of casualties in the whole belt. It must be kept in mind that this is a very indirect way of validating our model and flood fatalities are highly correlated with population density, infrastructure, and societal vulnerability.

The flashiness predictions are also compared to the Storm Data database of flooding and flash flooding reports from 2007-2013. This dataset is included in the flash flood observation database described in Gourley et al. (2013). NWS forecasters report locations of flooding impacts using bounding polygons defined by as many as eight vertices. Currently, there are around 35,000 events in the database with an ID mentioning whether the event was a flood or a flash flood according the NWS definitions. Using GIS software, the mean flashiness in all such polygons were calculated and beta distributions were fitted to the populations of flashiness values in the flood and flash flood categories. Figure 4.9(a) gives the fitted Probability Distribution Functions (PDFs) of mean flashiness for floods and flash floods according to actual NWS reports. The PDF shows a clear distinction between NWS-reported floods and flash floods between flashiness values of 0.75, which is the value we used initially to define flash flooding. The empirical and fitted cumulative distributions are shown in Figure 4.9(b). A Kolmogorov-Smirnov

test performed on the two distributions yielded a p-value of less than 2.2e-16 and D-value of 0.22. Here, D is the maximum absolute difference between the two Cumulative Distribution Functions (CDFs) which is maximum near the mean flashiness value of 0.75. The p-value being small indicates that the distributions are significantly different, accrediting the usefulness of flashiness to characterize the flash flood severity.

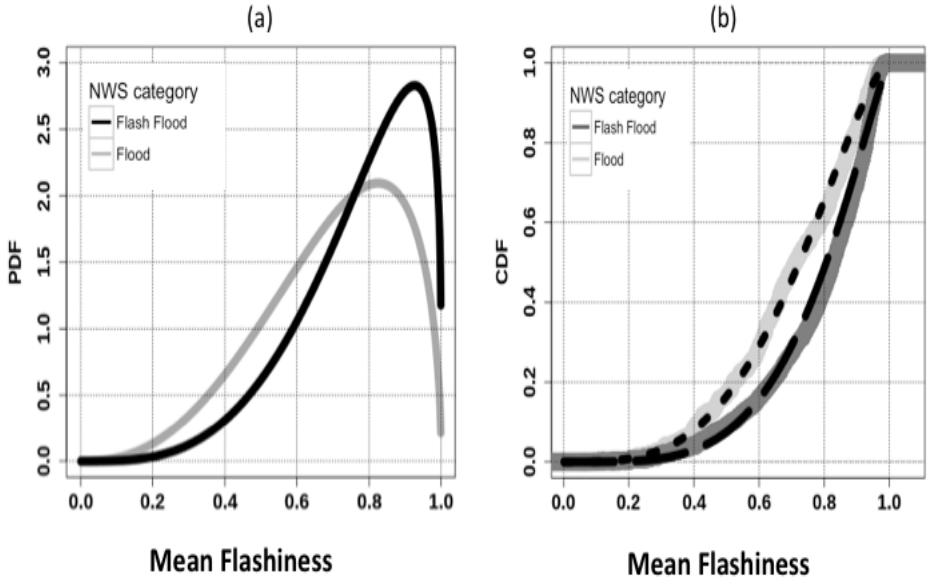

Figure 4.9: (a) PDF of fitted Beta models and (b) CDF of empirical mean flashiness by NWS categories of floods and flash floods. The fitted beta distribution models for floods (dotted line) and flash floods (dashed lines) are superimposed in (b).

4.5 Conclusions

A long flood database spanning 78 years over the continental U.S. was used to explore the dependency of flood severity on geomorphological variables and climatology. A new variable called flashiness was introduced in this paper as a measure of flood severity. Flashiness is not dependent on the annual likelihood of flash flooding, but rather gives the potential of a basin to produce a rapid and significant response to

heavy rainfall. Complex relationships between observed flashiness and a large number of geomorphologic and climatological variables were modeled using GAMLSS to predict flashiness at every location. The findings are summarized below:

- The spatial patterns of flood severity correlate well with regions that have been previously reported. Six flash flood hotspots were identified across the country: West Coast, Arizona, Front Range, Flash Flood Alley, Missouri Valley, and Appalachians.
- A monthly analysis of flash flooding in each of the hotspots revealed very different behavior in each region. The West Coast had the maximum frequency in flash flooding during the cool season while the interior regions were more commonly impacted during the warm season. Bimodal distributions in the monthly frequency of flash flooding were noted in both Arizona and in Flash Flood Alley in Texas.
- Several variables were used to model flashiness and the most influential ones were the basin area and the basin's slope index. Small, steep basins had the flashiest responses.
- The predicted flashiness values were trained on observed values with a correlation of 0.82; the same correlation was met with stations that were independent from the training data set.
- Additional spatial datasets related to flash flooding including fatalities and NWS reports showed good correspondence with the predicted flashiness map. The flashiness variable was shown to discriminate between NWS reports of flood and flash floods.

- Though the observation database showed Flash Flood Alley as being largely concentrated in central Texas hill country and Houston area, the model-predicted flashiness extends this flash flood prone area from southwest Texas through the Hill Country and continuing northeastward into adjoining states.
- Localized hotspots were identified within the broad flash flood prone areas as well as some of those outside of the originally defined regions including the western slopes of the Appalachians in Tennessee, Kentucky, and West Virginia.

This study proposes an overview of how flood severity varies across the United States using a model that can highlight flash flood-prone areas in ungauged locations. As an extension of this study, in the next chapter, the existing database will be augmented with event-level precipitation variability indices for improved modeling of flood severity.

Chapter 5. Impact of Rainfall Spatial Variability on Flash Flood Severity

In the previous chapters, flooding was characterized at climatological scale using a large number of geo-climatic variables. But to characterize flooding response at the event-scale, it is necessary to incorporate information on causative rainfall, especially the spatial organization of rainfall within a basin. In the absence of consensus on how spatial variability of rainfall impacts basin response, this study uses a high-resolution rainfall and flooding event dataset spanning 10 years to overcome a major limitation of existing studies basing their conclusions on limited case studies or simulations. The objective behind employing an observation-based big data approach is to develop a robust understanding of how rainfall spatial variability impacts flash flood severity and quantify its contribution relative to basin physiography.

Significant advances in radar measurement of rainfall has led to an unprecedented ability to investigate these relationships through an ensemble of approaches. Some studies have sought to compare performance of hydrologic models forced by rainfall estimated by gauge network, weather radar, or a blend of both (Cole and Moore, 2008, 2009; He et al., 2013; Jin-Hyeog Park et al., 2009; Philip B. Bedient et al., 2000; Smith et al., 2007). Other studies have investigated the impact of rainfall spatial variability on runoff modeling by comparing observed to modeled hydrographs forced by rainfall at a range of spatial scales from distributed to catchment averaged. Studies have found that the averaging effects of routing removed the majority of the impact of spatially variable rainfall at catchment scales such as 150 km^2 (Adams et al., 2012) and 384 km^2(Christian

Bernhofer et al., 2013). Adams et al. (2012)performed simulations using synthetic rainfall events typical of temperate climates in Melbourne, Australia while Christian Bernhofer et al. (2013) analyzed a single flood event in Eastern Germany, which limited the ability to extend the conclusions to a wider set of flooding scenarios. Contrasting results were reported by Zoccatelli et al. (2010) who found that not accounting for rainfall spatial variability reduced modeling efficiency in 30% of the cases while studying flash flood events in Romania.

Several researchers also found that accounting for spatial variability in rainfall could play a major role in flood modeling even for small basins (Faurès et al., 1995; Michaelides and Wainwright, 2002; Michaud and Sorooshian, 1994; Schuurmans and Bierkens, 2007). Other studies have found that the impact of rainfall spatial variability on modeled hydrographs depends not just on basin scale (Gabellani et al., 2007; Wood et al., 1988), but also on precipitation type (stratiform or convective) (Bell and Moore, 2000), soil properties (Anquetin et al., 2010; Sangati et al., 2009), and predominant hydrologic partitioning processes (Anquetin et al., 2010; Brath and Montanari, 2003; Gabellani et al., 2007). The Distributed Model Inter-comparison Project (DMIP) opined that distributed hydrologic modeling may not always yield better outlet simulations compared to lumped simulations (Reed et al., 2004), which may be due to non-linearities and/or many computational elements of distributed hydrologic models magnifying rather than smoothing errors in high-resolution radar rainfall data (Smith et al., 2004). Thus, past studies seeking to establish through simulations the importance of accounting for rainfall spatial variability on basin response may have unduly stressed on model sensitivity instead of observed sensitivity (Morin et al., 2001; Obled et al., 1994; Smith

et al., 2004; Winchell et al., 1998).An analysis of the impact of rainfall spatial variability on basin response using a database of observed events, as in this study, will remove some of the limitations of distributed hydrologic models compounding errors in data. Moreover, Smith et al. (2004) considered it important to not just determine where great spatial variability of rainfall exists but also to identify basins where the variability of rainfall overcomes filtering effects of a physical basin to significantly impact basin response. Overall, the determination of the most relevant rainfall spatial organization factors for flash floods in this study can be identified as an important exercise that will provide diagnostic capability to identify basins in which distributed hydrologic modeling is expected to be most effective.

The literature review of this topic reveals that our understanding of the nature of the impact of rainfall spatial variability on flooding under a wide variety of rainfall, physiographic, and antecedent conditions remains limited. Contrasting results have been reported and the extent of this influence is not fully understood. Most of these studies are performed on a case study basis covering a few events which severely limits our ability to make conclusions applicable to a wide variety of scenarios. A few studies have attempted to address this shortcoming. For example, Emmanuel et al. (2015) adopted a simulation chain that combines a stream network model, a rainfall simulator, and a distributed hydrologic model to disentangle the relationship between rainfall spatial variability and runoff. By synthetically generating 9,900 simulated hydrologic events for hundreds of varying catchment sizes and rainfall types, they found that the organization of rainfall has an important influence on the catchment response. The study tested the

spatial rainfall variability indices described in Zoccatelli et al. (2010) and proposed two new indices that summarizes the spatial organization of rainfall. However, using distributed hydrologic models to study the importance of rainfall spatial variability may introduce more uncertainty in the results due to errors in data, model structure, and model parameters as the experiments implicitly stress on model sensitivity rather than basin sensitivity (Smith et al., 2004). The key difficulty in evaluating the influence of rainfall spatial variability on basin responses remains the lack of a large real-world dataset of flood events and corresponding radar rainfall that captures a great diversity of situations and geographies. This study seeks to fill an important gap in our existing body of knowledge by investigating the impact of rainfall spatial variability by relying on observations instead.

Furthermore, existing studies (Douinot et al., 2016; Emmanuel et al., 2015; Zoccatelli et al., 2010) have reported the average relationships between rainfall variability indices and various aspects of flooding such as timing and level difference. But the complexity of the underlying processes necessitates investigating the variation in these relationships as well. Moreover, quantifying the impact of rainfall spatial variability on flash flood response is difficult due to limitations in monitoring rain and streamflow at those space and time scales using conventional instruments and methodologies (Creutin et al., 2013; Marchi et al., 2009). Investigation of flash floods have mostly been necessity event-based such as by using post-event surveys (Borga et al., 2007; Zoccatelli et al., 2010).

In this paper, we seek to understand, through a carefully-designed large-sample study based on observations of rainfall and flooding, how rainfall spatial variability influences

the hydrograph in basins of widely varying characteristics. The flooding data is derived from the publicly available Unified Flash Flood Database described in Gourley et al.(2013), which collates flooding events from three sources: USGS streamflow measurements, storm reports collected by the National Weather Service (NWS), and public survey responses during the SHAVE experiment (Gourley et al., 2010). This unique dataset has been subjected to extensive post-processing to harmonize data from a variety of sources over a long period. Quality-controlled radar rainfall data of high spatial and temporal resolution are used to compute the rainfall variability indices described in Zoccatelli et al. (2011)and Emmanuel et al. (2015). They are combined with large number of geomorphological attributes to develop an observation database suitable for clarifying the dependence between rainfall spatial organization, basin morphology, and catchment response. The goal is to quantify the relationship between rainfall spatial variability and flood response, and its contribution to flooding relative to basin morphology.

As severe floods cause great damage to life and property, we seek to investigate the severity of a flood in this paper, a hitherto unexplored aspect of the hydrograph in the context of rainfall spatial variability. To this end, a variable describing flash flood severity or "Flashiness", proposed in Saharia et al. (2016), is utilized in this study. It encompasses both the timing and magnitude aspect of a flood and represents the potential of a basin to produce severe floods. This study, to the best of our knowledge, explores for the first time, not only first-order dependencies but also the variability in these relationships. Finally, the relative impact of various rainfall and physiographic properties

on flooding are quantified using a multi-dimensional modeling framework and the impact of the individual attributes are disaggregated.

This provides an unprecedented opportunity to analyze the impact of event-level rainfall spatial variability on actual flooding using a big data approach. The purposes of this analysis are to (i) characterize flash flood severity (referred to as flashiness) using rainfall spatial variability and geomorphological parameters, (ii) quantify the relative impact of rainfall spatial variability and basin morphology on flashiness, and (iii) identify which variables are most important to explain flashiness. The chapter is organized as follows. Sections 5.1 describes the rainfall spatial variability indices and an overview of how the archive was developed. Section 5.2 presents a case study explaining these indices for a flooding event. Sections 5.3 and 5.4 characterizes flash flood severity based on rainfall spatial variability indices and large number of physiographic variables. Finally, Section 5.5 provides a summary of findings and concluding remarks.

5.1 Rainfall spatial variability indices

The indices found in Zoccatelli et al. (2010, 2011) and Emmanuel et al. (2015) are used in this study to quantify the impact of rainfall spatial variability on flooding. They provide metrics for space-time precipitation organization as a function of the flow distance i.e. distance measured from any point in the basin to the outlet along the flow path. The analytical framework in Zoccatelli et al. (2011) describes two indices by taking ratios of spatial moments of catchment rainfall [$p_0(t)$, $p_1(t)$, $p_2(t)$] and the moments of flow distance (g_1 and g_2). The n-th spatial moment of catchment rainfall is defined as:

$$p_n = \frac{1}{A}\int_A p(x,y,t)\, d(x,y)^n dA \tag{5.1}$$

Where A is the catchment area. The zeroth order spatial moment of catchment rainfall, $p_0(t)$, is the average catchment rainfall rate at time t. Analogously, the n^{th} moment of flow distance is given by:

$$g_n = \frac{1}{A}\int_A d(x,y)^n\, dA \tag{5.2}$$

Note that the first moment of flow distance is the catchment averaged flow distance. The non-dimensional (scaled) spatial moments of catchment rainfall correspond to spatial parameters characterizing rainfall and can be obtained by taking ratios of the moments of catchment rainfall and flow distance. The first two orders, δ_1 and δ_2, are as follows:

$$\delta_1(t) = \frac{p_1(t)}{p_0(t) g_1} \tag{5.3}$$

$$\delta_2(t) = \frac{1}{g_2 - g_1^2}\left\{\frac{p_2(t)}{p_o(t)} - \left[\frac{p_1(t)}{p_o(t)}\right]^2\right\} \tag{5.4}$$

According to the authors, δ_1 is the distance of the catchment rainfall centroid from catchment centroid. Values of δ_1 close to 1 reflect a rainfall distribution either concentrated close to the catchment centroid position or spatially homogeneous. While values less than one indicate a rainfall distribution near the basin outlet, and values greater than one indicate rainfall distribution towards the catchment headwaters.

The second moment (δ_2) describes the dispersion of the rainfall-weighted flow distances with respect to the dispersion of the flow distances. Values of δ_2 close to 1 represent a uniform-like rainfall distribution. Values of $\delta_2<1$ indicate that the rainfall is concentrated over a small region of the catchment with a spatially unimodal storm cell along the flow distance, while values greater than 1 indicate a multimodal rainfall distribution, which is generally rare.

The spatial moments described in equations (5.3) and (5.4) describe the instantaneous rainfall spatial organization at a time t. To describe spatial organization of rainfall accumulated during a particular time-period, say a storm event, these indices are integrated over time, in which case they are denoted as Δ_1 and Δ_2 and can be analyzed the same way as δ_1 and δ_2 respectively.

Emmanuel et al. (2015) proposed two additional indices based on comparing width function and the rainfall width function. The width function (w_x) is defined as the portion of the basin area at a flow distance x from the outlet (Rinaldo et al., 1993), which is constant for a given basin and represents the hydrologic response of a catchment to spatially uniform rainfall. They proposed an analogously defined rainfall width function (w_p) as the proportion of rainfall on the catchment falling at a flow distance x from the outlet, which combines rainfall spatial organization and the hydrologic response. The influence of rainfall spatial organization on the hydrologic response can be quantified by comparing the cumulative distribution functions of these two version of the width function. The index of Vertical Gap (VG) is defined as the absolute value of the maximum vertical difference between the two width functions while the Horizontal Gap (HG) is corresponding horizontal difference between the two width functions divided by

the longest flow path of the catchment. VG values close to zero indicates a rainfall distribution with weak spatial variability while higher VG values correspond to greater concentration of rainfall over a smaller portion of the catchment. Similarly, HG values close to zero represent a rainfall distribution either concentrated closer to the catchment centroid or spatially uniform. Greater than zero HG value (or lesser than zero) indicates a rainfall distributed upstream (or downstream) of the basin.

A large events database collating flooding events from diverse geographies and seasons allows, for the first time, the testing of the efficacy of these variability indices in capturing the influence of rainfall spatial variability on catchment response. The moments of precipitation (zeroth, first, and second), moments of flow distance (first and second), and the four spatial variability indices (Δ_1, Δ_2, HG, and VG) are computed for each of the 9,392 flooding events in the Unified Flash Flood Database between 2002 and 2011. The database was subjected to extensive post-processing based on radar beam height and snow percent of total precipitation in a basin to reduce input uncertainties in modeling results. Firstly, all events that fall in basins with mean radar beam height of greater than 2 kilometers above the ground level were discarded. This was to ensure that we only include events for which we have high-quality radar rainfall data from MRMS. Similarly, all events for basins that get less than 15% of their annual precipitation from snowpack were included. For basins that get greater than 15% of its annual precipitation from snowpack, only events in summer months (May-Oct) were included. Table 5.1 shows how the number of flooding events changed at different stages of post processing. Finally, a dataset of 9,392 flooding events enhanced with corresponding geomorphologic and climatologic variables was finalized for modeling.

Table 5.1: Quality control of the dataset based on radar beam height and percent snow

Quality control criteria	Number of flooding events
Initial dataset (2002-2011)	15,393
Radar beam height	12,595
Snow percent	9,392

The indices are computed on the rainfall accumulated before the peak of the hydrograph (T_q), i.e. [T_q – X*T_r], with T_r being the catchment response time and X denoting the multiplier for the accumulation period. A value of X=1.5 has been adopted in this study as it was found to be the most suitable by Emmanuel et al. (2015) after a duration sensitivity analysis on a simulated database. Moreover, they found that these indices are not very sensitive to the accumulation period and very similar results were obtained for a wide interval period. In this study, the catchment response time is derived from the conceptual definition of the time interval between the centroid of effective rainfall and peak of the hydrograph.

5.2 Case study

A flooding event occurring on 27th August 2006, in the Blue river at Blue Ridge Blvd Ext in Missouri (USGS ID: 6893150) is presented to illustrate the conceptualization of various rainfall spatial moments. Important flooding information such as start of the flooding event (t1, when streamflow crosses the action stage) and peak flow (t4), along with associated total catchment rainfall is shown in Figure 5.1. The corresponding lag

time (From t2 to t4) for this event is 8.4 hours while the rainfall is accumulated 1.5 times that period as explained in the previous section.

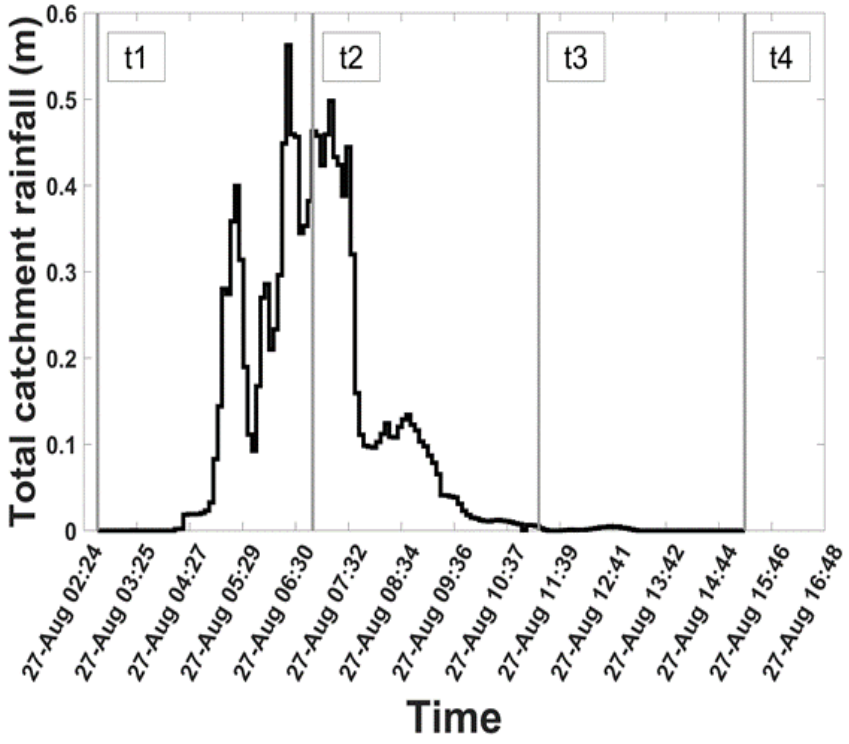

Figure 5.1: Illustration of rainfall and corresponding flooding for an event on 27th August, 2006, in the Blue river at Blue Ridge Blvd Ext in Missouri with a USGS gauge of ID 6893150. Here, t1 is the start of the rainfall accumulation period, t2 is the centroid of rainfall, t3 is the time at which the flooding starts (i.e. crosses action stage), and t4 is the peak of hydrograph.

Figure 5.2 shows the flow distance grid, rainfall accumulation grid, and the computation of rainfall moments and width functions. The first (Δ_1) and second order (Δ_2) scaled spatial moments of catchment rainfall for this flooding event are 1.1 and 0.886 respectively. Δ_1 values greater than 1 signify upstream distribution of rainfall as is confirmed by the rainfall accumulation map of Figure 5.2(b). A value of Δ_2 less than 1 represents a rainfall distribution characterized by a unimodal distribution along the flow

distance. This is further confirmed by Figure 5.2(c) where the higher rainfall accumulations are concentrated in the higher ranges of the flow distance (i.e. furthest from catchment outlet). Similarly, horizontal gap (HG) value of 0.071 (greater than zero) indicates rainfall is distributed upstream. While, vertical gap (VG) of 1.11 (greater than unity) represents concentration of rainfall over a small part of the catchment.

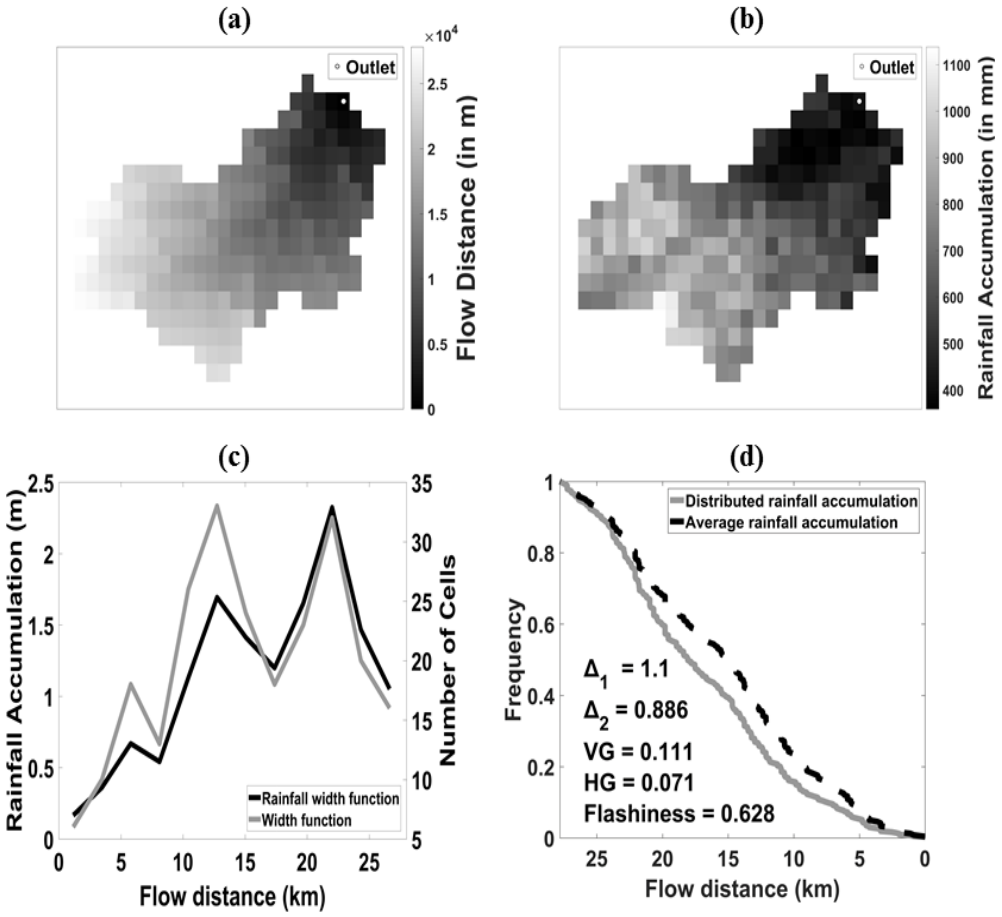

Figure 5.2: Rainfall spatial variability indices described in Zoccatelli et al. (2011)and Emmanuel et al.(2015) for a flooding event in the Blue river at Blue Ridge Blvd Ext in Missouri with USGS ID of 6893150 and a catchment area of 241 km^2. The peak flow of the event happened at 27-Aug-2006 15:15. Here, (a) shows the flow distances of the basin, (b) rainfall accumulation field for a period of 12.61 hours, (c) width function and rainfall width function, (d) distributions of average and distributed rainfall accumulation along with associated values of Δ_1, Δ_2, horizontal gap, vertical gap, and flashiness.

5.3 Association of flashiness with rainfall and basin properties

The influence of some of the rainfall and geomorphological properties on flashiness is further analyzed using quantile plots in Figure 5.3 and Figure 5.4. Traditional regression techniques summarize the average relationship between the explanatory and the target variables, which only provides a limited view of the relationship. But for relationships that explain substantial heterogeneity, it is prudent to look at the relationship at different points in the conditional distribution of the output variable, and this can be accomplished using quantile plots. The quantiles (1st, 10th, 25th, 50th, 75th, 90^{th}, and 99th) of event flashiness conditioned on the variability indices represents the variability in these relationships. The conditional median describes the first order information of the dependency, while the inter-quartile area estimates the variability in the relationship and 10^{th} and 90^{th} quantiles describe the uncertainty of extreme values of flashiness.

5.3.1 Spatial moments of catchment rainfall

Figure 5.3 shows the quantile plots of some of the derived variables that describe the spatial organization of catchment rainfall as described previously including the spatial variability indices mentioned in Zoccatelli et al. (2011) and Emmanuel et al. (2015). The zeroeth order of catchment rainfall (P0), i.e. the basin-averaged catchment rainfall, is intuitively expected to impact the severity of a flash flood. Figure 5.3(a) confirms this relationship where higher average rainfall rates lead to higher flashiness. However, this increasing relationship is more prominent among higher values of P0. In lower ranges, increase in P0 don't lead to corresponding increase in flashiness, indicating that there may be competing factors at play that dampen the impact of rainfall intensity on flash

flood severity. Similarly, Figure 5.3(b) shows the relationship of different quantiles of flashiness with second scaled spatial moment of catchment rainfall (Δ2) that reflects the mode of the rainfall. It is noted that large number of events have Δ_2 values close to 1 which represent uniform-like rainfall distributions. This relationship however, don't exhibit a gradual dependence throughout the entire range of values of Δ_1 and Δ_2. The influence of vertical gap (VG) on flashiness can be seen in Figure 5.3(c). Higher values of VG imply greater concentration of rainfall over a small part of the catchment. In the figure, flashiness decreases as VG values increase. Horizontal Gap (HG) exhibits a more complicated relationship in Figure 5.3(d) with large number of events having HG values close to 1, indicating a rainfall concentrated near the catchment centroid. However, these quantile plots describe two-dimensional relationships, but the severity of a flood being impacted by many factors, further analysis is required to disaggregate competing dependencies.

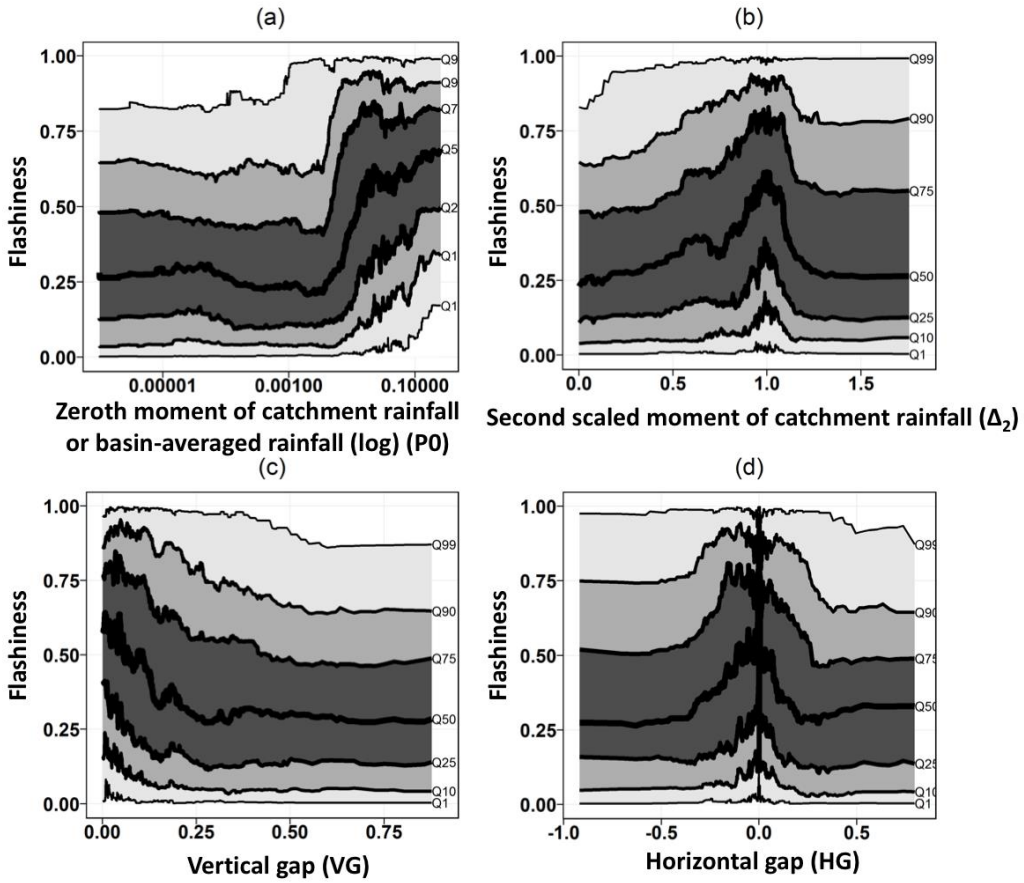

Figure 5.3: 1st-99th quantile of flashiness versus (a) zeroeth moment of catchment rainfall or basin-averaged rainfall (P0), (b) first scaled moment of catchment rainfall (Δ_1), (c) vertical gap (VG), and (d) horizontal gap (HG). These rainfall variability indices are from Zocatelli et al. (2010) and Emmanuel et al. (2015)

5.3.2 Basin properties

The influence of some of the physiographic variables on flashiness is analyzed using quantile plots in Figure 5.4. The first moment of flow distance (G1) is the catchment-averaged flow distance, with higher flow distances corresponding to increased travel times and lower flow peaks, and, thus, lower flashiness. Figure 5.4(a) shows how flashiness decreases with increasing G1 values, along with the variability in the relationship. Similarly, steeper basins are expected to experience flashier floods as water travels faster to the outlet along with increased runoff. The relationship between

flashiness and slope index is portrayed by Figure 5.4(b), where increase in slope index (describing steeper topography) leads to increase in flashiness. The percentage of imperviousness in a basin controls the proportion of rainfall converting into runoff or infiltrating into the ground. Higher percentage of impervious area will lead to more water running off towards the outlet at faster speeds, which is reflected in Figure 5.4(c). Finally, larger number of first-order channel frequency increases channel conveyance of runoff and we can see its mild increase with flashiness.

Quantile plots provide valuable insights into the influence of moments of precipitation and flow distances, spatial variability indices, geomorphologic variables etc. on flashiness. But flooding is a result of complex interactions between many factors and a one-dimensional approach is limited in its ability to explain competing behaviors. Thus, this technique is extended into a multi-dimensional approach in the next section to account for the collective influence of many explanatory variables on flashiness. This will help in uncovering the relative impact of different factors on any flood event, thus, dramatically improving our ability to diagnose causative processes behind flash floods.

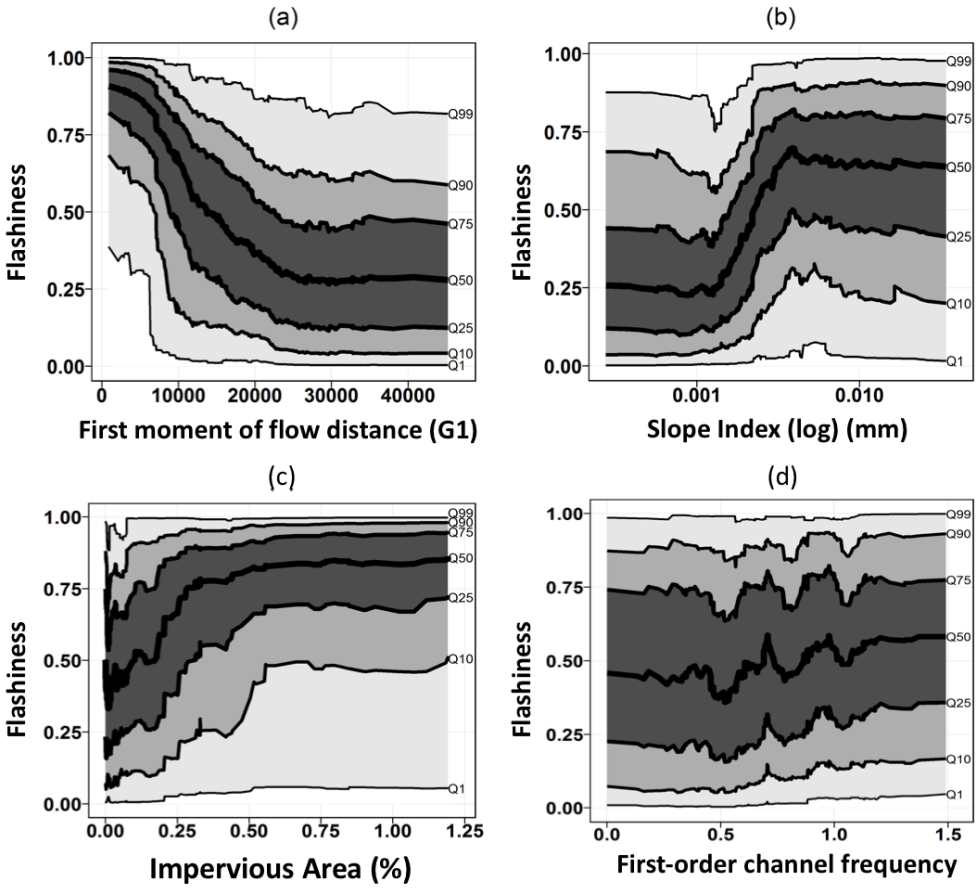

Figure 5.4: 1st-99th quantile of flashiness versus (a) first moment of flow distance (G1), (b) slope index, and (c) impervious area (%), and (d) first order channel frequency

5.4 Multi-dimensional modeling of flashiness

5.4.1 The model

In this work, the complex relationship between the explanatory variables and flashiness is analyzed through conditional distribution functions using the generalized additive models for location, scale, and shape (GAMLSS, Rigby and Stasinopoulos 2005) technique which has been discussed in detail in Section 4.4. To find the most suitable distribution for fitting event-level flashiness, several conditional two-parameter density functions (lognormal, normal, reverse gumbel, logistic, gamma, etc.) were tested

for goodness of fit using the AIC for each of the semi-parametric density fits as well as by checking the normality and independence of residuals. Finally, the beta distribution was selected as the most appropriate distribution for modeling the dependence of flashiness on various geomorphological, climatological, and rainfall variables. The original beta distribution is given by:

$$f(y|\alpha,\beta) = \frac{1}{B(\alpha,\beta)} y^{\alpha-1}(1-y)^{\beta-1} \tag{5.5}$$

for y = (0, 1), α > 0 and β > 0. In the GAMLSS implementation, α = μ and β > σ where μ (representing location) and σ (representing scale) are the distribution parameters. The function given in Eq. (5) was used to model the conditional flashiness distributions, where the location μ is linked to the expected flashiness value, and the scale σ gives the uncertainty around the expected flashiness. The model is further refined through an iterative procedure of trying various combinations of explanatory variables by using domain knowledge of individual variables and diagnostics. Instead of polynomials or fractional polynomials, penalized splines are used for fitting trends for each parameter as they offer more flexibility in modeling complex nonlinear relationships. The variables that were retained in the final model are presented in Table 5.2 along with their corresponding statistical significance values. Overall, variables such as zeroth moment of catchment rainfall (P0), vertical gap (VG), first-moment of flow distance, curve number etc. were found to be the most impactful when it comes to explaining flashiness of an event. Here, P0 is the catchment-averaged rainfall rate and represents the general

availability of water for a flood to occur. Along with average rain rate, higher VG values represent greater concentration of rainfall over a small portion of a basin, which leads to more severe floods. In case of extreme floods, river network geometry as represented by catchment-averaged flow distance (G1) plays a vital role as heterogeneities of land properties play lesser role in runoff generation than for moderate floods. Finally, curve number also impacts the severity of a floods as it is a measure of a watershed's runoff response to a rainstorm. Figure 5.7 shows a scatter plot of the systematic part of modeled versus observed flashiness with a correlation of 0.72. Thus, the model exhibits significant explanatory power in modeling event flashiness, thereby increasing our confidence in the results to explain the relative impact of various parameters.

Table 5.2: Statistical significance of explanatory variables in GAMLSS model. Not retained or not considered variable are marked with '-'. Significance is expressed as p-value.

Variable	p-value
Catchment-averaged rainfall rate (P0)	$<2x10^{-16}$
Vertical Gap (VG)	$<2x10^{-16}$
Catchment-averaged flow distance (G1)	$<2x10^{-16}$
Curve Number	$<2x10^{-16}$
Slope Index	$2x10^{-16}$
Impervious Area	$2.75x10^{-16}$
Frequency of first-order channels	$3.66x10^{-08}$
Horizontal Gap (HG)	$8.54x10^{-05}$
Δ_2	0.00235

5.4.2 Conditional estimates of explanatory variables

GAMLSS being an additive framework allows us to analyze the accuracy of individual predictors on the response variable (here, flashiness), which is a powerful diagnostic tool for disaggregating competing influences. Figure 5.5 and Figure 5.6

shows the partial prediction of the flashiness based on the rainfall and geomorphological variables included in the final model. Figure 5.5(a) illustrates how the effect of zeroeth moment of catchment rainfall (i.e. basin average rainfall) on flashiness is low for lower values but has a sharp inflection as it increases. This indicates that the physiography of the basin dampens the effect of rainfall at lower values, but rainfall overwhelms other factors resulting in a higher contribution to flashiness at upper ranges. The influence of second scaled moment of catchment rainfall (Δ_2) in Figure 5.6(b) indicates that floods are more severe for unimodal distribution of rainfall along the stream network characterized by lower Δ_2 values. Lower values of Δ_2 represent unimodal distribution of floods which translates to high peak discharges corresponding to higher flashiness due to resonance of rainfall and catchment flow distances. One can note that this relationship is not pronounced through a unidimensional approach of quantile plots as shown in Figure 5.5(b). Similarly, higher Vertical Gap (VG) values represent greater concentration of rainfall on a small part of the catchment which leads to higher flashiness. Overall, a combination of high basin average rainfall (P0), unimodal rainfall distribution along flow distance (Δ_2), and greater concentration of rainfall over a small part of the catchment (VG) will yield the most severe floods.

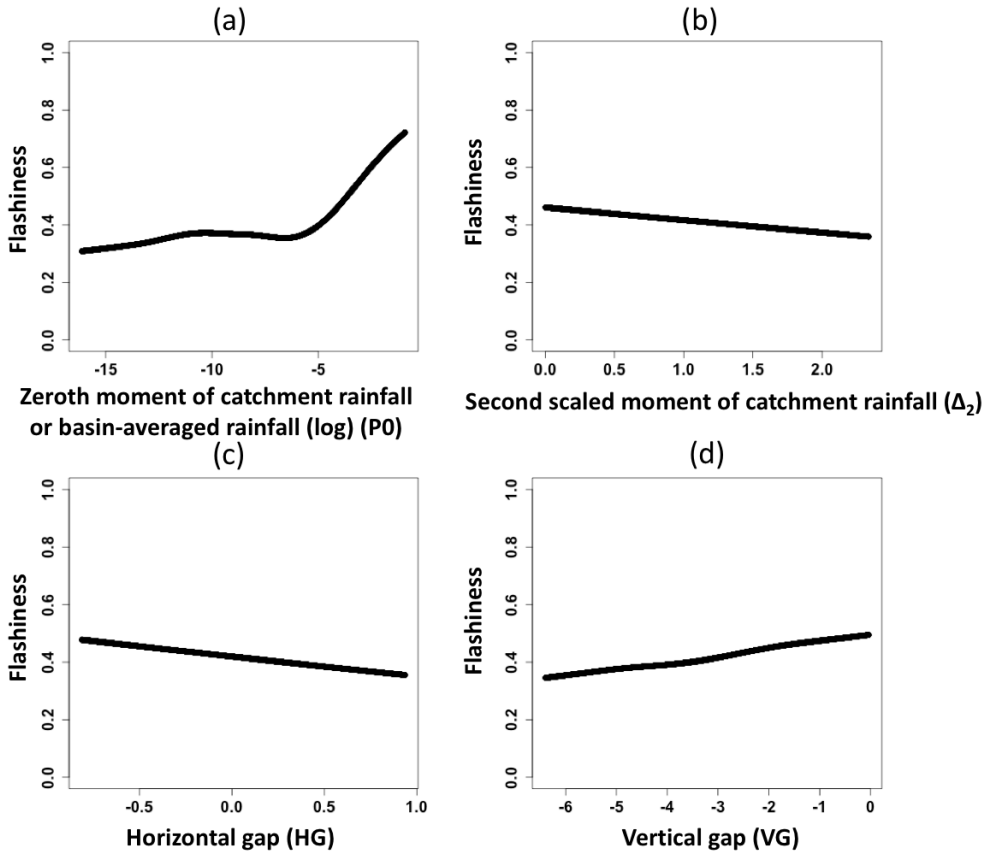

Figure 5.5: Relative contribution on flashiness by rainfall parameters such as: a) zeroeth moment of catchment rainfall or basin-averaged rainfall (P0), b) second scaled moment of catchment rainfall (Δ_2), (c) horizontal gap (HG), (d) vertical gap (VG)

The contribution of geomorphological variables is similarly exhibited in Figure 5.6. In Figure 5.6(a), the first moment of flow distance (G1), which is the average flow distance in the basin, is a proxy for how long it takes for water to reach the outlet and shows a sharp decreasing trend with flashiness. This variable is closely related to the size and shape of the basin which is known to have a large impact on flood response. The basin curve number is related to the runoff-producing potential of a basin and higher peak discharges and, expectedly, shows an increasing trend with flashiness in Figure 5.6(b). Curve numbers have a range of 30 to 100 where lower numbers indicate low runoff

potential corresponding to more permeable soil such as well-drained sands and gravels. Higher curve numbers indicate increasing runoff potential exhibited by soils with very low infiltration rates such as clay. According to Morisawa (1959), first-order channel frequency expresses the small-scale properties of a basin which complements G1. Higher number of first-order channels will carry more water into the main channel and, thus, shows increasing trend with flashiness in Figure 5.6(c). Greater imperviousness in a basin leads to greater percentage of rainfall converting into surface runoff as shown in Figure 5.6(d). Finally, greater slope of a basin leads to lower travel time for runoff, and hence an increasing trend with flashness as observed in Figure 5.6(e)

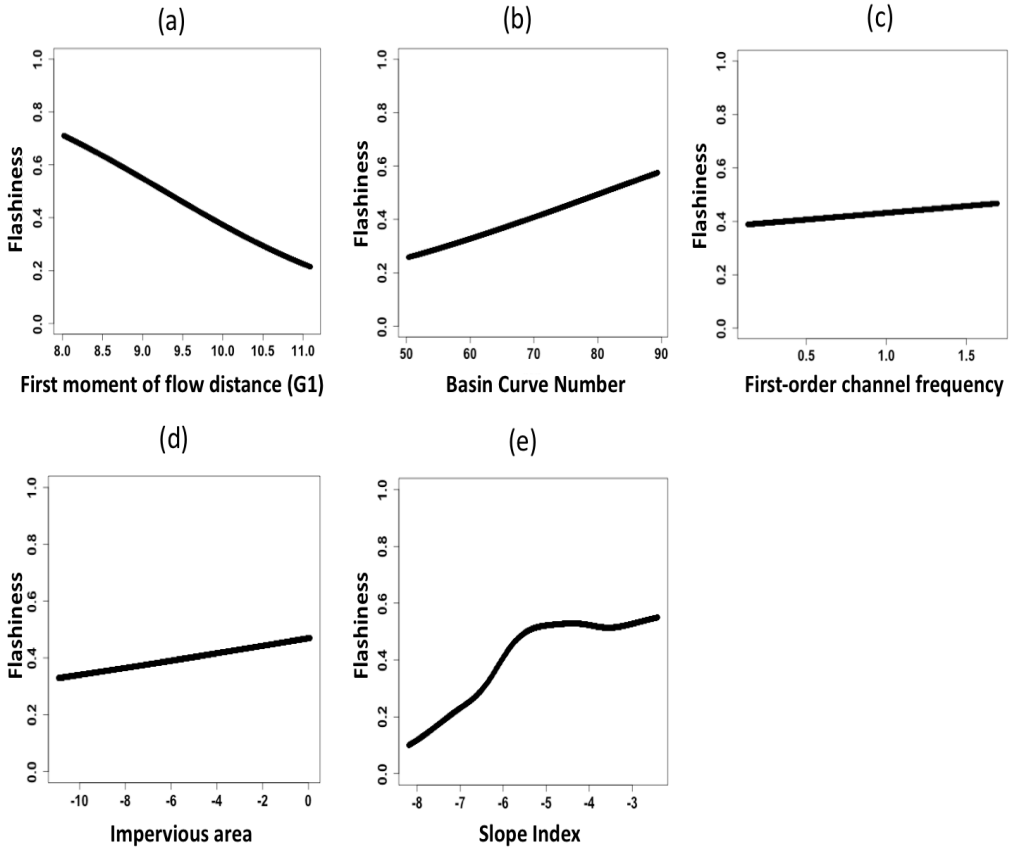

Figure 5.6: Relative contribution on flashiness by different geomorphologic parameters: (a) first moment of flow distance (G1), (b) basin curve number, (c) frequency of first-order channels, (d) impervious area, (e) slope index

5.4.3 Contrast between floods and flash floods

Using the GAMLSS model, the event-based flashiness was characterized using rainfall and geomorphological variables. The model is used to further investigate how the influence of contributing processes change from floods to flash floods. Though, there is no universally accepted definition of distinguishing floods and flash floods, but, Saharia et al. (2016) has previously identified a flashiness value of 0.75 as a reasonable cutoff between floods and flash floods by fitting probability distribution functions between them based on actual NWS storm reports. Accepting this as the baseline, the equivalent cutoff for event-based flashiness was found to be 0.58. Accordingly, 33% of the lowest (<0.29) and 33% of the highest (>0.58) flashiness cases were selected for floods and flash floods respectively. Based on this cutoff, the GAMLSS model was refitted and percentage contribution of the two groups of variables, rainfall variability and geomorphology, were quantified. The comparative analysis was performed for three cases: all floods, floods, and flash floods and results are reported in Table 5.3. We found that the contribution of geomorphology to flashiness is almost twice that of rainfall variability for the entire dataset. But, a clear increase in the percentage contribution of rainfall variability from 34% to 43% was found for floods and flash floods respectively. Thus, the percentage contribution of rainfall spatial variability on flashiness is 9% more for flash floods compared to floods. This clearly underscores the importance of accounting for rainfall spatial variability for modeling at flash flood scales and, so far as the authors are aware, is the first quantification of this dependence varying with scale.

Table 5.3: Percentage contribution of rainfall variability and geomorphology to flashiness

for all floods, floods, and flash floods.

Dataset	Percentage contribution to flashiness	
	Rainfall variability	Geomorphology
All floods	35%	65%
Floods (Flashiness <0.75)	34%	66%
Flash Floods (≥0.75)	43%	57%

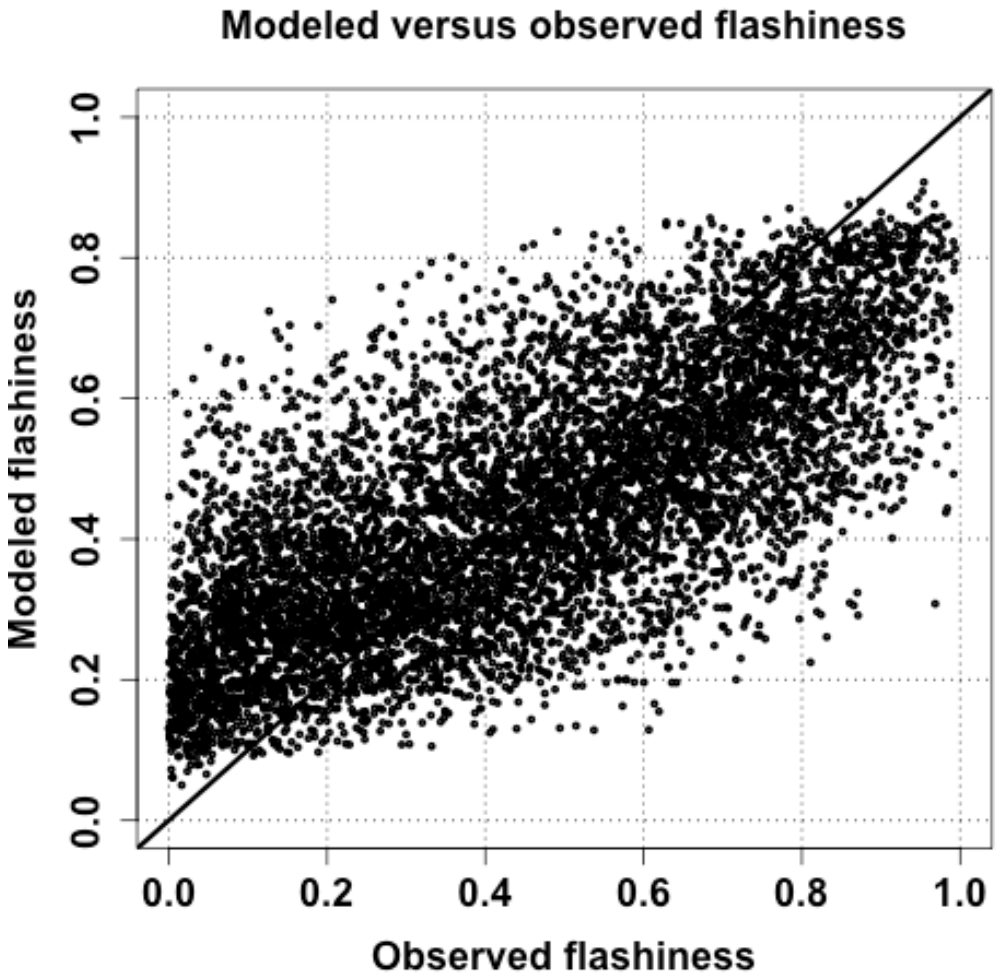

Figure 5.7: Scatter plot of modeled versus observed flashiness. Correlation R=0.72

5.5 Conclusions

The goal of this study is to quantify the impact of rainfall spatial variability on flash flood severity through a big data approach using a large dataset of observations. A robust methodology of including many rainfall spatial variability indices and morphological variables in analyzing 9,392 flooding events improves upon existing body knowledge replying on case studies and simulations. Complex relationships between the flashiness and a large number of explanatory variables such as the moments of rainfall and flow distance, spatial variability indices found in Zoccatelli et al. (2011) and Emmanuel et al. (2015), and geomorphologic factors were modeled using a multidimensional framework called GAMLSS. Along with the variability of these relationships, the relative influences of these factors on flashiness were also quantified, thereby, yielding an improved understanding of these dependencies. The findings are summarized below:

1. Large number of variables were used to model event flashiness, and zeroeth moment of catchment rainfall or basin-averaged rainfall, vertical gap, first-moment of flow distance, and curve number were found to be the most impactful.
2. Among rainfall spatial variables, the flashiest floods ae caused by a combination of high basin average rainfall (P0), unimodal rainfall distribution along flow distance (Δ_2), and greater concentration of rainfall over a small part of the catchment (VG).
3. The systematic part of the multidimensional model yielded a correlation of 0.72 between modeled and observed flashiness.
4. The relative percentage contribution of rainfall spatial variability on flashiness increased from 34% to 43% for floods to flash floods.

This work proposes a general overview of the impact of rainfall spatial variability on flash flood severity. In future, this framework will be extended to propose indices that better capture the spatial variability of rainfall within a basin.

Chapter 6. Summary and Future Work

Flash floods are a leading cause of fatalities caused by natural disasters worldwide. Characterizing floods and flash floods is the key to understanding the dominant mechanisms impacting flooding based on a multitude of rainfall, physiographic and climatologic variables at different spatial and temporal scales. However, this is difficult due to the inherently multidimensional and non-linear relationships that these processes exhibit. In this work, different aspects of the hydrograph, such as the flooding rise time, unit peak discharge, and flood severity were characterized over the conterminous United States using a big data approach. This large events sample approach requires intensive data collection. Different geospatial datasets were utilized to compute geophysical attributes at continental scale.

A unique database of USGS observations combined with NWS flood stage thresholds was used to perform the most spatial and temporally comprehensive characterization of floods in the United States. The monthly frequency of floods was found to greatly change depending on climate classes. The envelope curves were developed for unit peak discharges and basin area that were found to be consistent with those reported for Europe and worldwide in the literature.

Next, a new variable called “flashiness” was proposed as a proxy for flash flood severity of a basin. The variable was modeled using a large number of explanatory variables covering geomorphology and climatology. The multi-dimensional GAMLSS model showing a correlation of 0.83 and bias of 0.6% during the calibration exercise was used to map the flashiness variable all over CONUS. Several hotspots were identified within known flash flood prone regions but also some that were outside the areas covered

by observations, including the western slopes of the Appalachians in Tennessee, Kentucky, and West Virginia.

And, finally, the impact of spatial organization of rainfall on event-level flash flood severity was investigated using the high-resolution MRMS reanalysis precipitation dataset. The systematic part of the model yielded a correlation of 0.72 between modeled and observed flashiness at event scale and the relative percentage contribution of rainfall spatial variability on flashiness increased by 9% from floods to flash floods.

The hypotheses proposed in Chapter 1 were confirmed as information regarding geomorphology, climatic regimes, rainfall spatial variability, soil type, land use/land cover etc. was useful in explaining trends in unit peak discharges, flooding rise time, flash flood severity etc. The relationships were explored using both unidimensional approaches such as quantile plots and envelope curves as well as multi-dimensional modeling using GAMLSS. The model for basin-median flashiness was found to be skillful enough to reliably regionalize the variable outside the observation dataset. The results were successfully verified using flash flood fatalities and the NWS storm database. The model for event-level flashiness was also found to have sufficient explanatory power to systematically disaggregate the impact of rainfall spatial variability and physiographic variables.

The analysis framework presented herein is only a first-step towards improved characterization of flash floods. Several research endeavors are currently underway to explore other aspects of flooding such as the time of concentration of a basin and recession time. New rainfall spatial variables that describe the spatial organization of rainfall are being developed that accounts for precipitation intermittency. The flash flood

severity map would be connected to fatalities, demographic, and economic data to produce a CONUS-wide flood vulnerability map. The overarching goal is to augment the existing database and use sophisticated modeling techniques to improve predictions in gauged and ungauged locations. Moreover, the geomorphological and climatological variables included in this study can be computed globally and the flooding data available over the US is geographically diverse, thus the model could be extended to predict flashiness globally.

Improved understanding of the dependence of hydrologic process on organization of rainfall and geomorphology at catchment scale will be useful in improving physics-based hydrological models. Threshold values of the rainfall spatial variability indices will identify basins most amenable to distributed hydrologic modeling where significant variability in spatial rainfall lead to corresponding variability in basin response. Since this study determines the relative importance of different spatial variability and geomorphological indices in flash flooding, it could be used to improve upon the spatial flash flood guidance (SFFG) approach proposed by Douinot et al. (2016) which currently only uses the first and second scaled spatial moments proposed by Zoccatelli et al. (2010).

In the future, this analysis framework could be extended to serve as a baseline for evaluating distributed hydrologic model simulations from the Flooded Locations And Simulated Hydrographs Project (FLASH) (Gourley et al., 2017) under a variety of conditions. The flash flood climatologies derived from the hydrologic model could be verified for consistency against results in this study explaining the relative impact of

rainfall and geomorphology on flooding. The framework will also be extended to propose indices that better capture the spatial variability of rainfall within a basin.

References

Adams, R., Western, A.W., Seed, A.W., 2012. An analysis of the impact of spatial variability in rainfall on runoff and sediment predictions from a distributed model. Hydrol. Process. 26, 3263–3280. doi:10.1002/hyp.8435

Adhikari, P., Hong, Y., Douglas, K.R., Kirschbaum, D.B., Gourley, J., Adler, R., Brakenridge, G.R., 2010. A digitized global flood inventory (1998–2008): compilation and preliminary results. Nat. Hazards 55, 405–422. doi:10.1007/s11069-010-9537-2

Akantziliotou, C., Rigby, R., Stasinopoulos, D., 2002. The R implementation of generalized additive models for location, scale and shape, in: Statistical Modelling in Society: Proceedings of the 17th International Workshop on Statistical Modelling. Statistical Modelling Society, pp. 75–83.

Anquetin, S., Braud, I., Vannier, O., Viallet, P., Boudevillain, B., Creutin, J.-D., Manus, C., 2010. Sensitivity of the hydrological response to the variability of rainfall fields and soils for the Gard 2002 flash-flood event. J. Hydrol., Flash Floods: Observations and Analysis of Hydrometeorological Controls 394, 134–147. doi:10.1016/j.jhydrol.2010.07.002

Ashley, S.T., Ashley, W.S., 2008. Flood Fatalities in the United States. J. Appl. Meteorol. Climatol. 47, 805–818. doi:10.1175/2007JAMC1611.1

Bell, V.A., Moore, R.J., 2000. The sensitivity of catchment runoff models to rainfall data at different spatial scales. Hydrol Earth Syst Sci 4, 653–667. doi:10.5194/hess-4-653-2000

Bhaskar, N., French, M., Kyiamah, G., 2000. Characterization of Flash Floods in Eastern Kentucky. J. Hydrol. Eng. 5, 327–331. doi:10.1061/(ASCE)1084-0699(2000)5:3(327)

Borga, M., Boscolo, P., Zanon, F., Sangati, M., 2007. Hydrometeorological Analysis of the 29 August 2003 Flash Flood in the Eastern Italian Alps. J. Hydrometeorol. 8, 1049–1067. doi:10.1175/JHM593.1

Brakenridge, G.R., Karnes, D., 1996. The Dartmouth Flood Observatory: an electronic research tool and electronic archive for investigations of extreme flood events, in: Geoscience Information Society Proceedings. Presented at the Geological Society of America Annual Meeting.

Brath, A., Montanari, A., 2003. Sensitivity of the peak flows to the spatial variability of the soil infiltration capacity for different climatic scenarios. Phys. Chem. Earth Parts ABC, Hydrological Processes and Distributed Hydrological Modelling 28, 247–254. doi:10.1016/S1474-7065(03)00034-2

Castellarin, A., 2007. Probabilistic envelope curves for design flood estimation at ungauged sites. Water Resour. Res. 43, W04406. doi:10.1029/2005WR004384

Christian Bernhofer, Michele Tarolli, Nadine Jatho, Firas al Janabi, Marco Borga, Davide Zoccatelli, 2013. Rainfall Space-Time Organization and Orographic Control on Flash Flood Response: The Weisseritz Event of August 13, 2002. doi:10.1061/(ASCE)HE.1943-5584.0000569

Cole, S.J., Moore, R.J., 2009. Distributed hydrological modelling using weather radar in gauged and ungauged basins. Adv. Water Resour., Weather Radar and Hydrology 32, 1107–1120. doi:10.1016/j.advwatres.2009.01.006

Cole, S.J., Moore, R.J., 2008. Hydrological modelling using raingauge- and radar-based estimators of areal rainfall. J. Hydrol. 358, 159–181. doi:10.1016/j.jhydrol.2008.05.025

Collier, C.G., 2007. Flash flood forecasting: What are the limits of predictability? Q. J. R. Meteorol. Soc. 133, 3–23. doi:10.1002/qj.29

Collier, C.G., Fox, N.I., 2003. Assessing the flooding susceptibility of river catchments to extreme rainfall in the United Kingdom. Int. J. River Basin Manag. 1, 225–235. doi:10.1080/15715124.2003.9635209

Costa, J.E., 1987a. Hydraulics and basin morphometry of the largest flash floods in the conterminous United States. J. Hydrol. 93, 313–338. doi:10.1016/0022-1694(87)90102-8

Costa, J.E., 1987b. A comparison of the largest rainfall-runoff floods in the United States with those of the People's Republic of China and the world. J. Hydrol., Analysis of Extraordinary Flood Events 96, 101–115. doi:10.1016/0022-1694(87)90146-6

Creutin, J.D., Borga, M., Gruntfest, E., Lutoff, C., Zoccatelli, D., Ruin, I., 2013. A space and time framework for analyzing human anticipation of flash floods. J. Hydrol. 482, 14–24. doi:10.1016/j.jhydrol.2012.11.009

Crippen, J.R., Bue, C.D., 1977. Maximum floodflows in the conterminous United States (No. WSP-1887). United States Geological Survey.

Dade, W.B., 2001. Multiple Scales in River Basin Morphology. Am. J. Sci. 301, 60–73. doi:10.2475/ajs.301.1.60

Dawdy, D.R., Bergmann, J.M., 1969. Effect of rainfall variability on streamflow simulation. Water Resour. Res. 5, 958–966. doi:10.1029/WR005i005p00958

de Lima, J.L.M.P., Singh, V.P., 2002. The influence of the pattern of moving rainstorms on overland flow. Adv. Water Resour. 25, 817–828. doi:10.1016/S0309-1708(02)00067-2

Douinot, A., Roux, H., Garambois, P.-A., Larnier, K., Labat, D., Dartus, D., 2016. Accounting for rainfall systematic spatial variability in flash flood forecasting. J. Hydrol., Flash floods, hydro-geomorphic response and risk management 541, Part A, 359–370. doi:10.1016/j.jhydrol.2015.08.024

Emmanuel, I., Andrieu, H., Leblois, E., Janey, N., Payrastre, O., 2015. Influence of rainfall spatial variability on rainfall–runoff modelling: Benefit of a simulation approach? J. Hydrol. doi:10.1016/j.jhydrol.2015.04.058

Fabry, F., 1996. On the determination of scale ranges for precipitation fields. J. Geophys. Res. Atmospheres 101, 12819–12826. doi:10.1029/96JD00718

Fahrmeir, L., Lang, S., 2001. Bayesian semiparametric regression analysis of multicategorical time-space data. Ann. Inst. Stat. Math. 53, 11–30.

Faurès, J.-M., Goodrich, D.C., Woolhiser, D.A., Sorooshian, S., 1995. Impact of small-scale spatial rainfall variability on runoff modeling. J. Hydrol. 173, 309–326. doi:10.1016/0022-1694(95)02704-S

Fry, J.A., Xian, G., Jin, S., Dewitz, J.A., Homer, C.G., Yang, L., Barnes, C.A., Herold, N.D., Wickham, J.D., 2011. COMPLETION OF THE 2006 NATIONAL LAND

COVER DATABASE FOR THE CONTERMINOUS UNITED STATES. Photogramm. Eng. Remote Sens. 77, 858–864.

Furey, P.R., Gupta, V.K., 2005. Effects of excess rainfall on the temporal variability of observed peak-discharge power laws. Adv. Water Resour. 28, 1240–1253. doi:10.1016/j.advwatres.2005.03.014

Gabellani, S., Boni, G., Ferraris, L., von Hardenberg, J., Provenzale, A., 2007. Propagation of uncertainty from rainfall to runoff: A case study with a stochastic rainfall generator. Adv. Water Resour., Recent Developments in Hydrologic Analysis 30, 2061–2071. doi:10.1016/j.advwatres.2006.11.015

Gaume, E., Bain, V., Bernardara, P., Newinger, O., Barbuc, M., Bateman, A., Blaškovičová, L., Blöschl, G., Borga, M., Dumitrescu, A., Daliakopoulos, I., Garcia, J., Irimescu, A., Kohnova, S., Koutroulis, A., Marchi, L., Matreata, S., Medina, V., Preciso, E., Sempere-Torres, D., Stancalie, G., Szolgay, J., Tsanis, I., Velasco, D., Viglione, A., 2009. A compilation of data on European flash floods. J. Hydrol. 367, 70–78. doi:10.1016/j.jhydrol.2008.12.028

Gaume, E., Gaál, L., Viglione, A., Szolgay, J., Kohnová, S., Blöschl, G., 2010. Bayesian MCMC approach to regional flood frequency analyses involving extraordinary flood events at ungauged sites. J. Hydrol., Flash Floods: Observations and Analysis of Hydrometeorological Controls 394, 101–117. doi:10.1016/j.jhydrol.2010.01.008

Georgakakos, K.P., 2006. Analytical results for operational flash flood guidance. J. Hydrol. 317, 81–103. doi:10.1016/j.jhydrol.2005.05.009

Gochis, D., Schumacher, R., Friedrich, K., Doesken, N., Kelsch, M., Sun, J., Ikeda, K., Lindsey, D., Wood, A., Dolan, B., Matrosov, S., Newman, A., Mahoney, K., Rutledge, S., Johnson, R., Kucera, P., Kennedy, P., Sempere-Torres, D., Steiner, M., Roberts, R., Wilson, J., Yu, W., Chandrasekar, V., Rasmussen, R., Anderson, A., Brown, B., 2014. The Great Colorado Flood of September 2013. Bull. Am. Meteorol. Soc. 96, 1461–1487. doi:10.1175/BAMS-D-13-00241.1

Gourley, J.J., Erlingis, J.M., Smith, T.M., Ortega, K.L., Hong, Y., 2010. Remote collection and analysis of witness reports on flash floods. J. Hydrol., Flash Floods: Observations and Analysis of Hydrometeorological Controls 394, 53–62. doi:10.1016/j.jhydrol.2010.05.042

Gourley, J.J., Flamig, Z.L., Vergara, H., Kirstetter, P.-E., Clark, R.A., Argyle, E., Arthur, A., Martinaitis, S., Terti, G., Erlingis, J.M., Hong, Y., Howard, K.W., 2017. The FLASH Project: Improving the Tools for Flash Flood Monitoring and Prediction across the United States. Bull. Am. Meteorol. Soc. 98, 361–372. doi:10.1175/BAMS-D-15-00247.1

Gourley, J.J., Hong, Y., Flamig, Z.L., Arthur, A., Clark, R., Calianno, M., Ruin, I., Ortel, T., Wieczorek, M.E., Kirstetter, P.-E., Clark, E., Krajewski, W.F., 2013. A Unified Flash Flood Database across the United States. Bull. Am. Meteorol. Soc. 94, 799–805. doi:10.1175/BAMS-D-12-00198.1

Groisman, P.Y., Knight, R.W., Easterling, D.R., Karl, T.R., Hegerl, G.C., Razuvaev, V.N., 2005. Trends in Intense Precipitation in the Climate Record. J. Clim. 18, 1326–1350. doi:10.1175/JCLI3339.1

Groisman, P.Y., Knight, R.W., Karl, T.R., Easterling, D.R., Sun, B., Lawrimore, J.H., 2004. Contemporary Changes of the Hydrological Cycle over the Contiguous

United States: Trends Derived from In Situ Observations. J. Hydrometeorol. 5, 64–85. doi:10.1175/1525-7541(2004)005<0064:CCOTHC>2.0.CO;2
Gupta, V.K., Castro, S.L., Over, T.M., 1996. On scaling exponents of spatial peak flows from rainfall and river network geometry. J. Hydrol., Fractals, scaling and nonlinear variability in hydrology 187, 81–104. doi:10.1016/S0022-1694(96)03088-0
Hastie, T.J., Tibshirani, R.J., 1990. Generalized additive models. CRC Press.
He, X., Sonnenborg, T.O., Refsgaard, J.C., Vejen, F., Jensen, K.H., 2013. Evaluation of the value of radar QPE data and rain gauge data for hydrological modeling. Water Resour. Res. 49, 5989–6005. doi:10.1002/wrcr.20471
Herschy, R.W., 2002. The world's maximum observed floods. Flow Meas. Instrum. 13, 231–235. doi:10.1016/S0955-5986(02)00054-7
Herschy, R.W., Fairbridge, R.W., 1998. Encyclopedia of Hydrology and Water Resources. Springer Science & Business Media.
Hirsch, R.M., Archfield, S.A., 2015. Flood trends: Not higher but more often. Nat. Clim. Change 5, 198–199. doi:10.1038/nclimate2551
Hong, Y., Adhikari, P., Gourley, J.J., 2012. Flash Flood In: Bobrowsky, Peter (Ed.), in: Encyclopedia of Natural Hazards.
Jarvis, C.S., 1926. Flood Flow Characteristics. Trans. Am. Soc. Civ. Eng. 89, 985–1032.
Jin-Hyeog Park, Baxter E. Vieux, Boosik Kang, 2009. Distributed Hydrologic Prediction: Sensitivity to Accuracy of Initial Soil Moisture Conditions and Radar Rainfall Input. doi:10.1061/(ASCE)HE.1943-5584.0000039
Kirstetter, P.-E., Gourley, J.J., Hong, Y., Zhang, J., Moazamigoodarzi, S., Langston, C., Arthur, A., 2015. Probabilistic precipitation rate estimates with ground-based radar networks. Water Resour. Res. 51, 1422–1442. doi:10.1002/2014WR015672
Konrad, C.E., 2001. The Most Extreme Precipitation Events over the Eastern United States from 1950 to 1996: Considerations of Scale. J. Hydrometeorol. 2, 309–325. doi:10.1175/1525-7541(2001)002<0309:TMEPEO>2.0.CO;2
Kottek, M., Grieser, J., Beck, C., Rudolf, B., Rubel, F., 2006. World Map of the Köppen-Geiger climate classification updated. Meteorol. Z. 15, 259–263. doi:10.1127/0941-2948/2006/0130
Lins, H.F., Slack, J.R., 1999. Streamflow trends in the United States. Geophys. Res. Lett. 26, 227–230. doi:10.1029/1998GL900291
Lobligeois, F., Andréassian, V., Perrin, C., Tabary, P., Loumagne, C., 2014. When does higher spatial resolution rainfall information improve streamflow simulation? An evaluation using 3620 flood events. Hydrol Earth Syst Sci 18, 575–594. doi:10.5194/hess-18-575-2014
Mallakpour, I., Villarini, G., 2015. The changing nature of flooding across the central United States. Nat. Clim. Change advance online publication. doi:10.1038/nclimate2516
Marani, M., 2005. Non-power-law-scale properties of rainfall in space and time. Water Resour. Res. 41, W08413. doi:10.1029/2004WR003822
Marchi, L., Borga, M., Preciso, E., Gaume, E., 2010. Characterisation of selected extreme flash floods in Europe and implications for flood risk management. J. Hydrol., Flash Floods: Observations and Analysis of Hydrometeorological Controls 394, 118–133. doi:10.1016/j.jhydrol.2010.07.017

Marchi, L., Borga, M., Preciso, E., Sangati, M., Gaume, E., Bain, V., Delrieu, G., Bonnifait, L., Pogačnik, N., 2009. Comprehensive post-event survey of a flash flood in Western Slovenia: observation strategy and lessons learned. Hydrol. Process. 23, 3761–3770. doi:10.1002/hyp.7542

McCullagh, Peter, Nelder, J.A., McCullagh, P, 1989. Generalized linear models. Chapman and Hall London.

Mei, Y., Anagnostou, E.N., Stampoulis, D., Nikolopoulos, E.I., Borga, M., Vegara, H.J., 2014. Rainfall organization control on the flood response of mild-slope basins. J. Hydrol. 510, 565–577. doi:10.1016/j.jhydrol.2013.12.013

Merz, R., Blöschl, G., 2004. Regionalisation of catchment model parameters. J. Hydrol. 287, 95–123. doi:10.1016/j.jhydrol.2003.09.028

Merz, R., Blöschl, G., 2003. A process typology of regional floods. Water Resour. Res. 39, 1340. doi:10.1029/2002WR001952

Michaelides, K., Wainwright, J., 2002. Modelling the effects of hillslope–channel coupling on catchment hydrological response. Earth Surf. Process. Landf. 27, 1441–1457. doi:10.1002/esp.440

Michaud, J.D., Hirschboeck, K.K., Winchell, M., 2001. Regional variations in small-basin floods in the United States. Water Resour. Res. 37, 1405–1416.

Michaud, J.D., Sorooshian, S., 1994. Effect of rainfall-sampling errors on simulations of desert flash floods. Water Resour. Res. 30, 2765–2775. doi:10.1029/94WR01273

Miller, D.A., White, R.A., 1998. A Conterminous United States Multilayer Soil Characteristics Dataset for Regional Climate and Hydrology Modeling. Earth Interact. 2, 1–26. doi:10.1175/1087-3562(1998)002<0001:ACUSMS>2.3.CO;2

Morin, E., Enzel, Y., Shamir, U., Garti, R., 2001. The characteristic time scale for basin hydrological response using radar data. J. Hydrol. 252, 85–99. doi:10.1016/S0022-1694(01)00451-6

Morisawa, M.E., 1959. Relation of quantitative geomorphology to stream flow in representative watersheds of the Appalachian Plateau Province (Technical Report No. No. CU-TR-20). Columbia University, New York.

NWS, 2014. Annual Flood Loss Summary Reports [WWW Document]. URL http://www.nws.noaa.gov/hic/summaries/

Obled, C., Wendling, J., Beven, K., 1994. The sensitivity of hydrological models to spatial rainfall patterns: an evaluation using observed data. J. Hydrol. 159, 305–333. doi:10.1016/0022-1694(94)90263-1

O'Connor, J.E., Costa, J.E., 2004. Spatial distribution of the largest rainfall-runoff floods from basins between 2.6 and 26,000 km2 in the United States and Puerto Rico. Water Resour. Res. 40, W01107. doi:10.1029/2003WR002247

Ogden, F.L., Sharif, H.O., Senarath, S.U.S., Smith, J.A., Baeck, M.L., Richardson, J.R., 2000. Hydrologic analysis of the Fort Collins, Colorado, flash flood of 1997. J. Hydrol. 228, 82–100. doi:10.1016/S0022-1694(00)00146-3

Ortega, K.L., Smith, T.M., Manross, K.L., Kolodziej, A.G., Scharfenberg, K.A., Witt, A., Gourley, J.J., 2009. The Severe Hazards Analysis and Verification Experiment. Bull. Am. Meteorol. Soc. 90, 1519–1530. doi:10.1175/2009BAMS2815.1

Perucca, L.P., Angilieri, Y.E., 2011. Morphometric characterization of del Molle Basin applied to the evaluation of flash floods hazard, Iglesia Department, San Juan, Argentina. Quat. Int., Quaternary Landscape Evolution: Interplay of Climate,

Tectonics, Geomorphology, and Natural Hazards 233, 81–86. doi:10.1016/j.quaint.2010.08.007

Philip B. Bedient, Baxter E. Vieux, Dawn C. Gladwell, Brian C. Hoblit, 2000. NEXRAD Radar for Flood Prediction in Houston. doi:10.1061/(ASCE)1084-0699(2000)5:3(269)

Pielke, R.A., Downton, M.W., 2000. Precipitation and Damaging Floods: Trends in the United States, 1932–97. J. Clim. 13, 3625–3637. doi:10.1175/1520-0442(2000)013<3625:PADFTI>2.0.CO;2

Quintero, F., Sempere-Torres, D., Berenguer, M., Baltas, E., 2012. A scenario-incorporating analysis of the propagation of uncertainty to flash flood simulations. J. Hydrol. 460–461, 90–102. doi:10.1016/j.jhydrol.2012.06.045

Rafieeinasab, A., Norouzi, A., Kim, S., Habibi, H., Nazari, B., Seo, D.-J., Lee, H., Cosgrove, B., Cui, Z., 2015. Toward high-resolution flash flood prediction in large urban areas – Analysis of sensitivity to spatiotemporal resolution of rainfall input and hydrologic modeling. J. Hydrol., Hydrologic Applications of Weather Radar 531, Part 2, 370–388. doi:10.1016/j.jhydrol.2015.08.045

Reed, S., Koren, V., Smith, M., Zhang, Z., Moreda, F., Seo, D.-J., DMIP Participants, and, 2004. Overall distributed model intercomparison project results. J. Hydrol., The Distributed Model Intercomparison Project (DMIP) 298, 27–60. doi:10.1016/j.jhydrol.2004.03.031

Reed, S., Schaake, J., Zhang, Z., 2007. A distributed hydrologic model and threshold frequency-based method for flash flood forecasting at ungauged locations. J. Hydrol. 337, 402–420. doi:10.1016/j.jhydrol.2007.02.015

Rigby, R.A., Stasinopoulos, D.M., 2005. Generalized additive models for location, scale and shape. J. R. Stat. Soc. Ser. C Appl. Stat. 54, 507–554. doi:10.1111/j.1467-9876.2005.00510.x

Rigby, R.A., Stasinopoulos, D.M., 2001. The GAMLSS project: a flexible approach to statistical modelling, in: New Trends in Statistical Modelling: Proceedings of the 16th International Workshop on Statistical Modelling. pp. 337–345.

Rinaldo, A., Rodriguez-Iturbe, I., Rigon, R., Ijjasz-Vasquez, E., Bras, R.L., 1993. Self-organized fractal river networks. Phys. Rev. Lett. 70, 822–825. doi:10.1103/PhysRevLett.70.822

Rodriguez- Iturbe, I., Rinaldo, A., 1997. Fractal River Basins: Chance and Self-Organization. Cambridge University Press.

Ruiz-Villanueva, V., Díez-Herrero, A., Bodoque, J.M., Ballesteros Cánovas, J.A., Stoffel, M., 2013. Characterisation of flash floods in small ungauged mountain basins of Central Spain using an integrated approach. CATENA 110, 32–43. doi:10.1016/j.catena.2013.06.015

Safety, F., 2005. Flash flood alley. Boulder, CO: The Flood Safety Education Project.

Saharia, M., Kirstetter, P.-E., Vergara, H., Gourley, J.J., Hong, Y., 2017. Characterization of floods in the United States. J. Hydrol. 548, 524–535. doi:10.1016/j.jhydrol.2017.03.010

Saharia, M., Kirstetter, P.-E., Vergara, H., Gourley, J.J., Hong, Y., Giroud, M., 2016. Mapping Flash Flood Severity in the United States. J. Hydrometeorol. 18, 397–411. doi:10.1175/JHM-D-16-0082.1

Sangati, M., Borga, M., Rabuffetti, D., Bechini, R., 2009. Influence of rainfall and soil properties spatial aggregation on extreme flash flood response modelling: An evaluation based on the Sesia river basin, North Western Italy. Adv. Water Resour., Weather Radar and Hydrology 32, 1090–1106. doi:10.1016/j.advwatres.2008.12.007

Schröter, K., Llort, X., Velasco-Forero, C., Ostrowski, M., Sempere-Torres, D., 2011. Implications of radar rainfall estimates uncertainty on distributed hydrological model predictions. Atmospheric Res., Uncertainty Propagation in Advanced Hydro-Meteorological Forecast Systems 100, 237–245. doi:10.1016/j.atmosres.2010.08.014

Schumm, S.A., 1956. Evolution of Drainage Systems and Slopes in Badlands at Perth Amboy, New Jersey. Geol. Soc. Am. Bull. 67, 597–646. doi:10.1130/0016-7606(1956)67[597:EODSAS]2.0.CO;2

Schuurmans, J.M., Bierkens, M.F.P., 2007. Effect of spatial distribution of daily rainfall on interior catchment response of a distributed hydrological model. Hydrol Earth Syst Sci 11, 677–693. doi:10.5194/hess-11-677-2007

Sharif, H.O., Hassan, A.A., Bin-Shafique, S., Xie, H., Zeitler, J., 2010. Hydrologic Modeling of an Extreme Flood in the Guadalupe River in Texas1. JAWRA J. Am. Water Resour. Assoc. 46, 881–891. doi:10.1111/j.1752-1688.2010.00459.x

Sivapalan, M., TAKEUCHI, K., FRANKS, S.W., GUPTA, V.K., KARAMBIRI, H., LAKSHMI, V., LIANG, X., McDONNELL, J.J., MENDIONDO, E.M., O'CONNELL, P.E., OKI, T., POMEROY, J.W., SCHERTZER, D., UHLENBROOK, S., ZEHE, E., 2003. IAHS Decade on Predictions in Ungauged Basins (PUB), 2003–2012: Shaping an exciting future for the hydrological sciences. Hydrol. Sci. J. 48, 857–880. doi:10.1623/hysj.48.6.857.51421

Smith, B.K., Smith, J.A., 2015. The Flashiest Watersheds in the Contiguous United States. J. Hydrometeorol. 16, 2365–2381. doi:10.1175/JHM-D-14-0217.1

Smith, J.A., 1992. Representation of basin scale in flood peak distributions. Water Resour. Res. 28, 2993–2999. doi:10.1029/92WR01718

Smith, J.A., Baeck, M.L., Meierdiercks, K.L., Miller, A.J., Krajewski, W.F., 2007. Radar rainfall estimation for flash flood forecasting in small urban watersheds. Adv. Water Resour., Recent Developments in Hydrologic Analysis 30, 2087–2097. doi:10.1016/j.advwatres.2006.09.007

Smith, M.B., Koren, V.I., Zhang, Z., Reed, S.M., Pan, J.-J., Moreda, F., 2004. Runoff response to spatial variability in precipitation: an analysis of observed data. J. Hydrol., The Distributed Model Intercomparison Project (DMIP) 298, 267–286. doi:10.1016/j.jhydrol.2004.03.039

Stasinopoulos, D.M., Rigby, R.A., 2007. Generalized additive models for location scale and shape (GAMLSS) in R. J. Stat. Softw. 23, 1–46.

Sturdevant-Rees, P., Smith, J.A., Morrison, J., Baeck, M.L., 2001. Tropical storms and the flood hydrology of the central Appalachians. Water Resour. Res. 37, 2143–2168. doi:10.1029/2000WR900310

United States Soil Conservation Service, 1972. SCS national engineering handbook, Supplement A, Section 4, Chapter 10: hydrology. Soil Conservation Service, USDA.

US Department of Commerce, N., n.d. Flood and flash flood definitions [WWW Document]. URL http://www.srh.noaa.gov/mrx/hydro/flooddef.php (accessed 3.24.16).

Vergara, H., Kirstetter, P.-E., Gourley, J.J., Flamig, Z.L., Hong, Y., Arthur, A., Kolar, R., 2016. Estimating a-priori kinematic wave model parameters based on regionalization for flash flood forecasting in the Conterminous United States. J. Hydrol., Flash floods, hydro-geomorphic response and risk management 541, Part A, 421–433. doi:10.1016/j.jhydrol.2016.06.011

Viglione, A., Chirico, G.B., Komma, J., Woods, R., Borga, M., Blöschl, G., 2010. Quantifying space-time dynamics of flood event types. J. Hydrol., Flash Floods: Observations and Analysis of Hydrometeorological Controls 394, 213–229. doi:10.1016/j.jhydrol.2010.05.041

Villarini, G., Goska, R., Smith, J.A., Vecchi, G.A., 2014. North Atlantic Tropical Cyclones and U.S. Flooding. Bull. Am. Meteorol. Soc. 95, 1381–1388. doi:10.1175/BAMS-D-13-00060.1

Villarini, G., Krajewski, W.F., Ntelekos, A.A., Georgakakos, K.P., Smith, J.A., 2010. Towards probabilistic forecasting of flash floods: The combined effects of uncertainty in radar-rainfall and flash flood guidance. J. Hydrol., Flash Floods: Observations and Analysis of Hydrometeorological Controls 394, 275–284. doi:10.1016/j.jhydrol.2010.02.014

Villarini, G., Smith, J.A., 2010. Flood peak distributions for the eastern United States. Water Resour. Res. 46, W06504. doi:10.1029/2009WR008395

Vogel, R.M., Zafirakou-Koulouris, A., Matalas, N.C., 2001. Frequency of record-breaking floods in the United States. Water Resour. Res. 37, 1723–1731. doi:10.1029/2001WR900019

Wilson, C.B., Valdes, J.B., Rodriguez-Iturbe, I., 1979. On the influence of the spatial distribution of rainfall on storm runoff. Water Resour. Res. 15, 321–328. doi:10.1029/WR015i002p00321

Winchell, M., Gupta, H.V., Sorooshian, S., 1998. On the simulation of infiltration- and saturation-excess runoff using radar-based rainfall estimates: Effects of algorithm uncertainty and pixel aggregation. Water Resour. Res. 34, 2655–2670. doi:10.1029/98WR02009

Wood, E.F., Sivapalan, M., Beven, K., Band, L., 1988. Effects of spatial variability and scale with implications to hydrologic modeling. J. Hydrol., Hydrologic Research: The U.S. — Japan Experience 102, 29–47. doi:10.1016/0022-1694(88)90090-X

Zhang, J., Howard, K., Langston, C., Kaney, B., Qi, Y., Tang, L., Grams, H., Wang, Y., Cocks, S., Martinaitis, S., Arthur, A., Cooper, K., Brogden, J., Kitzmiller, D., 2015. Multi-Radar Multi-Sensor (MRMS) Quantitative Precipitation Estimation: Initial Operating Capabilities. Bull. Am. Meteorol. Soc. doi:10.1175/BAMS-D-14-00174.1

Zhang, J., Howard, K., Langston, C., Vasiloff, S., Kaney, B., Arthur, A., Van Cooten, S., Kelleher, K., Kitzmiller, D., Ding, F., Seo, D.-J., Wells, E., Dempsey, C., 2011. National Mosaic and Multi-Sensor QPE (NMQ) System: Description, Results, and Future Plans. Bull. Am. Meteorol. Soc. 92, 1321–1338. doi:10.1175/2011BAMS-D-11-00047.1

Zoccatelli, D., Borga, M., Viglione, A., Chirico, G.B., Blöschl, G., 2011. Spatial moments of catchment rainfall: rainfall spatial organisation, basin morphology, and flood response. Hydrol Earth Syst Sci 15, 3767–3783. doi:10.5194/hess-15-3767-2011

Zoccatelli, D., Borga, M., Zanon, F., Antonescu, B., Stancalie, G., 2010. Which rainfall spatial information for flash flood response modelling? A numerical investigation based on data from the Carpathian range, Romania. J. Hydrol., Flash Floods: Observations and Analysis of Hydrometeorological Controls 394, 148–161. doi:10.1016/j.jhydrol.2010.07.019